FIELD INVESTIGATION OF GEOSYNTHETICS USED FOR SUBGRADE STABILIZATION

FHWA/MT-09-003/8193

Final Report

prepared under the sponsorship of
NAUE GmbH & Co. KG

THE STATE OF MONTANA
DEPARTMENT OF TRANSPORTATION

in cooperation with
THE U.S. DEPARTMENT OF TRANSPORTATION
FEDERAL HIGHWAY ADMINISTRATION

RESEARCH AND INNOVATIVE TECHNOLOGY ADMINISTRATION

July 2009

prepared by
Eli Cuelho
Steve Perkins

Western Transportation Institute
Montana State University - Bozeman

RESEARCH PROGRAMS

MDT

FIELD INVESTIGATION OF GEOSYNTHETICS USED FOR SUBGRADE STABILIZATION

Final Project Report

by

Eli Cuelho and Steve Perkins

of the

Western Transportation Institute, College of Engineering
Montana State University – Bozeman

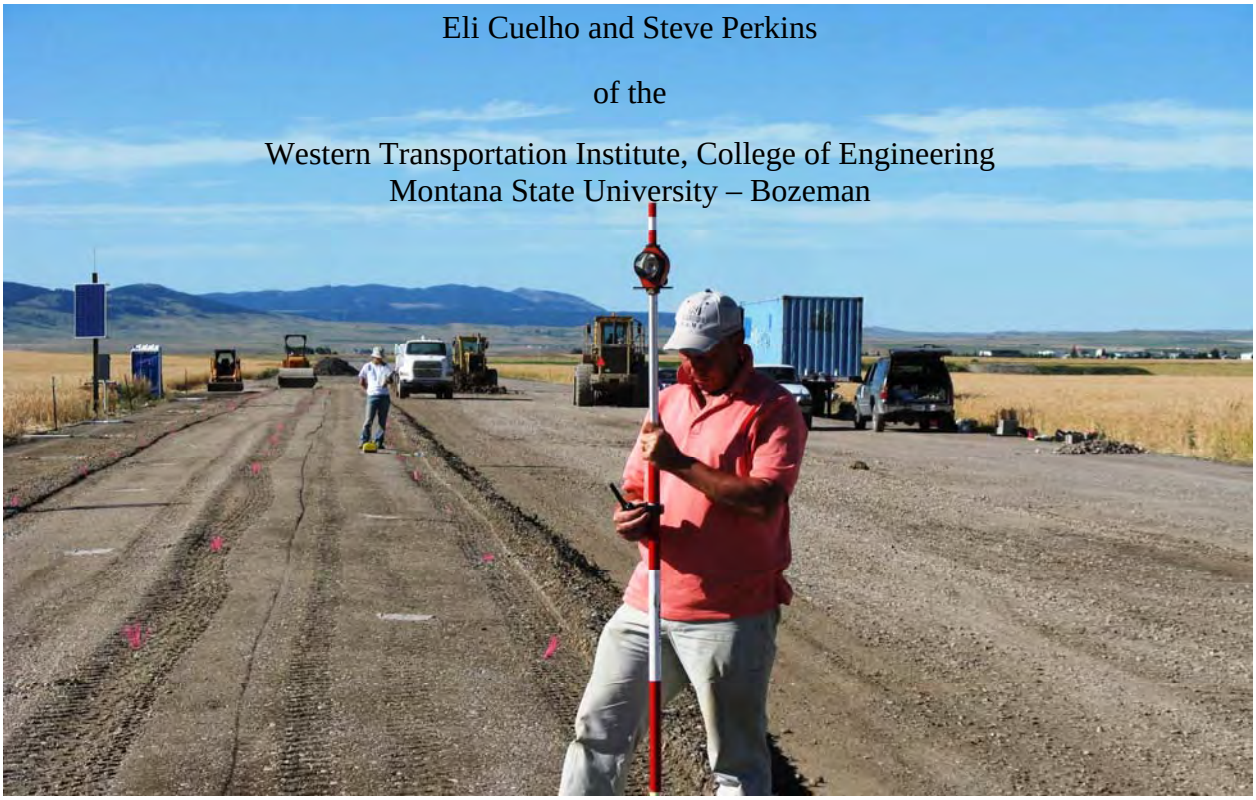

prepared for the

State of Montana, Department of Transportation
Research Programs

and

NAUE GmbH & Co. KG

in cooperation with the

U.S. Department of Transportation, Federal Highway Administration

July 2009

TECHNICAL REPORT DOCUMENTATION PAGE

1. Report No. FHWA/MT-09-003/8193	2. Government Access No.	3. Recipient's Catalog No.	
4. Title and Subtitle Field Investigation of Geosynthetics Used for Subgrade Stabilization		5. Report Date July 2009 6. Performing Organization Code	
7. Author(s) Eli Cuelho and Steve Perkins		8. Performing Organization Report Code	
9. Performing Organization Name and Address Western Transportation Institute PO Box 174250 Montana State University – Bozeman Bozeman, Montana 59717-4250		10. Work Unit No. (TRAIS) 11. Contract or Grant No. MSU G&C #4W2012 MDT Project #8193	
12. Sponsoring Agency Names and Addresses Research Programs Montana Department of Transportation 2701 Prospect Avenue Helena, Montana 59620-1001 NAUE GmbH & Co. KG Gewerbestraße 2 32339 Espelkamp-Fiestel Germany		13. Type of Report and Period Covered Final Report February 2008 – July 2009 14. Sponsoring Agency Code 5401	
15. Supplementary Notes Research performed in cooperation with the Montana Department of Transportation, the U.S. Department of Transportation, Federal Highway Administration and NAUE GmbH & Co. KG. This report can be found at http://www.mdt.mt.gov/research/docs/research_proj/subgrade/final_report.pdf.			
16. Abstract The use of reinforcement geosynthetics in unsurfaced roads built upon a soft subgrade is known to provide benefit through better distribution of applied loads and increased bearing capacity. This report describes a research project where field test sections were constructed to evaluate the performance of several geosynthetics commonly used for subgrade stabilization. A sandy clay soil was prepared as a weak roadbed material to a CBR strength of approximately 1.8 and a 20 cm thick aggregate layer was compacted over the geosynthetics. Trafficking was provided by a fully-loaded tandem axle dump truck. Longitudinal rut depth, along with discrete measurements of displacement and pore pressure were monitored throughout the trafficking period. Post-trafficking excavations were conducted to evaluate damage to the geosynthetic, base contamination and deformation of the layers. The construction and monitoring techniques employed during the course of this project helped establish a test bed of relatively similar conditions to facilitate more direct comparison of individual test sections to one another. An empirical analysis was used to normalize small differences between the subgrade strength after trafficking and base course thickness between test sections to facilitate a more direct comparison of performance. The results showed that the welded geogrids, woven geogrids and the stronger integrally-formed geogrid product seemed to provide the best overall performance, while the two geotextile products and the weaker integrally-formed geogrid provided significantly less stabilization benefit based on the normalized rutting performance at 50, 75 and 100 mm of longitudinal rut data, and this performance is likely directly related to the tensile strength of the materials in the cross-machine direction. Overall, this research provides additional and much needed insight regarding which properties have a significant role on performance, as well as an assessment of two design methodologies' ability to predict rutting performance using the test section parameters as design inputs. Additional work is needed to more fully understand which geosynthetic material parameters are most relevant in these situations.			
17. Key Words Geosynthetics, subgrade stabilization, reinforcement, separation, performance, field test		18. Distribution Statement No restrictions. This document is available through NTIS, Springfield, Virginia 22161.	
19. Security Classif. (of this report) Unclassified	20. Security Classif. (of this page) Unclassified	21. No. of Pages 140	22. Price

DISCLAIMER STATEMENT

This document is disseminated under the sponsorship of the Montana Department of Transportation and the United States Department of Transportation in the interest of information exchange. The State of Montana and the United States Government assume no liability of its contents or use thereof.

The contents of this report reflect the views of the authors, who are responsible for the facts and accuracy of the data presented herein. The contents do not necessarily reflect the official policies of the Montana Department of Transportation or the United States Department of Transportation.

The State of Montana and the United States Government do not endorse products of manufacturers. Trademarks or manufacturers' names appear herein only because they are considered essential to the object of this document.

This report does not constitute a standard, specification, or regulation.

ALTERNATIVE FORMAT STATEMENT

MDT attempts to provide accommodations for any known disability that may interfere with a person participating in any service, program, or activity of the Department. Alternative accessible formats of this information will be provided upon request. For further information, call (406) 444-7693, TTY (800) 335-7592, or Montana Relay at 711.

ACKNOWLEDGMENTS

The authors would like to acknowledge the generous financial support for this project from NAUE GmbH & Co. KG, Montana Department of Transportation, as well as the Research and Innovative Technology Administration (RITA) at the United States Department of Transportation through the Western Transportation Institute at Montana State University. Additional thanks are extended to those geosynthetic manufacturers that donated the materials used in this study. Lastly, the authors would like to thank the students and staff at the Western Transportation Institute, namely, Michelle Akin, Linsey Allen, Beker Cuelho, Ken Ellis, Justin Hauck and Jason Harwood, for all of their hard work in the laboratory and field, as well as Barry Christopher of Christopher Consultants for his advice during this project.

EXECUTIVE SUMMARY

In areas where excavation and replacement of inferior subsoils is not cost effective, soil stabilization using geosynthetics may provide a working platform so that the base course gravel layer can be properly constructed and overall rutting reduced. Historically, geotextiles were first used in these applications; however, geogrids have also been commonly used in more recent years. Montana Department of Transportation (MDT) has used both geotextiles and geogrids for subgrade stabilization and supported this research because currently there is a lack of: 1) a universally accepted standard design technique that incorporates non-proprietary material properties of geosynthetics when used as subgrade stabilization, and 2) agreement as to which geosynthetic properties are most relevant in these cases for purposes of specification development. This research was initiated to provide an understanding of which properties are most relevant as MDT seeks to update their specifications to more broadly encompass materials with which they have had good experience, as well as open up the application to other suitable materials. This is particularly important since new geosynthetics and manufacturing processes are regularly introduced into the market. To accomplish these goals, field sections were uniformly constructed, trafficked, and monitored at a transportation research facility to compare the relative performance of 12 test sections, ten with geosynthetics and two without geosynthetics.

Many test trials for geosynthetics have been constructed on native soil deposits as part of existing highway construction jobs. While this is generally more efficient and less costly, variations in the subgrade strength, depth and consistency are oftentimes significant enough to make it difficult to clearly distinguish differences between different products or construction practices. By conducting this research project at the TRANSCEND research facility in Lewistown, Montana on a decommissioned taxiway, three important aspects of construction were able to be controlled: 1) the strength of the roadbed subgrade, 2) the cross-sectional design of the road, and 3) the presence of traffic.

Three main steps were followed to construct the test sections in an excavated and plastic-lined test pit that was 4 meters wide by 1 meter deep by 195 meters long: 1) preparation and placement of the artificial subgrade soil, 2) installation of the geosynthetics and instrumentation, and 3) construction of the base course aggregate. A suitable subgrade soil, which consisted of natural overburden material and was typical of poor subgrade materials encountered in Montana construction projects, was obtained from a nearby gravel pit and delivered to the test site. A constructed CBR strength of 1.7 ±0.1 was targeted.

Laboratory tests were conducted to successfully relate CBR to vane shear. A mathematical relationship between these two parameters allowed the vane shear to be used as the primary method to monitor in-place shear strength of the subgrade as it was being constructed. A dynamic cone penetrometer (DCP) was also used as a comparison to monitor subgrade strength

before and after trafficking. Moisture content of the subgrade was used as a guide for the contractor to achieve the desired subgrade strength prior to compaction. The subgrade was prepared on site by adding water and discing. It was then transported to the test pit and compacted into 15 cm lifts using a single drum vibratory roller. Once constructed to the proper height, the geosynthetics were installed in each section by carefully rolling them out in the direction of traffic. Each geosynthetic test section was approximately 15 meters long, with the exception of the two control sections (Control 1 and Control 2) and the first geosynthetic test section in the direction of trafficking, which were each 20 meters long.

Crushed gravel was used as the base course aggregate for this project. The thickness of the base course was determined using the Federal Highway Administration (FHWA) design methodology (FHWA, 1995), which is based on the U.S. Forest Service method (Steward et al., 1977). A single layer of base course aggregate 20 cm thick was placed on top of the geosynthetics from the side so that the test sections would be in a virgin state (i.e., no trafficking) at the end of construction. A single-drum vibratory roller was used to compact the base aggregate.

Trafficking was accomplished using a fully loaded three-axle dump truck. Trafficking was applied to the test sections in a single direction until each of the individual test sections reached an average of 100 mm of rut as measured by changes in elevation over time. Test sections that failed early were repaired to allow the truck to pass over them without getting stuck. This repair was accomplished by placing additional base course aggregate in the rutted areas.

The analysis of respective performance of each of the test sections was based largely on rut depth as measured in the longitudinal direction. Rut depth was measured in each of the test sections at regularly scheduled intervals during trafficking (more frequently in the beginning and less frequently toward the end) to capture rutting as a function of truck passes. The depth of the rut was measured in the two outermost wheel tracks of the rear wheels at one-meter intervals along the length of each test section. In this case, rut was a function of the difference in the elevation of the measurement points over time. Total rut, therefore, was determined by comparing current measurements to a baseline measurement which was made before trafficking.

Slight differences in the strength of the subgrade and the depth of the base course aggregate between test sections made direct comparisons between test sections more challenging. A simple and direct comparison of performance was made using an empirical approach to account for these minor variations. Using this method to normalize the rut performance data, the welded geogrids, woven geogrids and the stronger integrally formed geogrid product seemed to provide the best overall performance, while the two geotextile products and the weaker integrally formed geogrid provided significantly less stabilization benefit based on the normalized rutting performance at 50, 75 and 100 mm of rut. These test sections failed rapidly (< 40 truck passes); therefore, it is probable that different results may be seen for sections that do not fail as quick.

Further research is needed to pinpoint which geosynthetic material properties most directly relate to stabilization of weak subgrade soils. However, based on the comparative analysis used during this study, tensile strength in the cross-machine direction of the geosynthetic (especially at 2 percent axial strain) likely plays a large roll in suppressing rut formation under these conditions.

The design method used to determine the thickness of the base (FHWA, 1995) was dependent upon two parameters: the strength of the subgrade and the level of traffic (in this case, 100 traffic passes for the control sections and 1000 traffic passes for the reinforced test sections). Since aggregate thickness needed to be the same for all sections, an average base course thickness of 20 cm was specified for a CBR of 1.7, which was greater than what was needed for the reinforced test sections, but less than what was needed for the unreinforced (control) test sections. Therefore, it was expected that the controls might fail somewhat prematurely, while the geosynthetic test sections may withstand greater traffic levels. Results from the test sections showed approximately one-tenth the number of traffic passes to reach 100 mm of rut as compared to the FHWA design. A second design method (Giroud and Han, 2004) that explicitly accounts for the number of traffic passes was also used to determine the base thickness necessary to support this level of traffic. In this case, the average post-trafficking subgrade CBR of each test section along with the observed number of axle passes were used as inputs into this design methodology. The method gave a predicted aggregate thickness that was approximately 16 to 85 percent of the actual constructed aggregate thickness. Aperture stability modulus is the main material property used to describe the properties of the geosynthetic reinforcement. This method underpredicts the required aggregate and provides for worse predictions for products with a larger aperture stability modulus. It is clear from the results of these test sections that both of these design methodologies were unable to predict rutting performance of the constructed test sections.

Instrumentation was installed on the geosynthetic after they were positioned. Three measurements of transverse displacement of the geosynthetic and a single measurement of pore pressure were measured within each test section. Linearly variable displacement transducers (LVDTs) were used to make displacement measurements in the vicinity of the rut bowl, and a stainless steel pressure transducer was used to measure pore pressure.

Live instrumentation was used to further understand the behavior of the geosynthetics during trafficking. Transverse displacement of the geosynthetic (cross-machine direction) within the rut area was measured using three LVDTs in each of the test sections. Displacement of the geosynthetics in each of the test sections was generally similar with respect to the direction and initial magnitude of response. Initially, the wheel loads pushed the geosynthetic away from the side of the vehicle toward the outer edge of the test sections. As the rut bowl began to form, these measurements showed that the geosynthetic began to move in the opposite direction (toward the rutted area). Therefore, using the displacement measurements, it was possible to perceive the geosynthetics shift from lateral restraint as the primary reinforcement mechanism to

the membrane effect. Three strain calculations were also possible using the displacement measurements. Dynamic strain during trafficking in the geosynthetic were relatively small (approximately 2 percent); static strain measurements were around 3 to 5 percent in most materials, and greatest in the non-woven geotextile (14+ percent).

Pore water pressure measurements were also made at a depth of 15 cm within the subgrade within the wheel path in all of the test sections. Dynamic measurements of pore pressure were measured during trafficking and static levels of pore pressure were extracted from these measurements to show pore pressure trends over time for increasing traffic passes. Dynamic pore pressures were generally similar to one another and ranged between 0.2 and 1.5 kPa. Using the maximum values of static pore water pressure, a prediction of the change in shear strength of the subgrade due to pore water pressure increase was made. Overall, the constructed CBR of the subgrade was predicted to decrease by approximately 0.1 due to pore pressure increase, which amounts to about a 6.5 percent decrease from the original strength measurement. Vane shear measurements conducted two weeks after trafficking showed that, overall, the subgrade had reduced in overall strength by about 0.5 CBR.

Post-trafficking, forensic investigations were conducted to evaluate damage to the geosynthetic from trafficking, as well as, to re-evaluate pertinent soil strength characteristics. Forensic evaluations were located in areas that had experienced approximately the same rutting (i.e., 100 mm average rut) so that a direct comparison of damage between products could be made. An area 1.5 meters wide (in the direction of traffic) and 4 meters long was selected in each of the test sections, including the control test sections. Excavation of the base course was accomplished using a large vacuum truck and a high-flow compressed air nozzle to minimize disturbance and damage of the geosynthetic. After exposing the entire area of geosynthetics, they were carefully removed to analyze damage to junctions and rib integrity and continuity. Post trafficking DCP measurements were taken in the excavated area prior to removal of the subgrade. The subgrade was then removed from these areas to comprehensively evaluate soil mixing between the subgrade and base course in the rutted areas, soil shear strength using the vane shear, soil moisture contents and a general evaluation of the rutted area.

Damage was quantified in three main ways depending on the material structural composition: 1) damage to junctions in welded and woven grid products, 2) damage to ribs in all grids and 3) a qualitative assessment of continuity in the cross-machine direction for the integrally-formed geogrids and the two textile products. The majority of junction and rib damage occurred in the rutted area. Junction damage was greatest in the WeG-1 material (27.4 percent damage) and least in the WoG-7 material (6.8 percent). Rib damage was minimal in the welded and woven products. Both of the integrally-formed grids sustained rupture damage during trafficking, which was seen to directly impact their ability to support the traffic loads, and this phenomenon had a more profound affect on the IFG-5 test section than in the IFG-3 test section.

This research was initiated to provide information from which a greater understanding of which geosynthetic material properties are most relevant when they are used as subgrade stabilization as the Montana Department of Transportation seeks to update their specifications to more broadly encompass materials with which they have had good experience, as well as open up the application to other suitable materials. This is particularly important since new geosynthetics and manufacturing processes are regularly introduced into the market.

TABLE OF CONTENTS

LIST OF TABLES

LIST OF FIGURES

1 INTRODUCTION AND BACKGROUND

Roadways are commonly constructed on weak native soil deposits. When excavation and replacement of these soils is not cost effective, soil stabilization may be necessary to provide a working platform so that the base course gravel layer can be properly constructed and overall rutting reduced. Geosynthetics are planar polymeric materials that have been extensively used in these situations (i.e., subgrade stabilization) to reinforce and/or separate the surrounding soils. Separation is typically attributed to geotextiles, while reinforcement may be derived from geotextiles and geogrids; however, under the right circumstances, geogrids may also offer separation (Maxwell et al., 2005). Subgrade stabilization is typically applicable for unpaved temporary roads such as haul roads, or construction platforms to support permanent roads. These roads are generally characterized by low volumes of heavy vehicles that can tolerate deeper ruts. According to the National Highway Institute (NHI), geosynthetic stabilization techniques used for these types of roads are "one of the more important uses of geosynthetics" (NHI, 2008). Historically, geotextiles were first used in these applications; however, geogrids have also been commonly used in more recent years.

Montana Department of Transportation (MDT) has used both geotextiles and geogrids for subgrade stabilization and supported this research because currently there is a lack of: 1) a universally accepted standard design technique that incorporates non-proprietary material properties of geosynthetics when used as subgrade stabilization, and 2) agreement as to which geosynthetic properties are most relevant in these cases for purposes of specification development (Gabr et al., 2006; Perkins et al., 2005; Watn et al., 2005). Therefore, this research was initiated to provide an understanding of which properties are most relevant as MDT seeks to update its specifications to more broadly encompass materials with which it has had good experience, as well as open up the application to other suitable materials. This is particularly important since new geosynthetics and manufacturing processes are regularly introduced into the market. To accomplish these goals, field sections were uniformly constructed, trafficked, and monitored at a transportation research facility to compare the relative performance of 12 test sections, ten with geosynthetics and two without geosynthetics.

Geosynthetics can improve the performance of weak subgrades under temporary unpaved roads by the following mechanisms: 1) reduction of plastic shear stresses that cause bearing capacity failure in the subgrade, 2) reduction of maximum normal stresses on the subgrade surface by improved load distribution, 3) increase in the bearing capacity of the subgrade by confining lateral movement at the subgrade-base interface and a reorientation of the induced shear stresses, 4) increase in the bearing capacity and stress reduction attributable to the "tensioned membrane effect" in rutted areas, 5) provide lateral restraint and reinforcement of base course aggregates and 6) reduction of mixing between subgrade and base soils (Hufenus et al., 2006; Maxwell et al., 2005; Giroud and Han, 2004; Leng, 2002; Perkins et al., 2005; Watn et

al., 2005). These improvements in subgrade performance can facilitate compaction, reduce the gravel surface thickness, delay rut formation, and extend the service life of unpaved roads, particularly in cases of very soft subgrades with a California Bearing Ratio (CBR) less than three (Benson et al., 2005; Hufenus et al., 2006).

The current practice of using geosynthetics for subgrade stabilization is primarily based on empirical evidence from constructed test sections. Field tests constructed strictly for research purposes instead of during scheduled rehabilitation or reconstruction activities offer better control over study variables, such as careful preparation of soil and reduced incidental trafficking. Despite this, it is still difficult to achieve uniform conditions throughout a project site utilizing the natural subgrade (e.g., Fannin and Sigurdsson, 1996; Edil et al., 2002; and Hufenus et al., 2006). Conversely, research studies in which a subgrade soil was artificially placed demonstrate better consistency (e.g., Santoni et al., 2001; Perkins, 2002; Tingle and Webster, 2003).

While laboratory studies can be conducted more quickly and usually include more alternatives, they are only able to simulate field conditions and, as Hufenus et al. (2006) point out, there "are no incontrovertible indications from laboratory tests of the influence that the geosynthetic will have on the performance of the pavement under trafficking" (p. 23). Thus the need still exists for field tests that provide uniform conditions and incorporate a variety of geosynthetics in order to develop a sufficient database of performance results. The need for such a database of information is resoundingly clear in light of the fact that there is still not an acceptable design method for unpaved roads (or construction platforms) that incorporate both soil and geosynthetic material properties.

A simple existing design published by the Federal Highway Administration (FHWA, 1995), is based on the U.S. Forest Service method developed by Steward et al. (1977). A more recent design method for unpaved roads that attempts to incorporate geosynthetic properties was theoretically derived based on the stresses that develop at the base-subgrade interface. The impact of these stresses and the subgrade bearing capacity were related to rut depth based on empirical data (Giroud and Han, 2004). However, only limited data were used to calibrate the model: 1) field data from Hammitt (1970) for unreinforced unpaved sections and 2) lab data from Gabr (2001) that involved two versions of one type of geosynthetic (integrally formed geogrid). One parameter in the model can take on three different values depending on whether the roadway is 1) unreinforced, 2) geotextile reinforced, or 3) geogrid reinforced design. If a geogrid is under consideration, the aperture stability modulus is used, but only if the material property is within the approximate range of the types of geogrids tested by Gabr (2001) for which the model was calibrated. Even though this design method was intended to be used to design reinforced and unreinforced unpaved roads, there are inherent limitations in how it models the contribution of various geosynthetics that should be considered. While this model is an improvement over less sophisticated designs from the 1980s (Giroud and Noiray, 1981 and

Giroud et al., 1985), there is still a need to investigate the performance of geosynthetics in controlled field tests. Calibrations with additional data sets may be sufficient, although most likely geosynthetic material properties other than aperture stability modulus should be considered.

2 FIELD TEST DESIGN

Many test trials for geosynthetics have been constructed on native soil deposits as part of existing highway construction jobs. While this is generally more efficient and less costly, variations in the subgrade strength, depth and consistency are oftentimes significant enough to make it difficult to clearly distinguish differences between different products or construction practices. Therefore, construction of the test sections reported for this project was done in a way to minimize these differences. By conducting this research project at the TRANSCEND research facility in Lewistown, Montana, on a decommissioned taxiway, three important aspects of construction were able to be controlled: 1) the strength of the roadbed subgrade, 2) the cross-sectional design of the road, and 3) the presence of traffic. The original cross section of the taxiway was modified by removing existing pavement and base materials so that an artificial subgrade material could be uniformly placed along the entire test site to ensure that underlying soil strength did not vary significantly. Traffic was not allowed on the test sections during construction and a single truck was used to apply traffic loads during testing.

2.1 Design and Layout of Test Site

The basic design and layout of the test area was centered on providing a uniform platform to compare the performance of several geosynthetics when used as subgrade stabilization. It was necessary to remove the natural soils at the TRANSCEND test site: 1) because they consisted mainly of large-stoned dense gravels topped by a layer of base course and asphalt which was too strong to evaluate geosynthetics as subgrade stabilization, and 2) to facilitate trafficking of the test sections, the final grade of the test site was designed to be close to the original level of the existing taxiway. The trench formed by the removal of the existing pavement and base materials provided an area to construct an “artificial” subgrade. Artificial, in this case, meant that the subgrade soil, which is typically the existing in-situ soil, was purchased off site and constructed to resemble naturally weak soil deposits. The top surface of the test sections was unpaved; therefore, trafficking occurred on the surface of the gravel base course layer.

The size of the excavation was designed to model a typical single lane roadway; therefore, the area needed was approximately 4 meters wide by 1 meter deep to sufficiently minimize boundary affects from the trench walls and floor. A length of 195 meters was necessary to evaluate ten geosynthetics and two control sections. The floor of the test pit was tapered at the ends to facilitate movement of the construction equipment into and out of the pit; the tapered area was not included in the experiment.

The surface of the subgrade was designed to have a slight crown (approximately 1 percent) so that water from precipitation would not pool on the surface and weaken it. Precipitation during construction and trafficking was minimal. The base course (which is the driving course) was also crowned for the same reason. The base aggregate extended past the outside edge of the

subgrade and tapered down to the original level of the original paved surface. Because the final level of the base aggregate was higher than the original level of the taxiway, a gradual ramp was built at each end using the base aggregate to allow the test vehicle to easily enter and exit the test sections during trafficking. A cross-sectional view of a typical test section is shown in Figure 1 with the test vehicle.

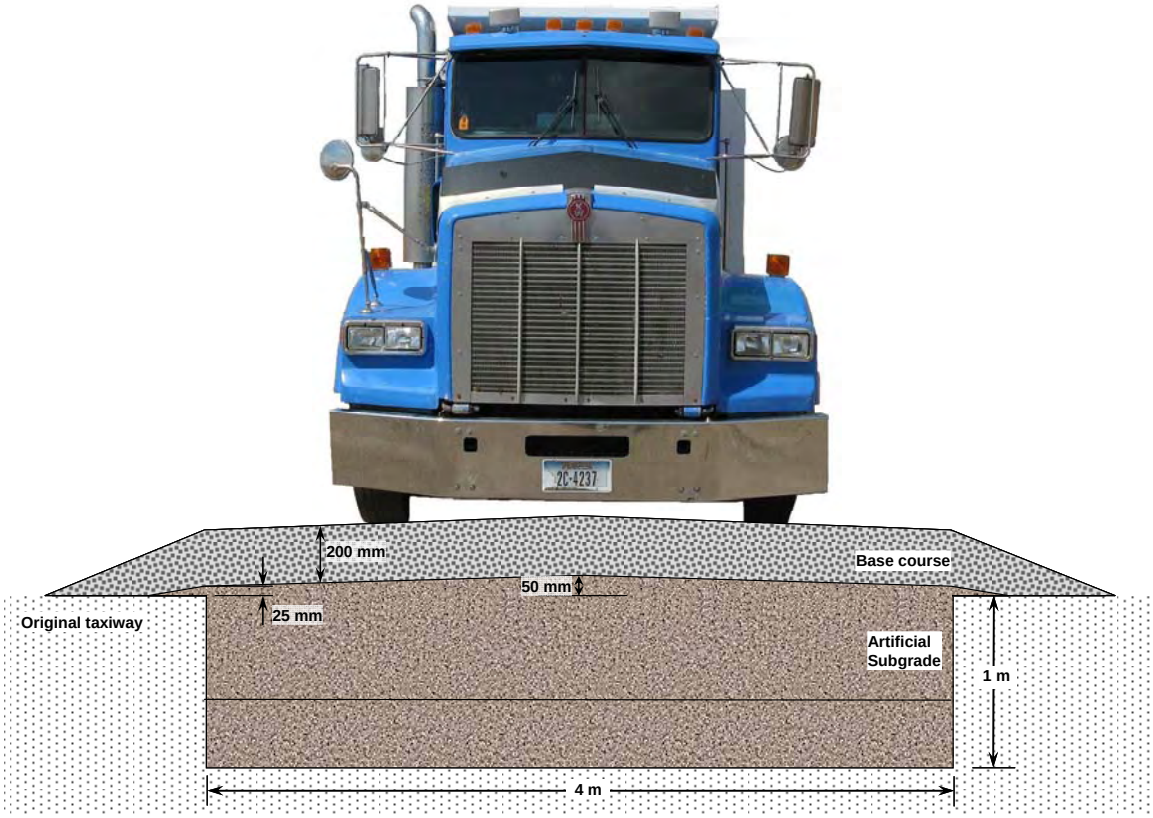

Figure 1. Cross-section of field test section with truck (truck scaled to approximate size).

2.2 Artificial Subgrade

It was desired to construct the artificial subgrade out of a soil that was weak when wet, in relatively close proximity to the test site, and was typical of poor subgrade materials encountered in Montana construction projects. A suitable subgrade soil, which consisted of natural overburden material, was obtained from a nearby gravel pit and delivered to the test site. The material was stockpiled along a vacant section of the abandoned taxiway adjacent to the test sections. This soil classified as A-2-6 according to the AASHTO classification system (AASHTO M-145) or SC (clayey sand with gravel) according to the USCS classification system (ASTM D 2487). Other relevant properties of the artificial subgrade are listed in Table 1. The gradation for the subgrade material for particle sizes less than 38.1 mm is shown in Figure 2. Because the subgrade material was natural and unprocessed, it occasionally contained some particles larger than 38.1 mm, such as small cobbles, that were mostly removed during

construction. The R-value of the subgrade listed in Table 1 indicates greater strength than what was measured during this research project, because the subgrade was prepared at a moisture content greater than optimum which, in this case, greatly reduced its overall strength.

Table 1. General Properties of the Artificial Subgrade

Property	
Liquid Limit	32
Plastic Limit	17
Plasticity Index	15
% passing #200 sieve	32%
Max. dry density†	1842 kg/m^3
Optimum moisture content†	15%
R-value	18

† using standard Proctor procedure (AASHTO T-99)

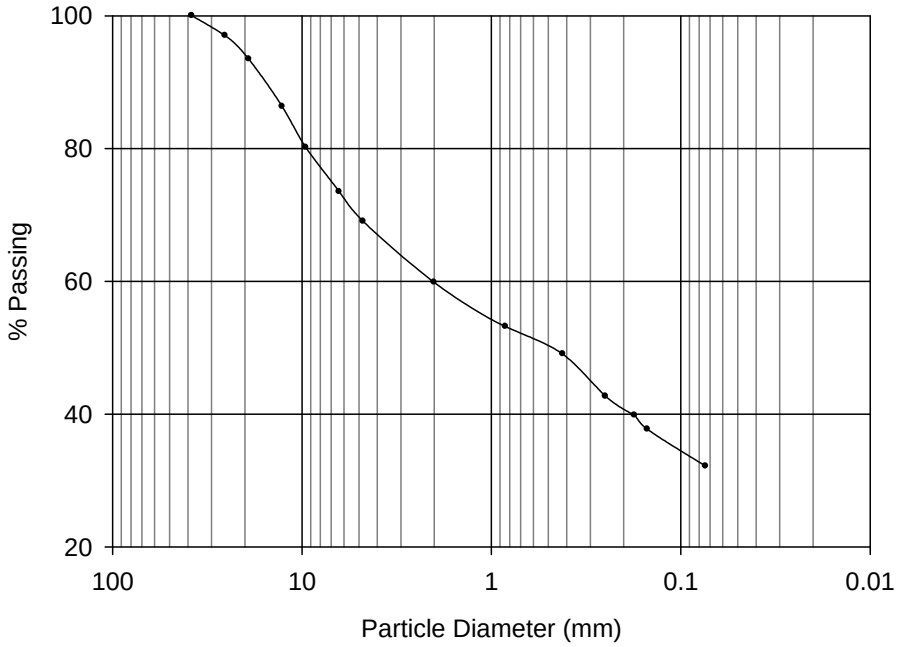

Figure 2. Grain-size distribution of the artificial subgrade soil.

Laboratory tests were conducted to determine the appropriate method to prepare the subgrade soil so that it had the desired strength characteristics (i.e., CBR strength of 1.7 ±0.1). A hand-held vane shear device was chosen as the primary method to monitor in-place shear strength of the subgrade as it was being constructed because it was: 1) simple to operate, 2) able to provide a rapid assessment of strength, and 3) was more precise than other devices. A dynamic cone penetrometer (DCP) was also used as a comparison to monitor subgrade strength before and after trafficking. Unsaturated CBR tests were conducted in the lab prior to

construction to determine a relationship between soil strength and moisture content. Vane shear tests were also conducted on the laboratory CBR samples to relate CBR to vane shear strength. The linear relationship that was developed in the lab using both of these tests was generally good (linear regression $R^2 = 0.8068$), as shown in Figure 3. According to this data, the shear strength as determined using the vane shear device must be between roughly 52 and 62 kPa to achieve the desired CBR strength (1.7 ±0.1). Attempts to relate moisture content or density to CBR in the laboratory did not yield satisfactory results (R^2 values = 0.1071 and 0.0374, respectively).

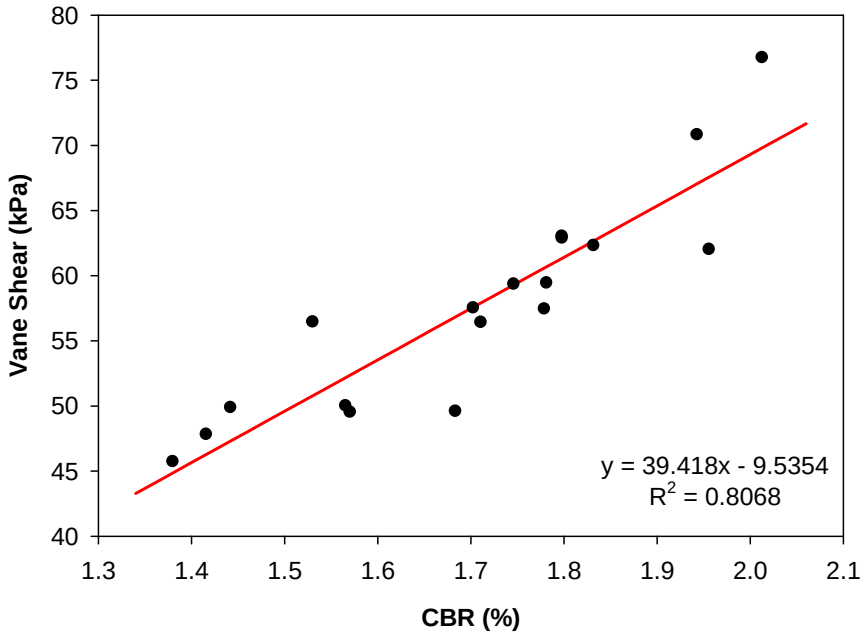

Figure 3. Relationship between California Bearing Ratio and the hand-held vane shear device.

2.3 Base Course Aggregate

The base course aggregate for this project was a crushed gravel Grade "6A" according to MDT standard material specifications, having the gradation shown in Figure 4. It classified as A-1-a according to the AASHTO classification system (AASHTO M-145) or GW-GM (well-graded gravel with silt with sand) according to the USCS classification system (ASTM D 2487). Other relevant properties of the base course aggregate are listed in Table 2. Multiple CBR tests run on the base course aggregate resulted in bearing ratios that were higher at 0.2 inches displacement than at 0.1 inches displacement, meaning that the CBR at 0.2 inches should be used. Corrections were also necessary to account for the concave upward shape of the load-displacement curve from the CBR tests. The base aggregate satisfied the natural filter gradation requirements as specified in Holtz et al. (2008), meaning a geotextile separation layer was not needed to prevent contamination of the gravel layer. This meant that any benefit provided by a geosynthetic could be attributed to reinforcement.

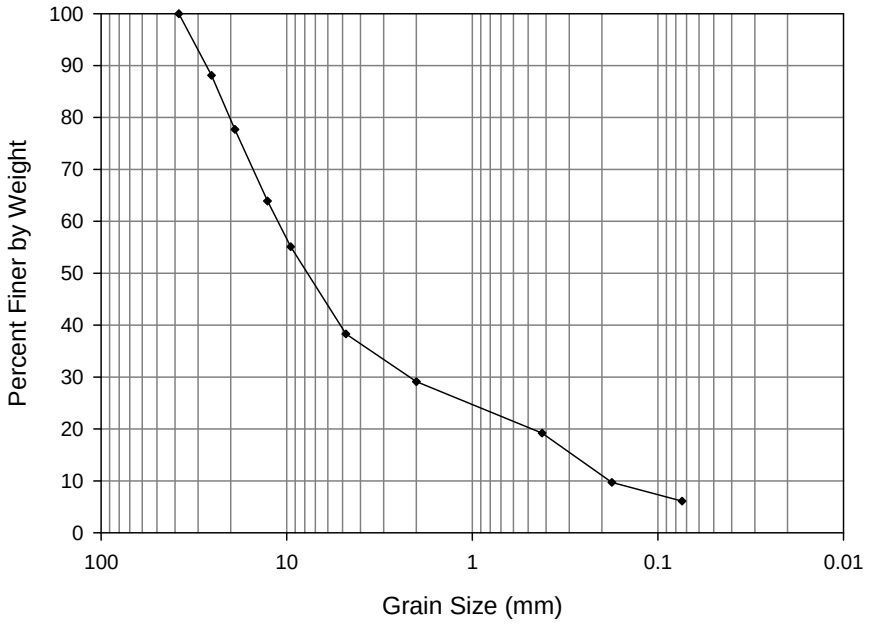

Figure 4. Base course aggregate grain-size distribution.

Table 2. General Properties of the Base Course Aggregate

Property	
Liquid Limit	NP
Plastic Limit	NP
Plasticity Index	NP
% passing #200 sieve	6%
Max. dry density†	2310 kg/m^3
Optimum moisture content†	5%
% fractured faces	36%
CBR† (ρ_{dry} = 2200 kg/m^3)	>100

† using modified Proctor procedure (ASTM D1557)
NP = non-plastic

The thickness of the base course was determined using the Federal Highway Administration design methodology (FHWA, 1995), that is based on the U.S. Forest Service method (Steward et al., 1977). The design process begins by selecting an appropriate bearing capacity factor, N_c, which depends on 1) presence of geosynthetics, 2) allowable rutting, and 3) traffic levels. Bearing capacity factors for a matrix of these conditions are listed in Table 3. It was assumed that test sections which utilized geosynthetics for subgrade stabilization would have less rutting and would therefore fail less rapidly as compared to sections that did not use geosynthetics (i.e., the control test sections). Consequently, bearing capacity factors of 5.0 and 3.3 were selected for sections with and without geosynthetic stabilization, respectively. The thickness of the base

course was then determined using the design curve for tandem (dual)-wheel loads (assumes 550 kPa tire pressure and each axle carries 80 kN of load). From this analysis a relationship of CBR to base course thickness was created (Figure 5). Since aggregate thickness needed to be the same for all sections, an average base course thickness of 20 cm was specified for a CBR of 1.7, which was greater than what was needed for the reinforced test sections, but less than what was needed for the unreinforced (control) test sections. Therefore, it was expected that the controls might fail somewhat prematurely, while the geosynthetic test sections may withstand greater traffic levels. Using the aforementioned design methodology and input values, it was anticipated that the control test sections would reach 10 cm of rut at less than 45 truck passes (~100 traffic passes) and that the majority of the geosynthetic-stabilized test sections would reach 10 cm of rut at greater than 455 truck passes (~1000 traffic passes). Based on Yoder and Witczak (1975), one passage of the truck equals about 2.2 traffic passes, also known as axle passes.

Table 3. Bearing Capacity Factors (after Steward et al., 1977)

	Allowable Rut (mm)	No. of Traffic Passes	Bearing Capacity Factor, N_c
Without Geosynthetic	< 50	> 1000	2.8
	> 100	< 100	3.3
With Geosynthetic	< 50	> 1000	5.0
	> 100	< 100	6.0

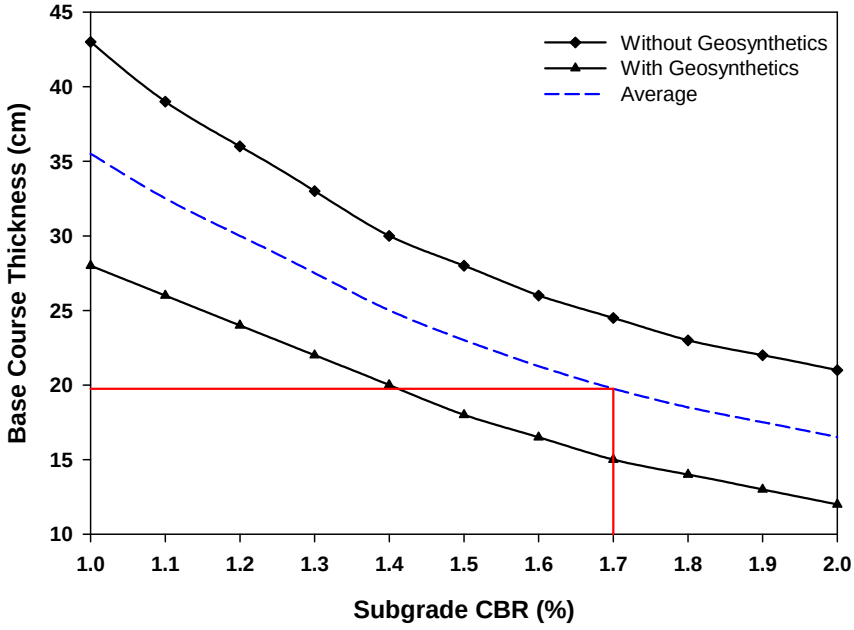

Figure 5. Relationship of subgrade strength to base course thickness.

2.4 Geosynthetics

Ten geosynthetic products were used in this research project to evaluate their relative performance under the conditions presented herein. Pertinent information for each of these products is listed in Table 4. The general layout of the test sections and the direction of traffic are illustrated in Figure 6. All of the geogrids met the aperture size criteria based on the gradation of the base course material and the Class 1 survivability requirements, as specified in Holtz et al. (2008).

Table 4. Summary of Geosynthetic Properties Provided by Manufacturers

Geosynthetic Test Section*	Structure	Polymer[a]	Roll Width (m)	Mass per unit area (g/m^2)	Aperture Size[b] (mm)
WeG-1	biaxial welded geogrid	PP	5.00	240	44 x 40
WeG-2	vibratory-welded geogrid	PP	4.75	155	32 x 32
IFG-3	integrally-formed biaxial geogrid	PP	4.88	NP	25 x 33
CoG-4†	composite vibratory-welded geogrid with integrated non-woven geotextile	PP	4.75	200 150	32 x 32 N/A
IFG-5	integrally-formed biaxial geogrid	PP	4.00	NP	25 x 33
WeG-6	vibratory-welded geogrid	PP	4.75	200	32 x 32
WoG-7	PVC coated woven geogrid	PMY	4.00	308.5	25.4 x 25.4
WoG-8	polymer coated woven geogrid	PMY	3.66	NP	25.4 x 25.4
WoT-9	fibrillated woven geotextile	PPY	3.81	342	0.425[c]
NWoT-10	non-woven needle-punched geotextile	PP	4.57	271	0.18[c]

* Acronym meanings: WeG = welded grid, IFG = integrally-formed grid, CoG = composite grid, WoG = woven grid, WoT = woven textile, NWoT = non-woven textile; numbers represent position along length of test site

† Material is a composite; the top row of values is for the grid component and the bottom row is for the non-woven textile

[a] PP = polypropylene, PMY = polyester multifilament yarn, PPY = polypropylene yarn

[b] Dimensions are listed as MD x XMD (Machine Direction x Cross-Machine Direction)

[c] Apparent Opening Size (AOS), ASTM D 4751

NP – information was not provided by the manufacturer; N/A – information not applicable

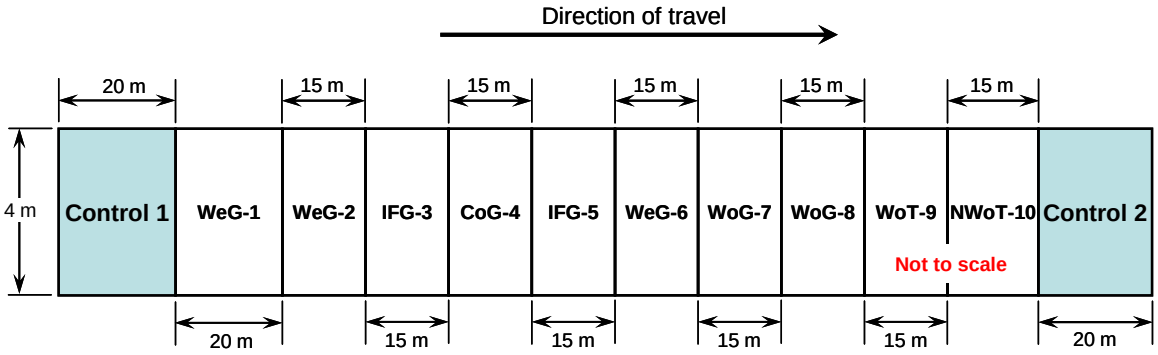

Figure 6. General layout of test sections.

Samples of each of the geosynthetics were collected and used to evaluate wide-width tensile strength (ASTM D4595) and junction strength (GRI-GG2) in the two principal strength directions (machine direction – MD and cross-machine direction – XMD). The tensile strength, independently determined by the Western Transportation Institute (WTI), is shown in comparison to the published tensile strength from each of the geosynthetic manufacturers in Table 5. Roll values as supplied by individual manufacturers are summarized in Appendix A along with the test results from the WTI laboratory.

Table 5. Tensile Strength Properties of Geosynthetics

Geosynthetic Test Section*	Tested by WTI						Published by Manufacturers[a]					
	Strength[b] @ 2% (kN/m)		Strength[b] @ 5% (kN/m)		Ultimate[b] Strength (kN/m)		Strength[b] @ 2% (kN/m)		Strength[b] @ 5% (kN/m)		Ultimate[b] Strength (kN/m)	
	MD	XMD	MD	XMD	MD	XMD	MD	XMD	MD	XMD	MD	XMD
WeG-1	9.5	9.7	19.6	20.4	29.9	35.3	10.7	10.7	21.3	21.3	32.0	32.0
WeG-2	13.2	13.0	25.7	26.1	38.4	39.6	8	8	16	16	20	20
IFG-3	7.5	12.8	15.2	24.8	22.6	32.4	6.0	9.0	11.8	19.6	19.2	28.8
CoG-4[c]	13.6	14.4	27.3	28.0	41.8	43.8	12	12	24	24	30[d]	30[d]
IFG-5	5.7	8.3	11.3	14.5	16.0	21.6	4.1	6.6	8.5	13.4	12.4	19.0
WeG-6	13.9	13.7	27.1	27.2	40.7	41.2	12	12	24	24	30	30
WoG-7	6.9	9.9	16.3	16.4	33.9	48.9	7.3	7.3	13.4	13.4	29.2	29.2
WoG-8	7.0	8.6	13.1	12.2	31.3	53.7	7.7	8.4	11.5	15.2	34.9	56.5
WoT-9	7.5	12.5	20.8	27.2	59.8	71.1	8.8	8.8	21.9	21.9	52.5	47.3
NWoT-10	0.1	0.2	0.6	0.7	17.5	12.7	NP		NP		912[e]	

* Acronym meanings: WeG = welded grid, IFG = integrally-formed grid, CoG = composite grid, WoG = woven grid, WoT = woven textile, NWoT = non-woven textile; numbers represent position along length of test site
[a] Manufacturers' minimum average roll values (MARV)
[b] ASTM D4595 and ASTM D6637
[c] Tested by WTI as a composite, i.e., not separately
[d] Non-woven portion of this material increases the ultimate strength by 6 kN/m in the MD and by 10 kN/m in the XMD
[e] Grab tensile strength (ASTM D-4632) in Newtons at 50% elongation
NP – information was not provided by the manufacturer

2.5 Instrumentation

Three measurements of transverse displacement of the geosynthetic and a single measurement of pore pressure in the subgrade were measured at a single location within each test section. Linearly variable displacement transducers (LVDTs) were used to make displacement measurements in the vicinity of the rut bowl, and a stainless steel pressure transducer was used to measure pore pressure, as illustrated in Figure 7. The pore pressure transducer had a range of 0 to 207 kPa. Dynamic measurements of displacement and pore pressure were collected at 200 Hz during all of the truck passes while trafficking. Static measurements of displacement and pore pressure were attempted, but problems with the data logger resulted in the loss of much of this data during trafficking. Displacement data were used to calculate strain in the geosynthetic during trafficking. These four measurements were made at the center of each test section along their length, and only pore pressure was measured in the control sections due to the absence of geosynthetics.

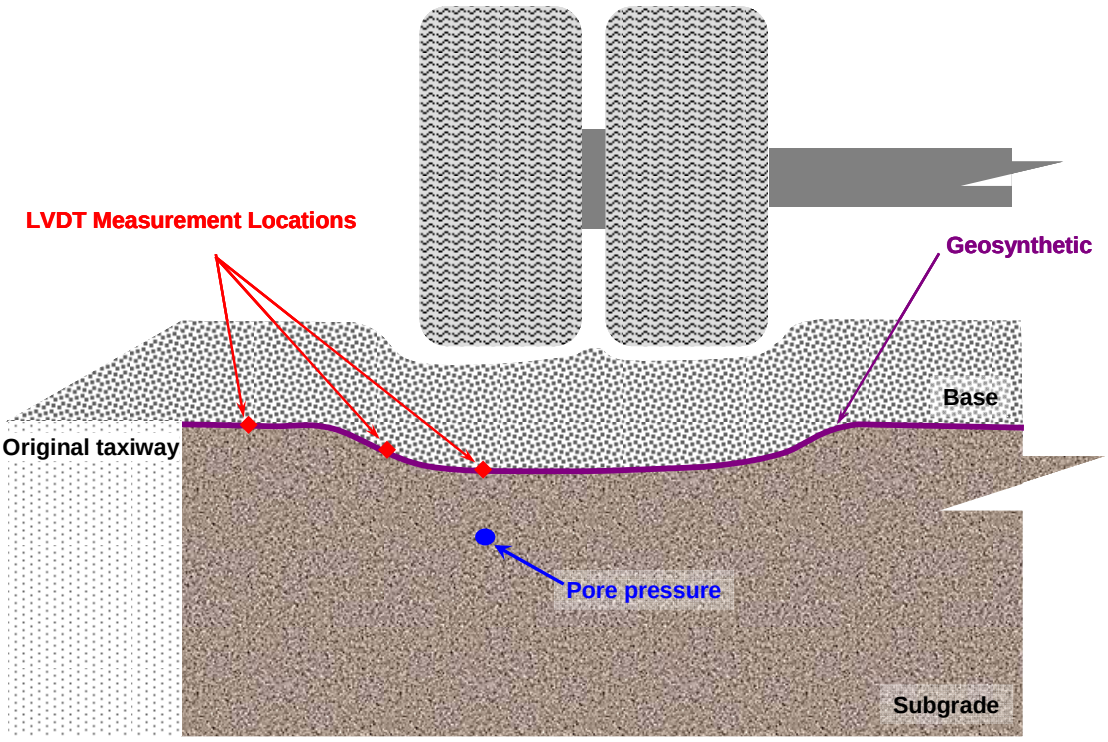

Figure 7. Cross-sectional view of instrumentation layout.

All sensors were mounted in a box that was rigidly attached to the existing pavement away from the edge of the test pit to minimize the influence of the presence of these gages in the rut bowl area (Figure 8). For displacement measurements, lead wires were attached to the geosynthetic using the methodology outlined in Cuelho et al. (2008) to bring the point of measurement on the geosynthetic back to the sensor. The four main steps to installing lead wires on the geosynthetics were: 1) creating a receptacle for the lead wire using a 0.5 mm in diameter

drill bit (not necessary for the geotextiles), 2) threading the 0.4 mm diameter, stainless steel, spring tempered lead wire through the receptacle and securing it, 3) stringing the lead wire through the protective brass tubing, and 4) attaching the lead wire to the LVDT. The protective brass tubing was also run inside small diameter, schedule 80, PVC pipes for two reasons: 1) to provide additional protection of the brass tubes during trafficking and 2) to facilitate plumbing the lead wires into the sensor box. A completed lead wire installation and protective tubing arrangement is provided in Figure 9.

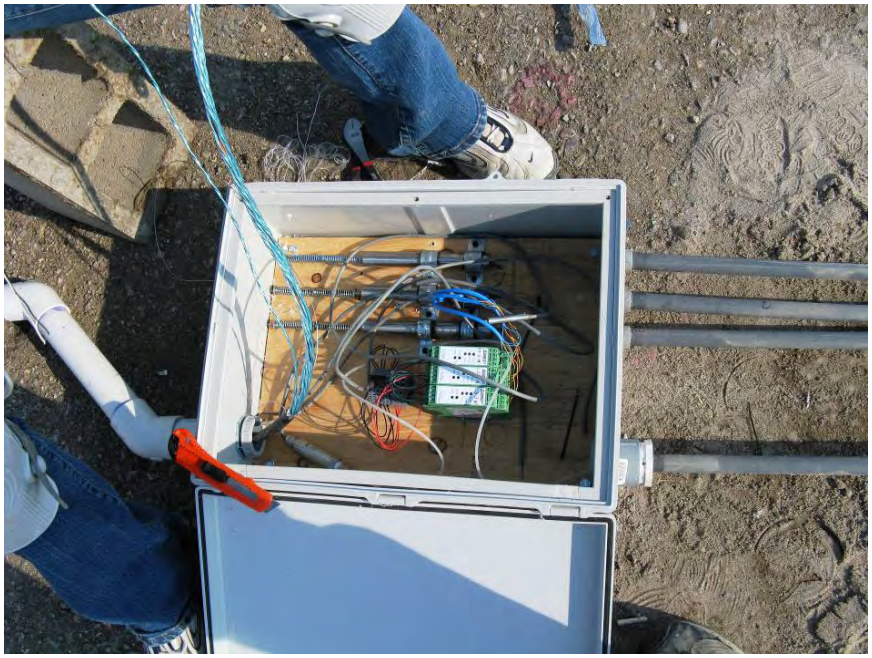

Figure 8. Installation of sensor box.

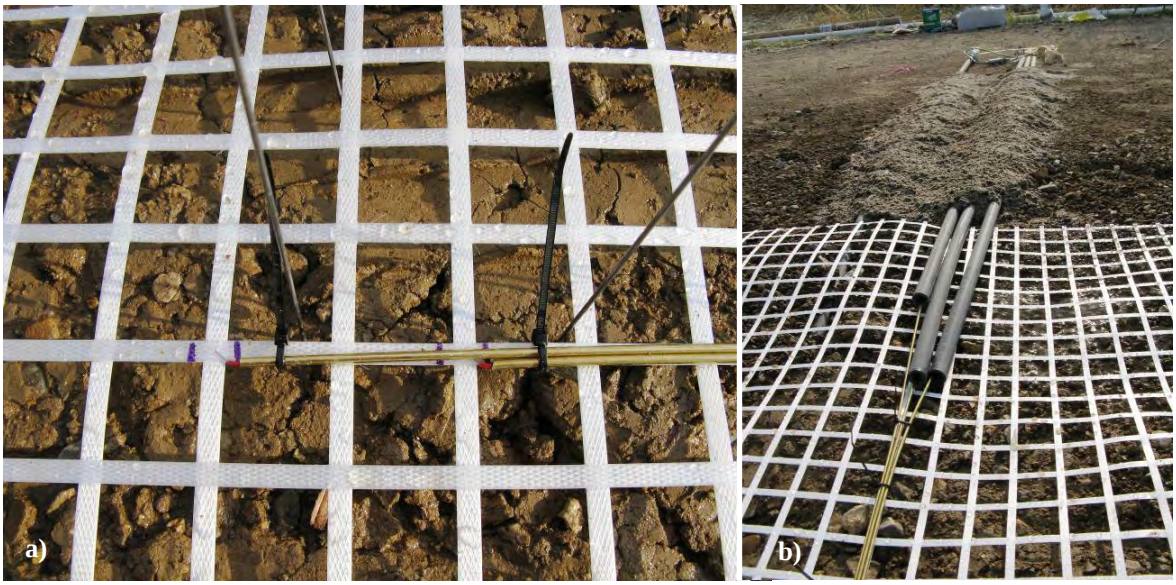

Figure 9. Displacement measurements: a) completed lead wire installation, b) protective tubing.

Pore pressure sensors were housed in the same box as the LVDTs, and 3 meters of high-pressure, flexible plastic tubing was used to extend the point of measurement to a position 15 cm below the top surface of the subgrade directly in the wheel path (Figure 7). Porous ceramic stone tips were attached to the end of the tube using epoxy and the entire system was fully saturated with de-aired water. The stone tips were kept fully saturated at all times prior to their installation. Saturated subgrade soil was carefully packed around each stone during installation to keep air from entering the sensor and tubing arrangement (Figure 10a). As it was placed in the subgrade, saturated soil was gently packed around the sensor to keep it from drying out or allowing air to enter the system during installation and testing (Figure 10b). As with the lead wire installation, small diameter, schedule 80 PVC pipes were used to protect the pressure tubing from damage during construction and trafficking. Using these installation techniques, all pore water pressure sensors were active and in good working condition after construction.

Figure 10. Installation of pore water pressure sensors: a) encapsulating porous stone with saturated subgrade, b) burying in subgrade.

2.6 Data Acquisition and Power Systems

Three independent data acquisition computers were used to store and transfer data during testing. Each data acquisition computer was connected to the sensors of four test sections, as illustrated in Figure 11. Power to the sensors and data acquisition systems were provided by solar panels and batteries installed adjacent to the testing area (Figure 12). All wires to and from the sensors were run through PVC conduit to one of the three metal cabinets to protect them from damage during construction, as well as water and varmints.

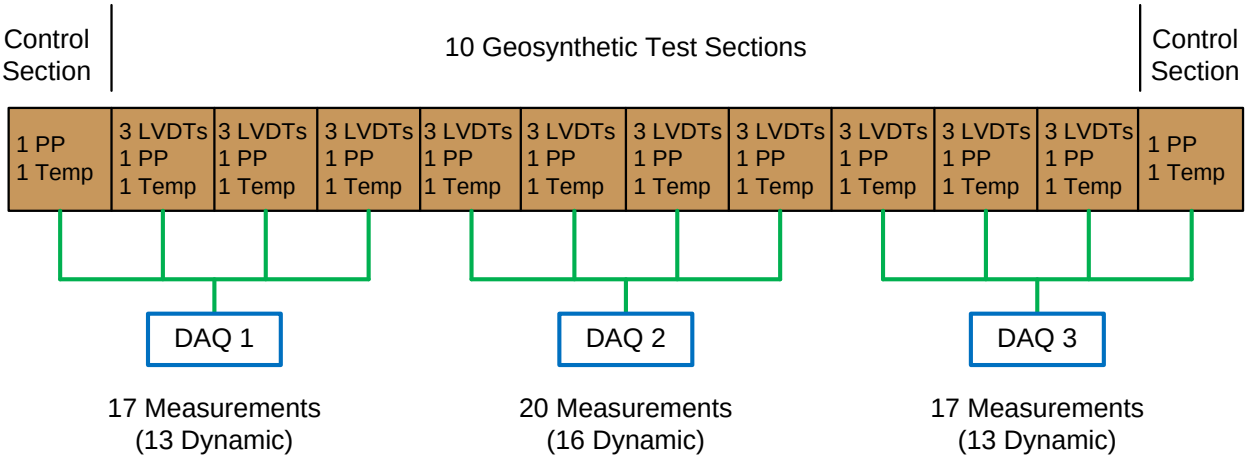

Figure 11. Data acquisition and instrumentation layout.

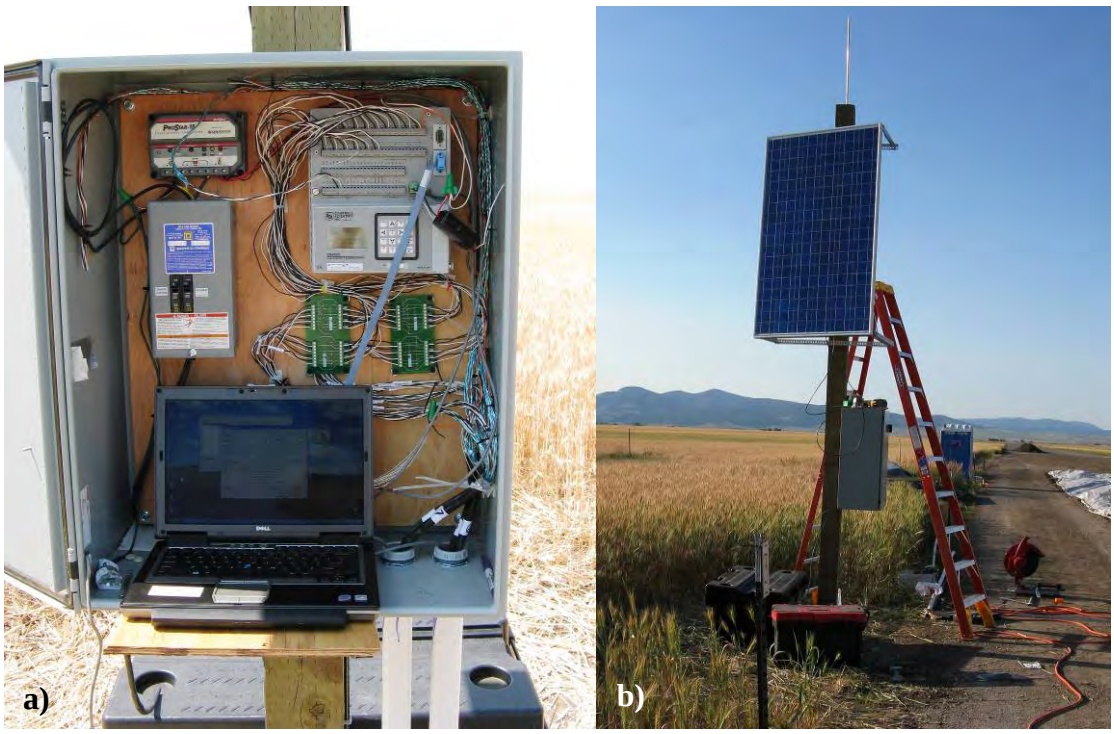

Figure 12. Data acquisition and power systems: a) data acquisition cabinet, b) full system.

3 CONSTRUCTION AND TRAFFICKING

Four main steps were followed to construct the test sections. They are described in more detail in the following subsections:

a. excavation of existing roadbed to make a trench, and installation of a plastic liner,
b. preparation and placement of the artificial subgrade soil,
c. installation of the geosynthetics and instrumentation, and
d. construction of the base course aggregate.

Trafficking of the test sections began approximately two weeks after construction.

3.1 Construction of the Test Pit

The existing pavement, base course and subgrade were removed to create a pit 1 meter deep by 4 meters wide by 195 meters long. Final grading of the test pit that would eventually contain the artificial subgrade is shown in Figure 13. The floor of the test pit was tapered at the ends to facilitate movement of the construction equipment into and out of the pit; the tapered area was not included in the experiment and is in addition to the 195 meters of length. The bottom of the test pit was compacted using a vibratory roller to create a level surface of uniform strength. Density was measured at 12 locations along the length of the test pit using a nuclear densometer at a depth of 100 mm, and the average density of the trench floor was 2159 kg/m^3. All measured densities were relatively uniform, being approximately ±5 percent from the average along the length of the test pit after compaction. After compaction, the entire length of the test pit was lined with a 6-mil plastic liner to help maintain uniform moisture conditions in the artificial subgrade during the experiment (Figure 14). The liner extended past the top of the trench and was secured in place during construction. Another sheet of 6-mil plastic was used as a temporary cover for the surface of the subgrade to minimize moisture loss after its completion and prior to placement of the aggregate base. This top plastic sheet was tied into the underlying sheet to create a tight seal during that time as discussed later.

Figure 13. Final grading of the test pit.

Figure 14. Installation of plastic liner in test pit.

3.2 Preparation and Placement of the Artificial Subgrade

The subgrade was prepared using a motor grader by scalping off portions of the subgrade stockpile and then tilling the material as water was added from a water truck with a spray bar. Once the subgrade was processed to have a uniform water content close to the target value, the material was brought to the trench with a front-end loader operating on the existing taxiway and dumping its load into the trench from the side. A track-driven, skid-steer tractor operating inside the trench was then used to distribute the subgrade evenly into a layer approximately 15 cm thick (Figure 15). Once a significant area was covered in this way (approximately half of the length of the test site), a large roto-tiller attached to a small tractor was used to even out the surface and further mix the soil mass (Figure 16). After tilling, soil samples were taken to determine the average moisture content of the layer. Water was then added using a large water truck (if too low) or the tilled surface was allowed to dry (if too wet).

Figure 15. Delivery and distribution of the artificial subgrade in the test pit.

Figure 16. Mixing the subgrade layer with large roto-tiller.

Compaction was performed with a single cylinder, smooth-drum, vibratory roller (Figure 17). Immediately after compaction, the vane shear device was used to determine in-place shear strength. If the shear strength of the artificial subgrade was not relatively close to the specified limits, two basic remedies were used: 1) shear strength too low—re-till the layer, allow soil to dry, and recompact the soil layer, or 2) shear strength too high—re-till the layer, add water, allow the water to penetrate the tilled soil mass, re-till the soil again, and recompact the soil layer. Altogether, seven layers were necessary to fill the trench (one layer at a time along the entire length of the trench) until the top surface of the subgrade was approximately equal to the original level of the existing pavement. A slight crown was set into the surface of the subgrade so that water from rain or the water truck would not accumulate on the surface.

Figure 17. Compacting subgrade with smooth drum, vibratory roller.

The quality and consistency of the artificially constructed subgrade was mainly monitored using a hand-held vane shear device and moisture content. Between three and nine strength measurements were randomly taken (average of four) at a particular location along the length of the test pit within each layer during construction using the vane shear device (shown in Figure 18). Data was not always collected in every layer at a particular location due to the many construction activities that were ongoing at the site. Multiple measurements taken at a particular position were averaged together into a single value for that location within that layer. These averaged values are plotted by layer for all the test sections in Figure 19. In general, there was more variability in earlier (i.e., lower) layers of the subgrade and less in the upper layers, so data from layers 2 through 5 were removed to show only results from layers 6 and 7 (Figure 20). Vane shear data from the first layer of subgrade was not taken and was therefore not included in the analysis. Moisture content did not correlate well with the vane shear as seen in the plot of moisture content versus vane for all of the field measurements taken during construction of the subgrade (Figure 21). Therefore, moisture content was mainly used to ensure uniform conditions in the subgrade prior to compaction while vane shear was used to monitor and control subgrade strength after compaction.

Figure 18. Field measurement of vane shear (inset is close-up of vane shear device).

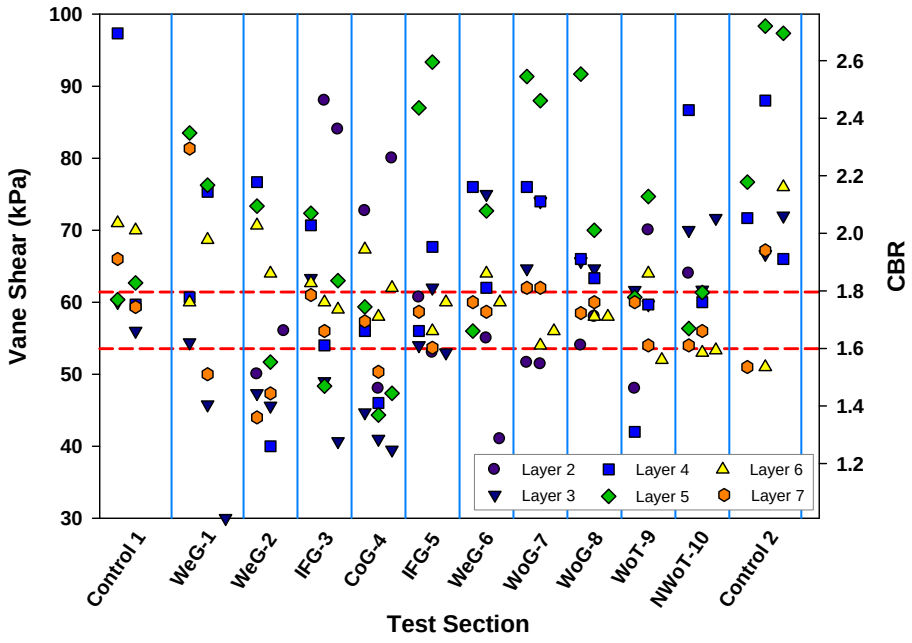

Figure 19. Averaged vane shear strength measurements of the artificial subgrade.

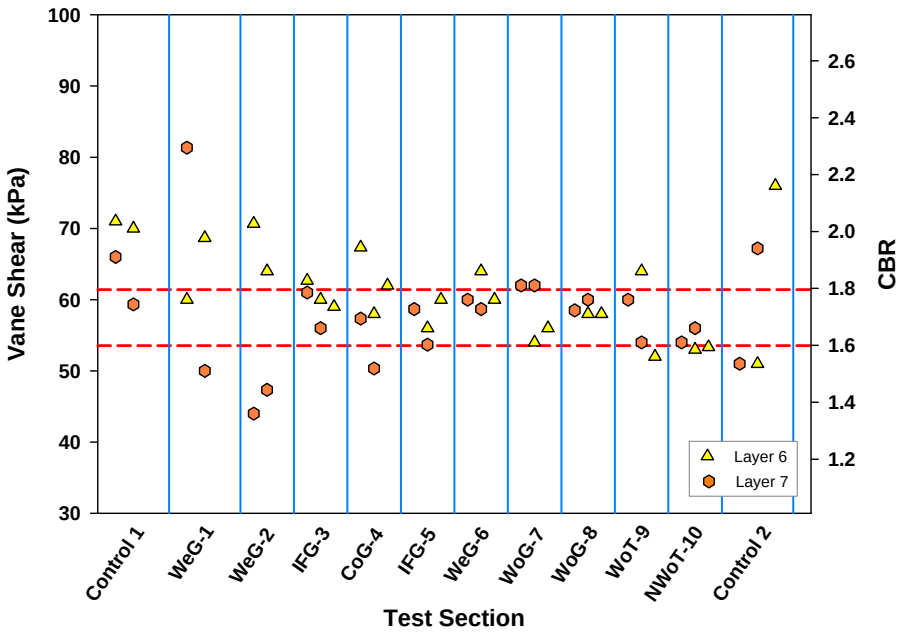

Figure 20. Averaged vane shear strength measurements of upper two layers of the artificial subgrade.

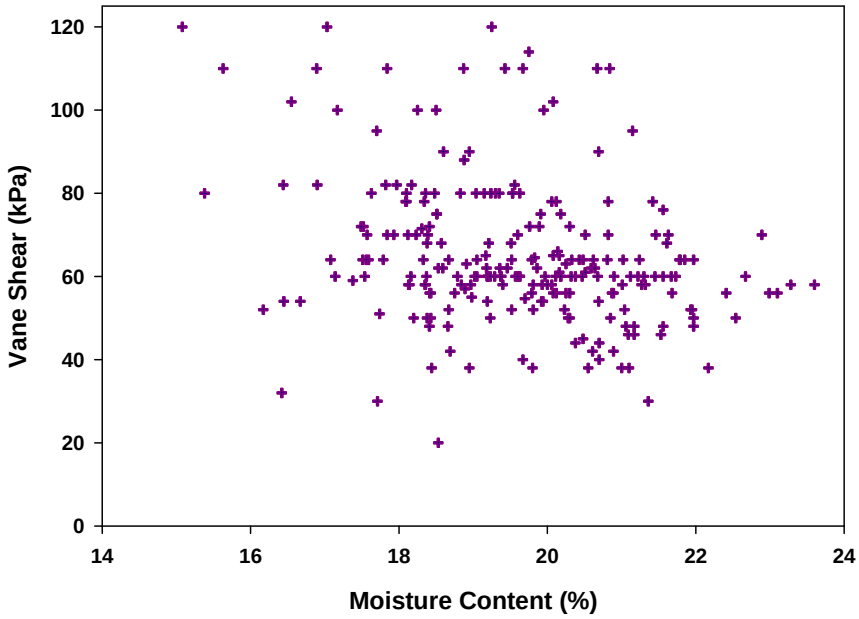

Figure 21. Moisture content versus vane shear from field test sections.

The upper layers of subgrade are responsible for supporting the majority of the load applied during trafficking. Consequently, the strength of the subgrade at the lower depths was less

important than the strength nearer the surface. In order to characterize the subgrade and assign an average value of strength to each test section, a strategy for weighting the strength of the subgrade layers was developed based on Boussinesq elastic stress distribution theory. Influence values can be determined using Boussinesq's theory based on the area of the load applied at the surface and the depth to the point of interest. Knowing that upper layers have more influence on behavior, the percent of the total influence was determined for each layer and was applied to vane shear measurements in those layers.

Weighting factors for subgrade layers 2 through 7 were calculated as the percent of the total influence of each layer using Equation 1, where I_i is the influence value, based on Boussinesq's theory, for a particular layer of subgrade. Values for the weighting factor (n_i) are tabulated in Table 6.

$$n_i = \frac{I_i}{\sum_{i=2}^{7} I_i} \qquad \textbf{Equation 1}$$

Table 6. Weighting Factors for the Artificial Subgrade

Subgrade layer	Depth to Center of Layer (cm)	I_i	n_i
7 (top)	7.5	0.967	0.396
6	22.5	0.650	0.266
5	37.5	0.340	0.139
4	52.5	0.229	0.094
3	67.5	0.150	0.061
2	82.5	0.108	0.044
1	97.5	---	---

The upper three layers of subgrade influenced the weighted average of the shear strength the most (cumulative weight is over 80 percent for these layers), as shown in Table 6. Weighted shear strength values were calculated at various locations along the test pit (Figure 22). Average strength values during construction ranged from 50.5 kPa to 79.3 kPa, which correspond to CBR strengths of 1.52 and 2.25, respectively (calculated using the regression equation in Figure 3).

$$\tau_{weighted} = \frac{\sum_{i=2}^{7} n_i \tau_i}{\sum_{i=2}^{7} n_i} \qquad \textbf{Equation 2}$$

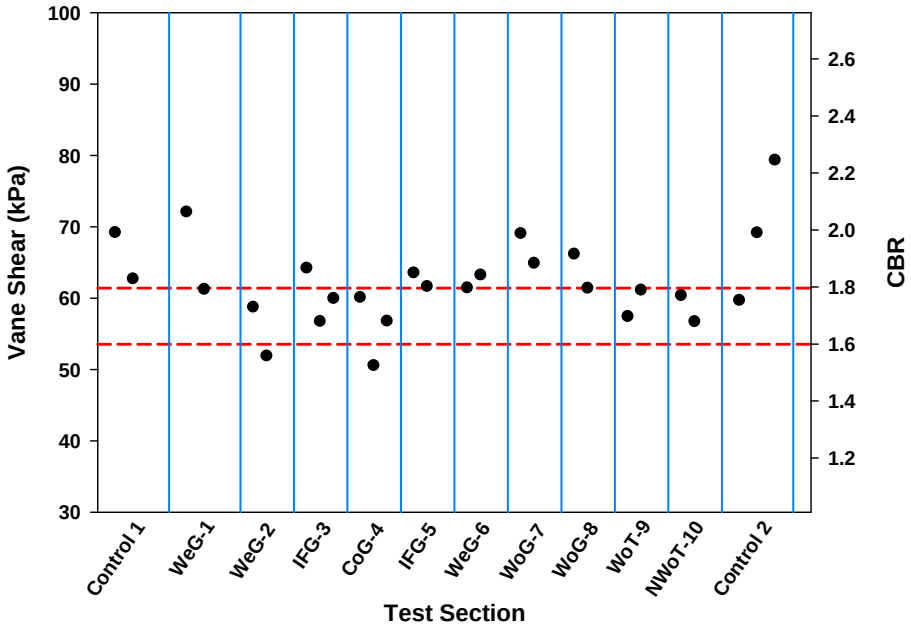

Figure 22. Weighted vane shear strength of the artificial subgrade.

A Kessler Dual Mass Dynamic Cone Penetrometer (DCP) was also used to evaluate the strength of the subgrade after it had been fully constructed (i.e., after placement of all seven layers), despite the fact that the DCP device was not necessarily well suited to evaluate very small differences in soil strength. One to three DCP measurements were made at a single location near the center of each test section to get an indication of the strength of the soil using this method, prior to installation of the base course. DCP results were averaged where multiple measurements were made. Conversion of the DCP information into CBR was achieved using the correlation equation provided by Kessler in the User's Manual, Equation 3. Using this equation and the methodology suggested by Kessler Soils Engineering Products, Inc., CBR was calculated as a function of depth, as shown in Figure 23.

$$CBR = \frac{292}{DCP^{1.12}} \qquad \textbf{Equation 3}$$

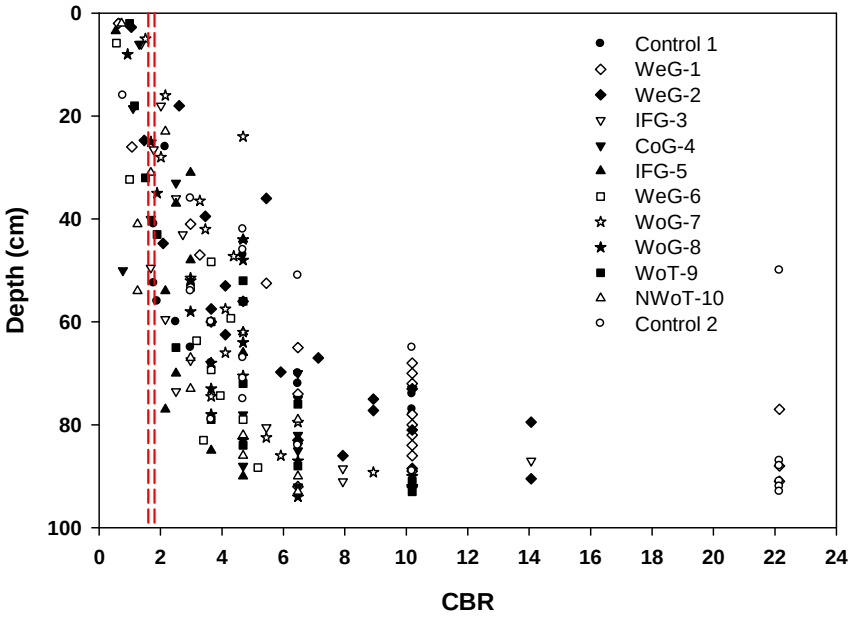

Figure 23. CBR strength of the artificial subgrade from the DCP, as a function of depth.

As in the previous analysis of the vane shear data, a weighted average approach was employed to estimate a single CBR value for each test section using the DCP data. As before, the influence of the load in the subgrade as a function of depth was calculated using Boussinesq's theory. Weighting factors for the subgrade were calculated as the percent of the total influence at each point using Equation 4, where n_z is the weighting factor at depth z beneath the surface of the subgrade, I_z is the influence factor at depth z, and d_{tot} is the total number of drops to reach depth z. Many of the CBR values were much higher than those estimated from the vane shear data, especially at lower depths; therefore, values of CBR greater than 7 (deemed unreasonably high) were not used in the weighted average calculation. The DCP device does not account for overburden, which likely contributes to the increased CBR with depth. The weighted CBR was calculated using Equation 5. Using this methodology, a weighted CBR value was calculated for each test section, as shown in Figure 24 along with the weighted vane shear results. Note that, overall, the CBR values calculated using this methodology are still higher than expected. This is mainly because the correlation equation tended to over-predict the CBR, but to a lesser degree may also be from higher than expected CBR values at lower depths which still influenced the overall weighted average CBR. In general, however, the majority of the CBR values are close to one another, indicating uniformity within the artificial subgrade.

$$n_z = \frac{I_z}{\sum_{z=1}^{d_{tot}} I_z}$$

Equation 4

$$CBR_{weighted} = \frac{\sum_{z=1}^{d_{tot}} n_z CBR_z}{\sum_{z=1}^{d_{tot}} n_z}$$ **Equation 5**

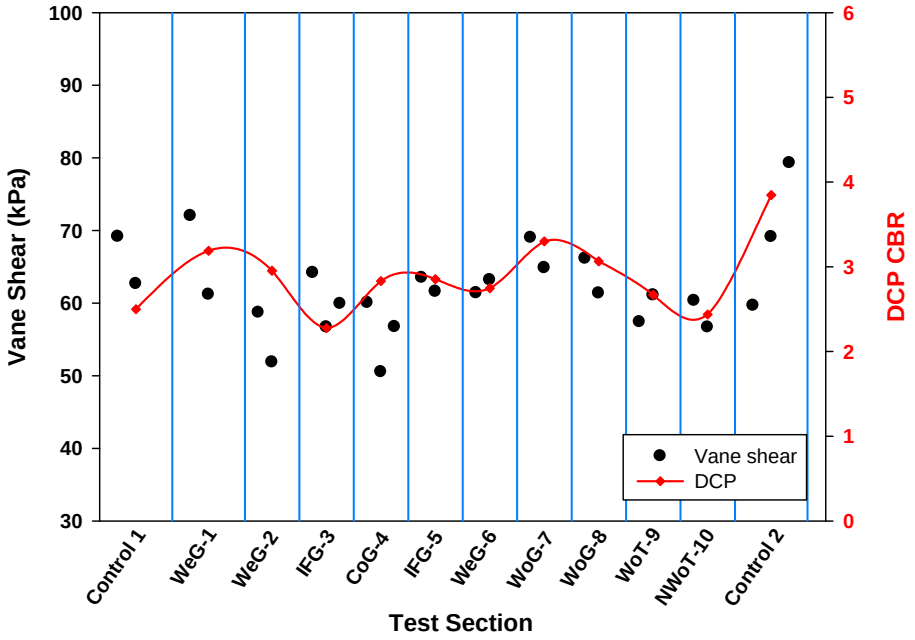

Figure 24. Weighted CBR strength of the artificial subgrade from the DCP and vane shear.

Overall, strength characteristics as determined by the vane shear and DCP devices were similar between test sections prior to installing the base course aggregate and applying traffic loads; however the predicted strengths determined using the DCP device were greater than those obtained using the vane shear device. Data obtained using both of these methodologies are useful; therefore, data was combined together to summarize the overall strength of each of the test sections. This was accomplished by applying a weighting factor to the CBR strengths from the DCP device so that it was in the range of values predicted by the vane shear. A weighting factor of 0.63 was used to do this. Vane shear strength values were converted to CBR using the best fit linear equation from Figure 3. All subgrade strength values for a particular test section were averaged together to create a composite strength value to generally describe the strength of the artificial subgrade, as shown in Figure 25.

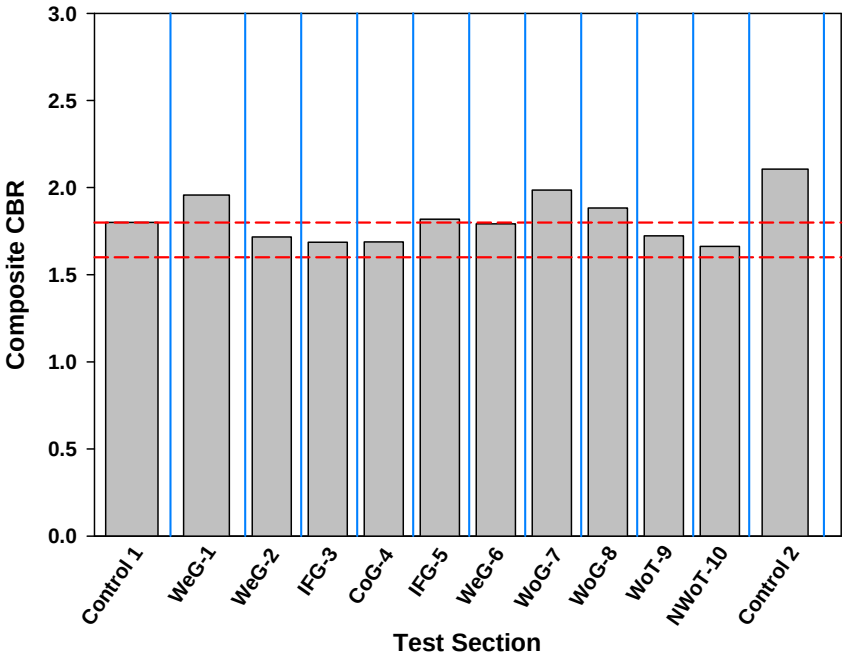

Figure 25. Composite subgrade strength after construction determined from vane shear and DCP.

3.3 Installation of Geosynthetics

Geosynthetics were installed in each section by carefully rolling them out in the direction of traffic. Any wrinkles were removed by gently pulling on the end of the material (Figure 26). The edges of the geosynthetic were not tensioned or staked in place; however, grade stakes were used during the installation of the base course. Instrumentation was installed on the geosynthetic after they were positioned. As indicated in Table 4, the widths of the geosynthetics varied between products; therefore, they were centered on the subgrade so that the vehicle would be centered on the material during trafficking and properly positioned in relation to the displacement and pore pressure sensors. Each geosynthetic test section was approximately 15 meters long, with the exception of the two control sections (Control 1 and Control 2) and the first geosynthetic test section (WeG-1), which were approximately 20 meters long. The geosynthetics in adjacent test sections overlapped one another by approximately 1 meter such that "upstream" geosynthetics overlapped "downstream" geosynthetics (i.e., WeG-1 was on top of WeG-2, WeG-2 was on top of IFG-3, etc.).

Figure 26. Installation of geosynthetics.

3.4 Construction of the Base Course Layer

The base course aggregate was delivered and stockpiled along the abandoned taxiway directly adjacent to the test sections so that water could be mixed into it prior to compaction. After placement of the geosynthetics, installation of the instrumentation and preparation of the base course, a single layer of base course aggregate 20 cm thick was placed on top of the geosynthetics from the side using a track-driven, skid-steer tractor (Figure 27). The installation of the base course aggregate was carefully monitored to prevent damage to the geosynthetics during construction. Final grading of the surface of the base course was done from the side using a road grader with an extended blade attachment so that the test sections would be in a virgin state (i.e., it had experienced no trafficking from construction equipment) prior to trafficking (Figure 28). A slight crown that matched the crown in the subgrade was set into the base course so that water did not accumulate on the finished surface. A ramp was built at both ends of the test site to allow the test vehicle to transition smoothly between the existing taxiway and the test area using the base course aggregate.

The same single-drum vibratory roller used to construct the artificial subgrade was used to compact the base aggregate. Three passes of the compactor were necessary to reach at least 90 percent of the maximum dry density (determined according to AASHTO T-180, modified Proctor) within of the test sections, as measured using a nuclear densometer (Figure 29). The thickness of the base material was monitored using survey equipment at the beginning, center and ends of each test section. The overall average depth of the base course was 20.1 cm after

compaction. Survey measurements of the finished subgrade and finished base course were made to determine the thickness of the base along the test sections, which is illustrated in Figure 30. The base course varied between a maximum thickness of 22.3 cm, minimum thickness of 18.0 cm and had a standard deviation of 1.4 cm.

Figure 27. Placement of base course aggregate.

Figure 28. Final grading of the base course surface.

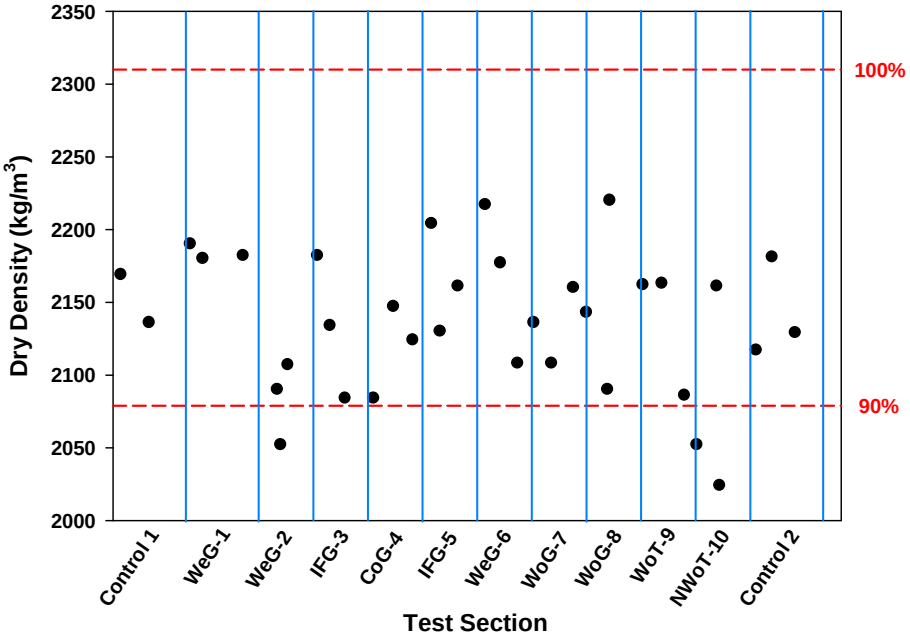

Figure 29. In-place density of base course aggregate after compaction.

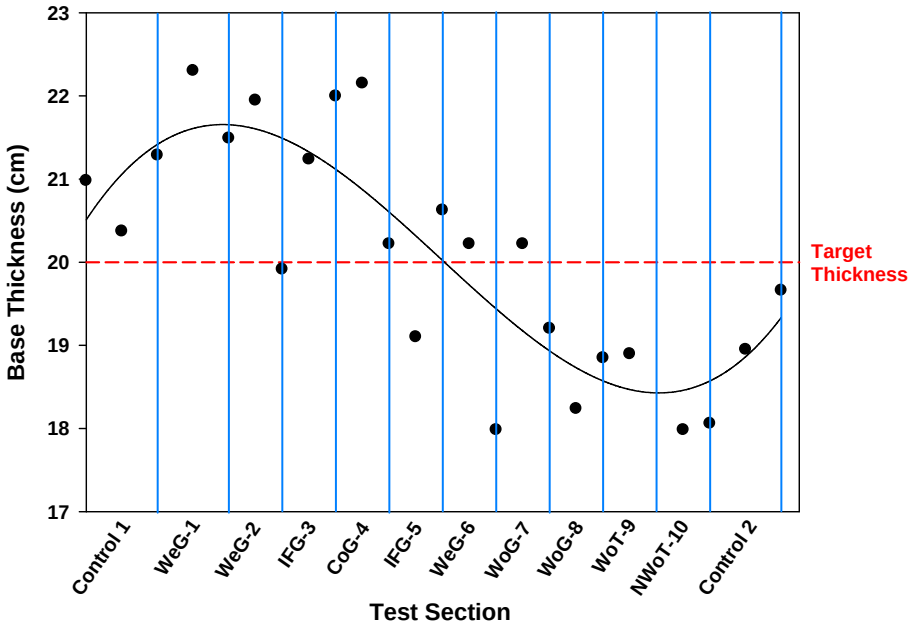

Figure 30. In-place thickness of the base course aggregate after compaction.

3.5 Trafficking

Trafficking was accomplished using a fully loaded three-axle dump truck. A photo of the truck and the associated weights and dimensions of the vehicle are shown in Figure 31 and Figure 32, respectively. The bed of the truck was filled with concrete blocks, which were carefully loaded to ensure similar applied loads on each tire (tire pressures were approximately 690 kPa). Individual axles and wheels were weighed using a calibrated scale at a nearby gravel pit. Lines were painted on the gravel surface prior to loading so that the truck was properly positioned on the test sections (Figure 33), that is, centered over the geosynthetics. The truck traversed the test sections at approximately 15 kph beginning at the first control section (Control 1) through the geosynthetic stabilized sections and exiting out of the second control section (Control 2).

Figure 31. Side view of three-axle dump truck used for trafficking.

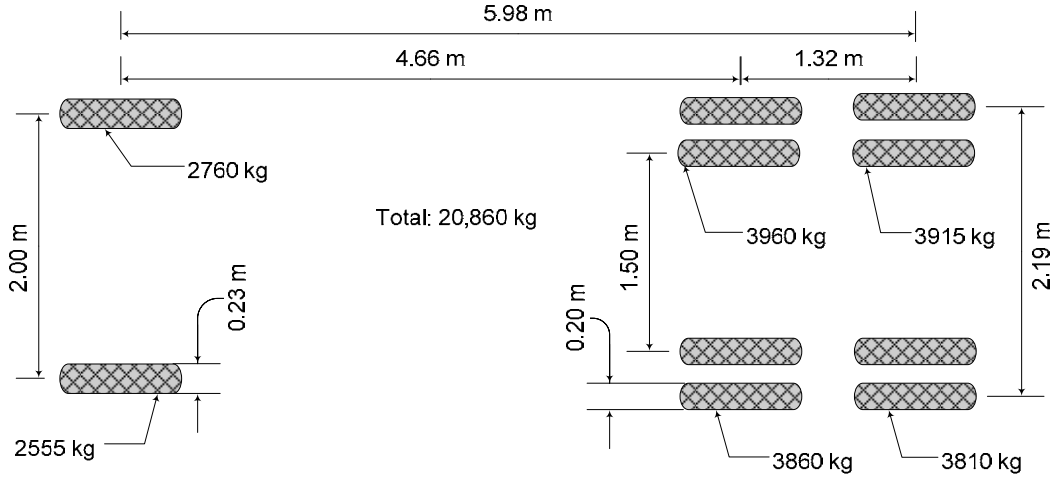

Figure 32. Axle dimensions and associated weights of test vehicle.

Figure 33. Full view of test area prior to trafficking.

Trafficking was applied to the test sections until each of the individual test sections reached an average of 100 mm of rut as measured by changes in elevation over time. Test sections that failed early were repaired to allow the truck to pass over them without getting stuck. This repair was accomplished by adding extra base course aggregate in the rutted areas and smoothing the area out with a skid-steer tractor.

4 POST-TRAFFICKING FORENSIC INVESTIGATIONS

Post-trafficking, forensic investigations were conducted to evaluate damage to the geosynthetic from trafficking, as well as, to re-evaluate pertinent soil strength characteristics. Forensic evaluations were located in areas that had experienced approximately the same rutting since a major component of this research was to evaluate damage to the geosynthetic due to trafficking. Therefore, elevation rut data was evaluated to find an area within each test section that had experienced approximately 100 mm average rut. Three of the ten geosynthetic-stabilized test sections failed earlier than the rest which made it necessary to fill in the ruts with gravel to facilitate trafficking. In those cases, areas that had experienced an average of 100 mm of rut prior to filling were selected for forensic investigation. The additional gravel added as part of this process, increased the overall strength of these sections so that further truck passes would induce much less damage in these geosynthetics as the remaining sections were trafficked. An area 1.5 meters wide (in the direction of traffic) and 4 meters long was selected in each of the test sections, including the control test sections. Transverse profiles of the edges of these areas were taken prior to and during excavation to evaluate rut shapes and layer thicknesses.

Excavation of the base course was accomplished using a large vacuum truck and a high-flow compressed air nozzle to minimize disturbance and damage of the geosynthetic (Figure 34a). After exposing the entire area of geosynthetics, they were carefully removed to analyze damage to junctions and rib integrity and continuity. Post trafficking DCP measurements were taken in the excavated area prior to removal of the subgrade. The subgrade was then removed from these areas (Figure 34b) to comprehensively evaluate soil mixing between the subgrade and base course in the rutted areas, soil shear strength using the vane shear, soil moisture contents, as well as provide a general evaluation of the rutted area.

4.1 Post-Trafficking Assessment of Geosynthetics

Approximately 6 square meters of geosynthetic were carefully extracted from each test section to visually quantify damage caused by construction and traffic. Damage was quantified in three main ways depending on the material structural composition: 1) damage to junctions in welded and woven grid products, 2) damage to ribs in all grids and 3) a qualitative assessment of continuity in the cross-machine direction for the integrally-formed geogrids and the two textile products. This approach was taken because of the manner in which the various products failed, as discussed in more detail below.

Figure 34. Forensic investigations: a) air and vacuum removal of base course, b) excavation of subgrade.

4.1.1 Damage Assessment of the Welded Geogrids

Junction damage was assessed in the welded geogrid materials (WeG-1, WeG-2, CoG-4, and WeG-6) test sections. Each junction was scrutinized to determine how "intact" it was. The methodology used to evaluate each junction assigned one of four values (ranging from 0 to 3) to each junction that corresponded to how intact it was (refer to Table 7). Junctions that were noticeably damaged during excavation or transport were marked as such and not included in the analysis. The junctions on the welded grids were the most susceptible to damage during excavation; therefore, a section of geosynthetic was excavated from each of the welded geogrid test sections from the bottom up to reduce the risk of damage during the excavation process to assess this type of damage. This process is referred to as "reverse excavation" and is discussed in greater detail below. The score was accumulated for each row of junctions in the machine direction of the material (the direction of traffic) and across the entire width of the material (cross-machine direction). The overall level of intactness was calculated from the individual scores using Equation 6, where n_0, n_1, n_2, and n_3, correspond to the number of junctions that contained the values 0, 1, 2 and 3, respectively, and n_{tot} is the total number of junctions evaluated along a particular line.

Table 7. Scoring Methodology for Junction Damage Assessment in the Welded Geogrids

Percent Intact	Score	Damage Description
100	3	No visible damage
50-99	2	More than half of the junction is welded
1-49	1	Less than half of the junction is welded
0	0	Junction is completely separated

$$Intactness = \left[\frac{n_0 \cdot 0 + n_1 \cdot 1 + n_2 \cdot 2 + n_3 \cdot 3}{n_{tot} \cdot 3} \right] * 100\% \qquad \textbf{Equation 6}$$

The majority of junction damage was near the vicinity of the wheel tracks, as shown in Figure 35. Average values of junction damage were calculated using the entire area of extracted geosynthetic, and are tabulated in Table 8. The WeG-2 and WeG-6 products sustained similar damage, and the CoG-4 and WeG-1 products sustained the most junction damage of the welded geogrids.

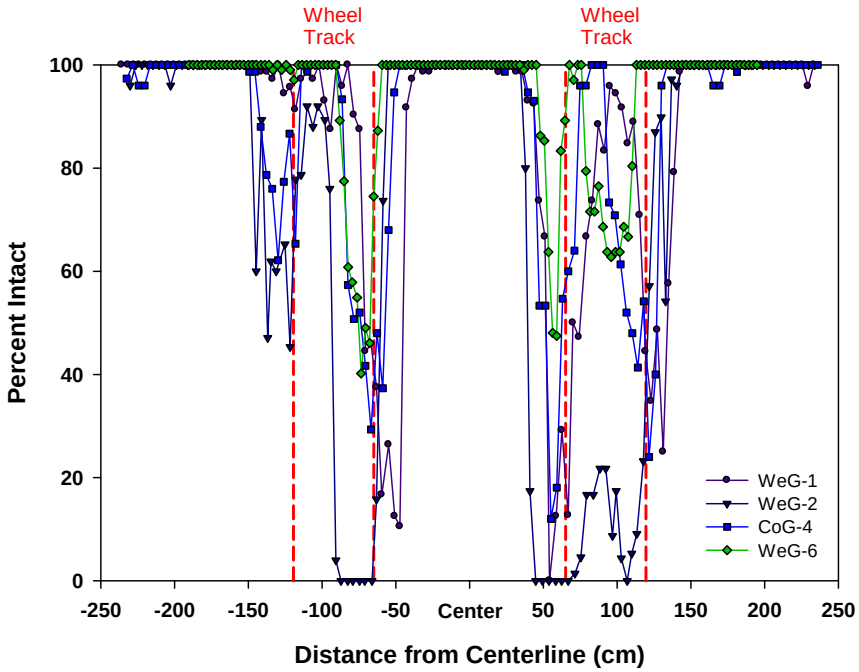

Figure 35. Junction damage in the cross-machine direction of the welded geogrids.

Table 8. Average Junction Damage for Welded Geogrids

Test Section	Percent Intact
WeG-1	72.7
WeG-2	86.7
CoG-4	73.6
WeG-6	87.8

As previously mentioned, each of the welded geogrid products was excavated from underneath to further minimize damage to the junctions during the excavation process as a way to assess excavation-induced damage. These excavations were done from the side in the trench that was created from the excavator during the forensic investigations. Hand tools were carefully used to remove the subgrade from under the geosynthetics while the base course remained on top (Figure 36a and b). This methodology was intended to keep the junctions from moving relative to one another during the excavation process. After all the supporting subgrade was removed, the base aggregate was carefully removed from the top (Figure 36c) by hand until the entire geosynthetic in the wheel path was freely hanging over the excavated area (Figure 36d). Finally, the geosynthetic was cut free and analyzed for junction and rib damage. Junction damage of the wheel path areas of the reverse excavations are compared to damage within the wheel path areas of the standard excavations (Table 9 and Figure 37). In general, the standard excavation method produced similar results to the reverse excavation method, and differences are thought to be within the accuracy of these assessments.

Figure 36. Pictorial overview of the reverse excavation method: a) excavating underneath the geosynthetic, b) subgrade fully removed and geosynthetic exposed, c) removal of the base from the top and d) fully exposed geosynthetic.

Table 9. Average Junction Damage for Standard and Reverse Excavated, Welded Geogrids

Test Section	Percent Intact	
	Standard	Reverse
WeG-1	53.7	56.3
WeG-2	87.8	73.2
CoG-4	46.3	43.9
WeG-6	76.5	86.0

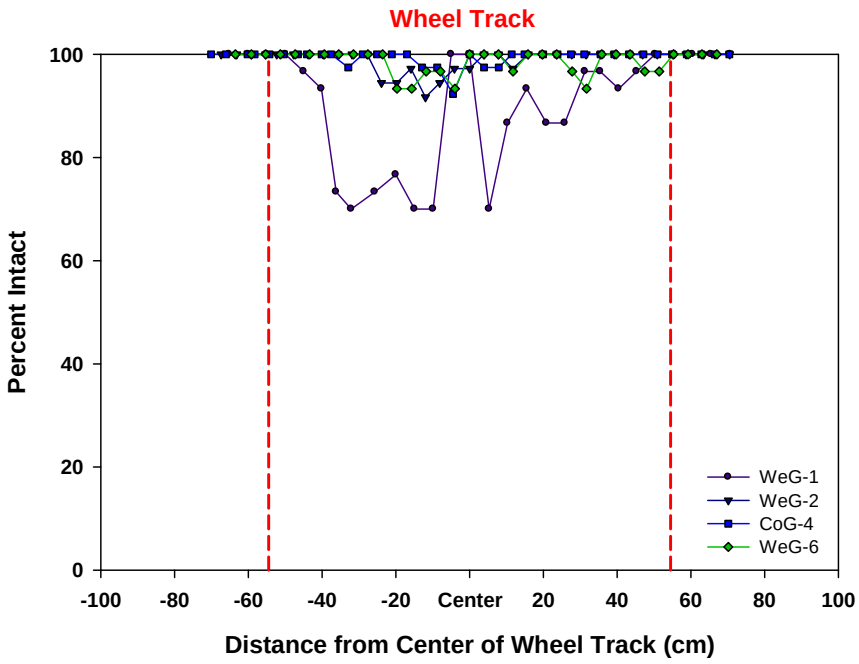

Figure 37. Junction damage in the reverse excavated, welded geogrids.

Rib damage was also assessed in the welded geogrid products. Machine and cross-machine ribs were scrutinized to evaluate how intact they were. Most of the damage sustained in the geogrids was in the cross-machine direction because of the tensile stresses induced in the material from ruts formed during trafficking. The scoring methodology was similar to the junction assessment, as described in Table 10. Ribs that were damaged during excavation or transport were not included in the analysis. Rib damage in the cross-machine direction was assessed at positions of the ribs oriented in the machine direction so that the entire width of the material was evaluated. Overall rib intactness was calculated from the individual scores using Equation 6, where n_0, n_1, n_2, and n_3, correspond to the number of rib segments that contained the values 0, 1, 2 and 3, respectively, and n_{tot} is the total number or rib segments evaluated along a particular line.

Table 10. Scoring Methodology for Rib Damage Assessment

% Intact	Score	Damage Description
100	3	No visible damage
50-99	2	More than half of the rib is intact
1-49	1	Less than half of the rib is intact
0	0	Rib is completely broken

Similar to the junction damage results, the majority of the rib damage was sustained in the wheel track areas, as shown in Figure 38. Average rib damage is tabulated in Table 11. Average rib damage in these products was similar and very low. The WeG-1 geogrid had the highest damage (6.9%), but the majority of the damage was from ribs in the cross-machine direction that were cracked along their length but not broken across their width (scored as a 2), as shown in Figure 39. Outside of the WeG-1 geogrid, the remaining welded geogrids were mostly intact with, again, most of the damage occurring in the wheel paths, and that damage generally occurred randomly.

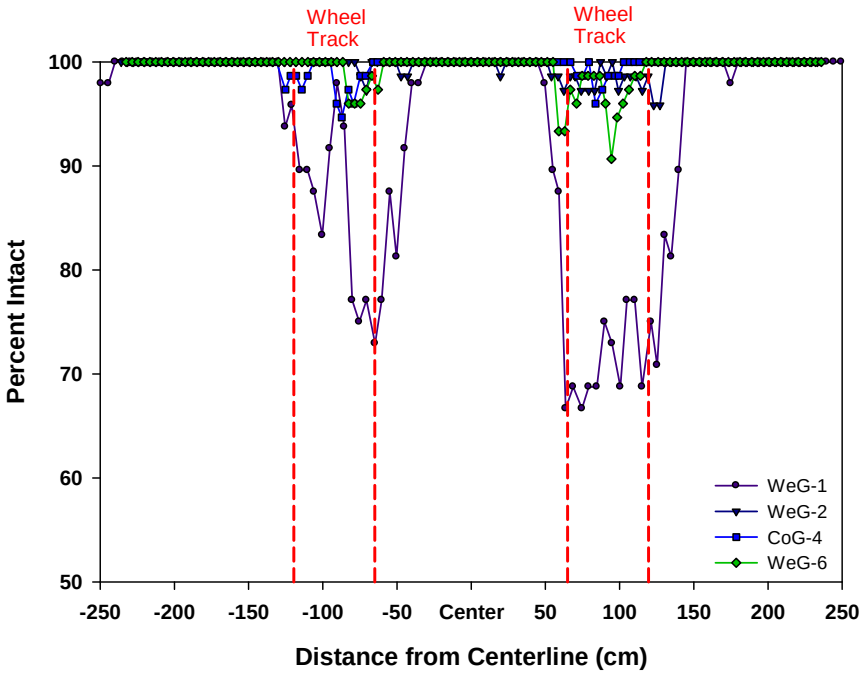

Figure 38. Rib damage in the cross-machine direction of the welded geogrids.

Table 11. Average Rib Damage for Welded Geogrids

Test Section	Percent Intact
WeG-1	93.1
WeG-2	99.6
CoG-4	99.7
WeG-6	99.4

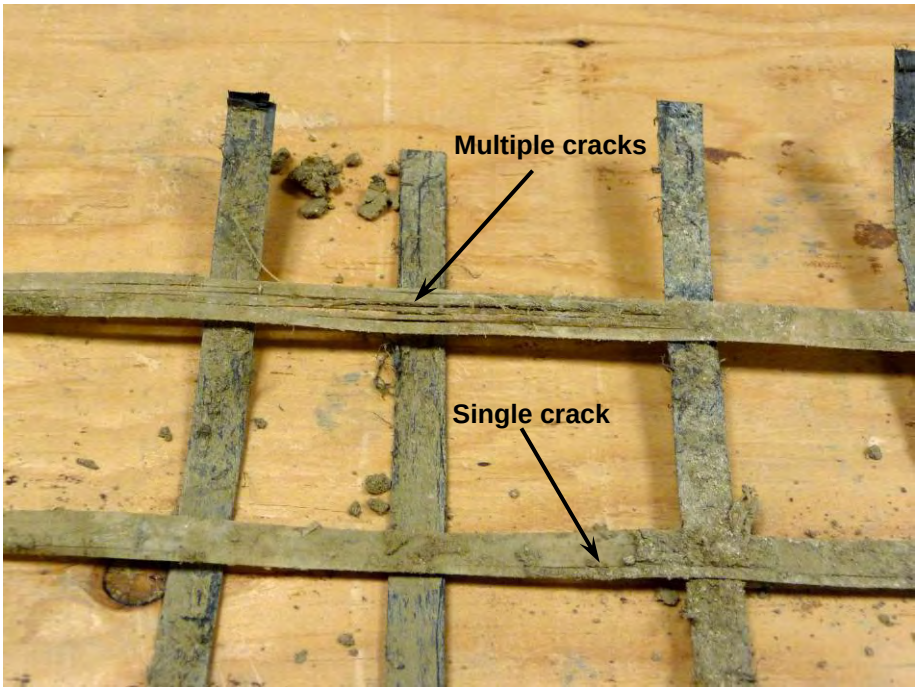

Figure 39. Example of damaged cross-machine members of WeG-1 geogrid.

4.1.2 Damage Assessment of the Woven Geogrids

Damage in the woven geogrid products (WoG-7 and WoG-8) was assessed using the same methodology as the welded products; however, the junction damage that manifested itself in these geogrids was somewhat different. Because of the woven structure, full separation of the junction was rare; however, individual ribs at the junctions were able to move independently of one another. The scoring methodology used for assessing junction damage in the woven geogrids is summarized in Table 12, and the overall intactness was calculated using Equation 6.

Table 12. Scoring Methodology for Junction Damage Assessment in the Woven Geogrids

Percent Intact	Score	Damage Description
100	3	No visible damage
50-99	2	Cross members are somewhat independent
1-49	1	Cross members are mostly independent
0	0	Cross members are totally independent

Similar to the welded products, the majority of the junction damage was near the vicinity of the wheel paths, as shown in Figure 40. Average values of the junction damage differed significantly between the WoG-7 and WoG-8 geogrids, being 93.2 and 67.6 percent intact, respectively.

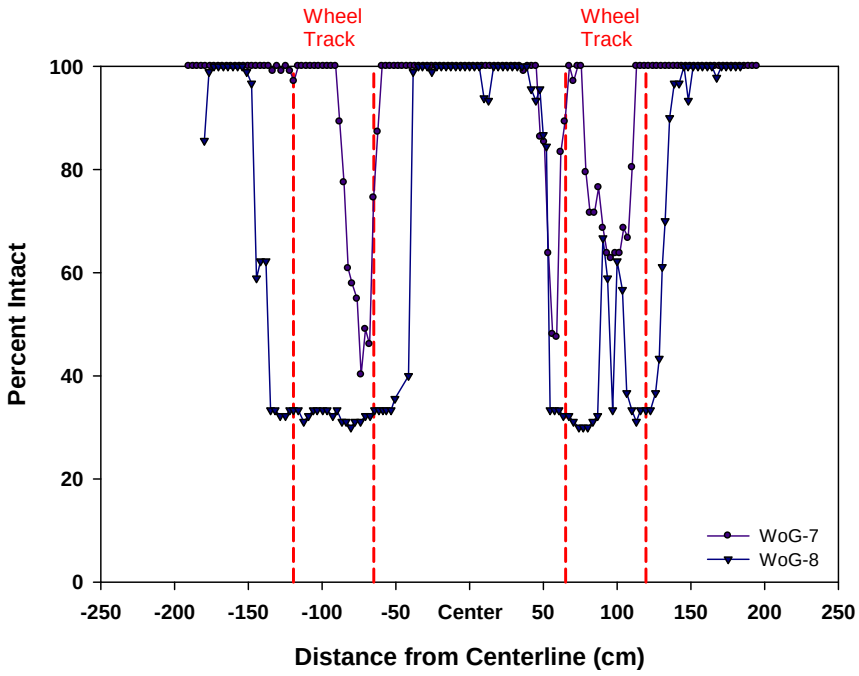

Figure 40. Junction damage in the cross-machine direction of the woven geogrids.

Rib damage in the woven geogrids was also assessed in the same way as the welded products (refer to Table 10 and Equation 6). Machine and cross-machine ribs were scrutinized to evaluate how intact they were. Very little rib damage was sustained in the woven geogrids; the WoG-7 and WoG-8 test sections were 99.9 and 99.7 percent intact, respectively.

4.1.3 Damage Assessment of the Integrally-Formed Geogrids

The two integrally-formed geogrids were not assessed in the same way as the welded and woven grids because their structural configuration and mode of failure differed significantly from the other geogrids. The welded and woven geogrids contained minimal broken and damaged ribs (as discussed in the previous sections), but sections IFG-3 and IFG-5 experienced failure by rupture along a line parallel to the roadway alignment and generally through the middle of a machine-direction rib (Figure 41). Test section IFG-3 experienced less rupture damage than the IFG-5 section, likely due to its higher tensile strength. The extracted IFG-5 sample was observed to have completely ruptured in both wheel tracks, while the IFG-3 sample was approximately 90 percent ruptured in one wheel path and fully ruptured in the other within the excavated areas. Rupture failure in both of these geogrids significantly limited their ability to carry load in the cross-machine direction, which consequently reduced their ability to stabilize the weak subgrade soils during trafficking.

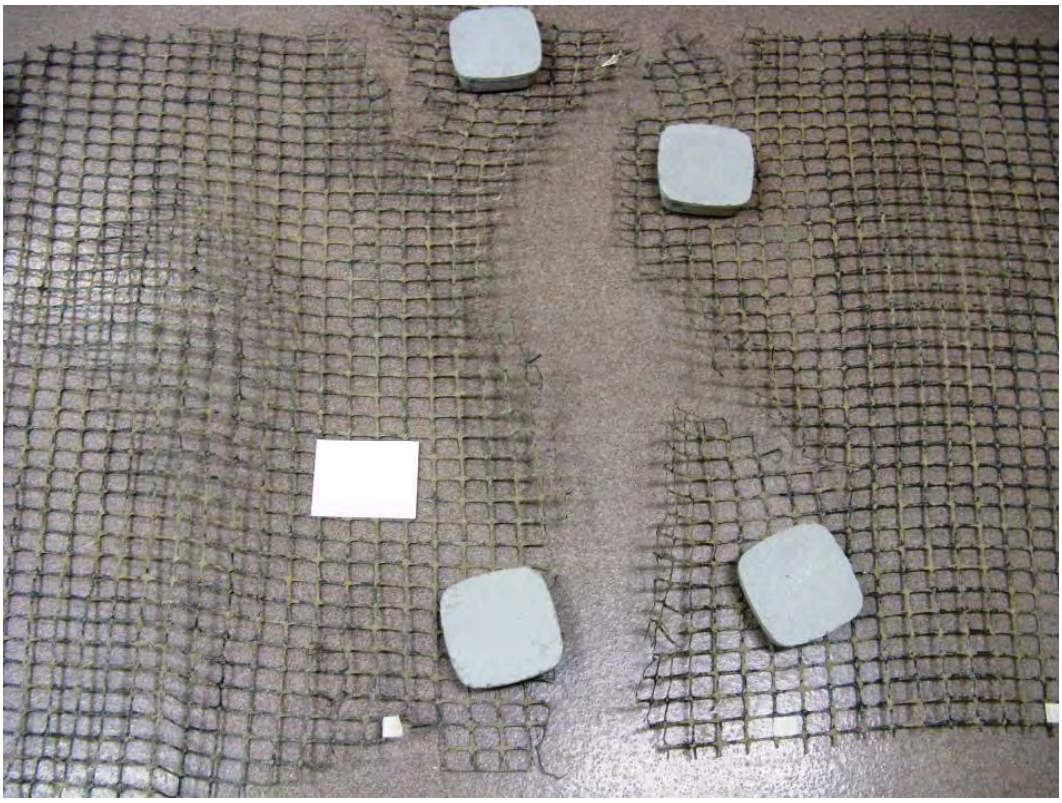

Figure 41. Example of rupture failure in wheel path of the IFG-5 geogrid.

4.1.4 Damage Assessment of the Geotextiles

The two geotextile products sustained very little damage during construction and trafficking, having only minor abrasions. The woven geotextile (WoT-9) was the second narrowest product (3.81 m wide), and it was noticed during trafficking that portions of the textile outside of the rut bowl were pulling out (Figure 42). This pullout failure did not allow the material to mobilize its tensile strength in the cross-machine direction and most likely contributed to reduced performance overall.

Figure 42. Pullout failure of the WoT-9 geotextile.

4.1.5 General Observations

All of the geosynthetics that were extracted from the test area were distorted in the rut bowl area due to the torsion of the truck tire as it propelled its way along the test site (Figure 43). Movement of the geosynthetics was north as the truck travelled south across the test site. This distortion was measured using a straight rod to qualitatively evaluate the severity of this movement between the different products. Table 13 summarizes the horizontal distance that the geosynthetic moved near the center of the rut as compared to the undistorted members outside of the rut bowl. This effect was not measured in the IFG-5 test section because the damage to the geosynthetic was too severe. This effect was also not measured in the NWoT-10 test section because there were no visible markers on the geosynthetic by which these measurements could be made.

Figure 43. Example of horizontal distortion of a geosynthetic due to trafficking.

Table 13. Summary of Horizontal Distortion of the Geosynthetics Due to Trafficking

Geosynthetic Test Section	Horizontal Displacement (cm)
Control 1	N/A
WeG-1	7.0
WeG-2	5.1
IFG-3	7.9
CoG-4	7.6
IFG-5	Not measured
WeG-6	6.4
WoG-7	7.9
WoG-8	8.4
WoT-9	9.2
NWoT-10	Not measured
Control 2	N/A

4.2 Post-Trafficking Assessment of Subgrade Soils and Base Aggregate

After trafficking, three measurements of subgrade strength were taken using the DCP device in the excavated areas prior to removal of the subgrade. The subgrade was then removed from these areas to also evaluate soil shear strength using the vane shear. In addition, soil moisture contents as well as mixing between the subgrade and base course in the rutted areas were also evaluated.

DCP measurements were made in each of the wheel paths and in the center of the areas where the base course was removed, within each test section. Horizontal vane shear measurements and corresponding moisture contents were taken at 10, 20, 40 and 60 cm below the subgrade/base course interface in each of the wheel paths and the center on each side of the excavated trench for a total of six measurements at each depth. The three DCP measurements were weighted and averaged together to form a single value for each test section using the same methodology described in Section 3.2 of this report. Overall, the post-trafficking subgrade strength from the DCP (average CBR = 2.90) were more similar to one another and did not change dramatically from the pre-trafficking strength (average CBR = 2.88), as shown in Figure 44. In contrast, however, the post-trafficking subgrade strength from the vane shear (average CBR = 1.29) measured using the vane shear was significantly lower than the pre-trafficking subgrade strength (average CBR = 1.82), as shown in Figure 45. As discussed in Section 5.4, this decrease is due in part to an increase in pore water pressure during trafficking. Overall, subgrade strengths were relatively close to the specified ranges, thus making differences between test sections relatively small. Figure 46 shows a plot of the moisture content versus the vane shear strength for all the corresponding measurements taken during construction and the post-trafficking excavations.

As previously noted, the predicted strengths determined using the DCP device were greater than those obtained using the vane shear device. Like before, the data obtained using both of these methodologies were combined together to summarize the overall strength of each of the test sections. A weighting factor of 0.45 was used to adjust the CBR strengths from the DCP device so that it was in the range of values predicted by the vane shear. All subgrade strength values for a particular test section were averaged together to create a composite strength value to generally describe the strength of the artificial subgrade, as shown in Figure 47.

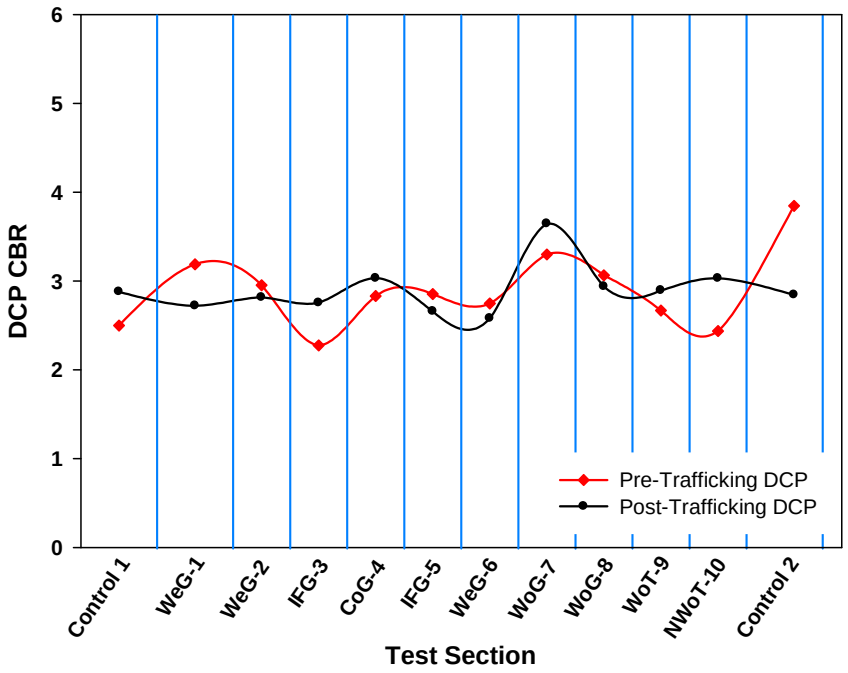

Figure 44. Pre- and post-trafficking, weighted, subgrade strength values from the DCP device.

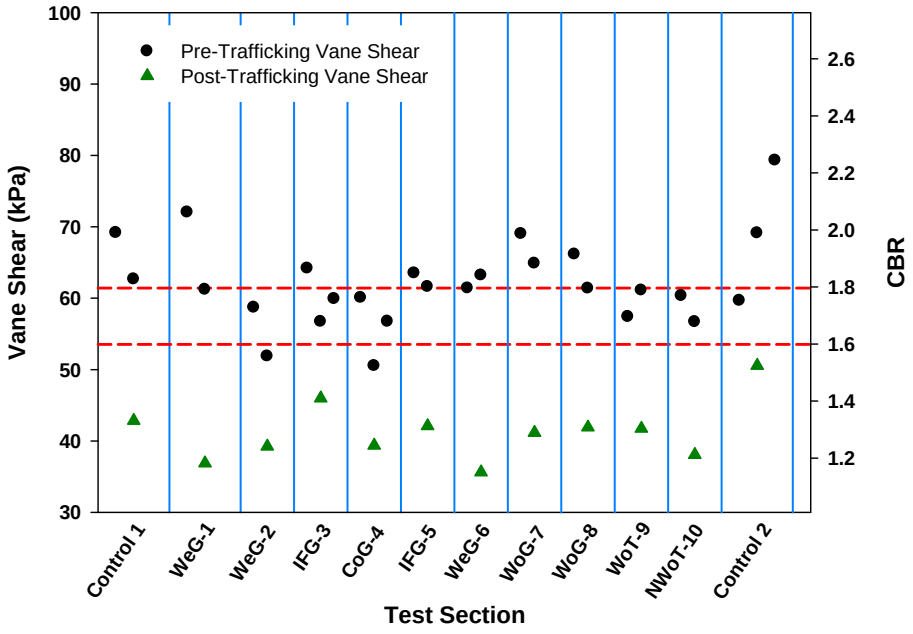

Figure 45. Pre- and post-trafficking, weighted, subgrade strength values from the vane shear.

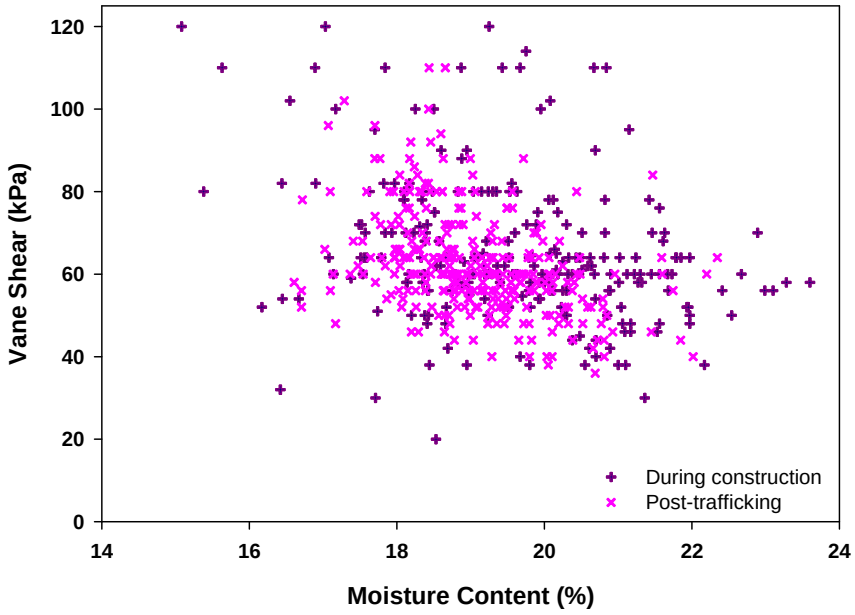

Figure 46. Construction and post-trafficking moisture content vs. vane shear for all test sections.

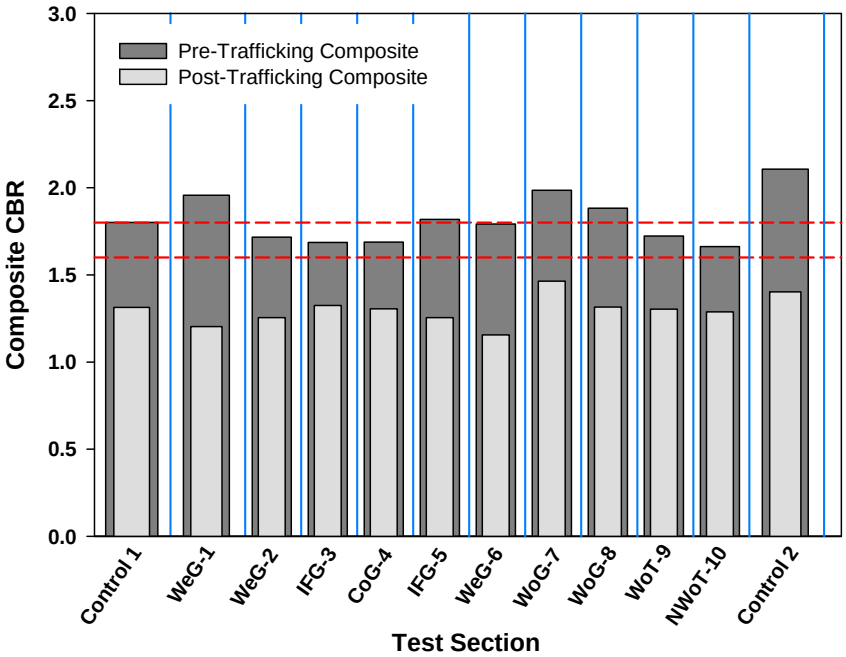

Figure 47. Post-trafficking composite subgrade strength determined from the vane shear and DCP.

The migration of soil particles from the subgrade to the base course layers was evaluated after trafficking by removing samples of the base course above the geosynthetic and measuring the amount of fines (percent passing the #200 sieve). A wet sieve analysis was conducted on

multiple samples extracted during the forensic investigations. Fines contents were generally greater in the soils directly above the geosynthetic when compared to the fines in the base course, as seen in Figure 48. Samples of base course from the WoG-8, WoT-9 and NWoT-10 test sections were inadvertently not taken during this analysis, but can be compared using the average fines content in the base (7.9 percent). No samples were taken in the Control 1 section because of the difficulty in determining the interface between the subgrade and base course layers.

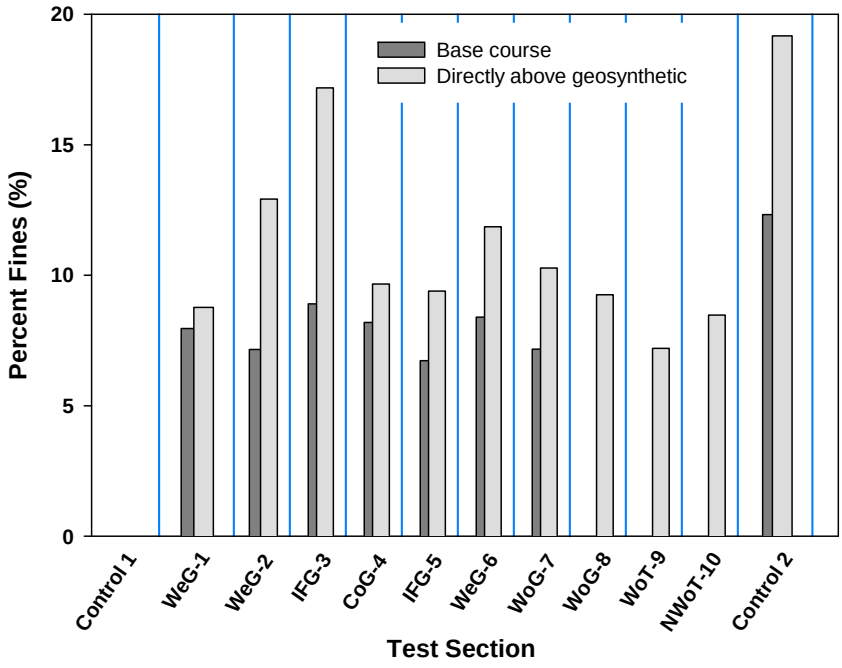

Figure 48. Fines content in the base course and directly above geosynthetic.

5 ANALYSIS AND RESULTS

Several types of data were used to analyze the performance of each of the test sections, including:

- longitudinal and transverse rut measurements during trafficking,
- displacement measurements of the geosynthetics in the rut bowl at one position within each test section,
- pore pressure measurements near the top of the subgrade at one position within each test section,
- in-air tension testing of the geosynthetics, and
- forensic investigations after trafficking.

5.1 Rut Analysis

The analysis of respective performance of each of the test sections was based largely on rut depth. Rut depth was measured in each of the test sections at regularly scheduled intervals during trafficking (more frequently in the beginning and less frequently toward the end) to capture rutting as a function of truck passes. The depth of the rut was measured in the two outermost wheel tracks of the rear wheels at one-meter intervals along the length of each test section using a digital level with ±1.0 mm accuracy. In this case, rut was a function of the difference in the elevation of the measurement points over time. Total rut, therefore, was determined by comparing current measurements to a baseline measurement which was made before trafficking. This type of rut is referred to as "elevation rut", as illustrated in Figure 49. The "apparent rut", however, is typically greater and can be defined as the vertical distance from the upper crest of the rut bowl to the bottom of the rut bowl (Figure 49). The apparent rut is generally greater than the elevation rut because bearing failure in the soil beneath the wheel load is shoved outward and upward adjacent to the wheel path. Measurement of the transverse surface contour was also made during trafficking to quantify the apparent rut at a single location in each test section.

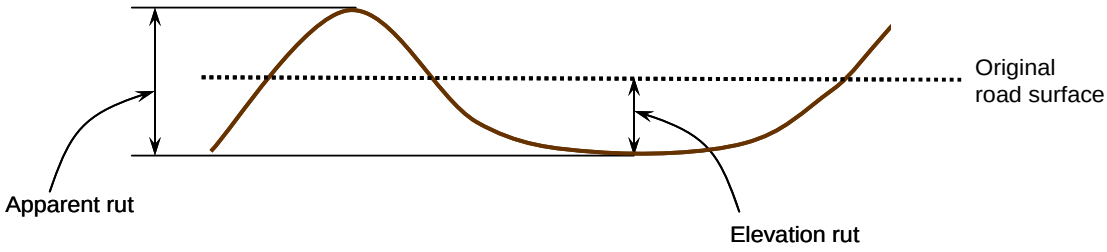

Figure 49. Illustration of rut measurements.

A maximum of 40 truck passes (120 axle passes) was necessary to cause an average of 100 mm rutting (elevation rutting) in the strongest test sections, at which trafficking of the test sections terminated. Because these test sections failed rapidly, it is probable that other results may be seen for sections that do not fail as quick. These 40 passes occurred over a one week period. Rut measurements were generally made more frequently during earlier passes and declined over time based on rut development. The schedule of rut data collection is provided in Table 14, where an **X** indicates that rut data was collected for a particular test section after a specific number of truck passes. For test sections that failed more rapidly, additional rut measurements were taken to better describe their behavior as a function of the number of passes made by the test vehicle. Overall, rut was measured in most test sections during truck passes 1, 2, 3, 5, 10, 15, 25 and 40 and will therefore be the focus of the statistical analysis contained in this report.

Table 14. Rut Data Collection Schedule

	Number of Truck Passes													
Test Section	1	2	3	4	5	6	7	8	10	15	16	17	25	40
Control 1	X	X	X	X	X	X	X		X	◯				
WeG-1	X	X	X		X				X	X			X	X
WeG-2	X	X	X		X				X	X			X	X
IFG-3	X	X	X		X				X	X			X	X
CoG-4	X	X	X		X				X	X			X	X
IFG-5	X	X	X		X				X	X		◯ X		
WeG-6	X	X	X		X				X	X			X	X
WoG-7	X	X	X		X				X	X			X	X
WoG-8	X	X	X		X				X	X			X	X
WoT-9	X	X	X		X				X	X			◯ X	
NWoT-10	X	X	X	X	X			X	X	X	X		◯	
Control 2	X	X	X	X	X	X		X	X	◯ X				

◯ indicates when ruts were filled in to facilitate further trafficking of the test site

The raw rut data obtained from the two outermost wheel ruts within each test section were averaged together to form a single rut measurement at a particular distance along the test section, as illustrated in the example test section in Figure 50. In this example, x_n and y_n represent rut measurements at a particular distance from the end of the test section. These values were averaged together to form a single point, z_n, the average rut at that longitudinal position in the test section; however, rut data collected near the ends of adjacent test sections (1 to 2 meters long) were omitted from the analysis because they were near the overlapped areas. This process was repeated for all corresponding measurements within a particular test section. The averaged

rut along the length for all of the test sections is presented in Figure 51 as a function of increasing number of truck runs. As expected, rut increases in all the test sections as truck passes increase.

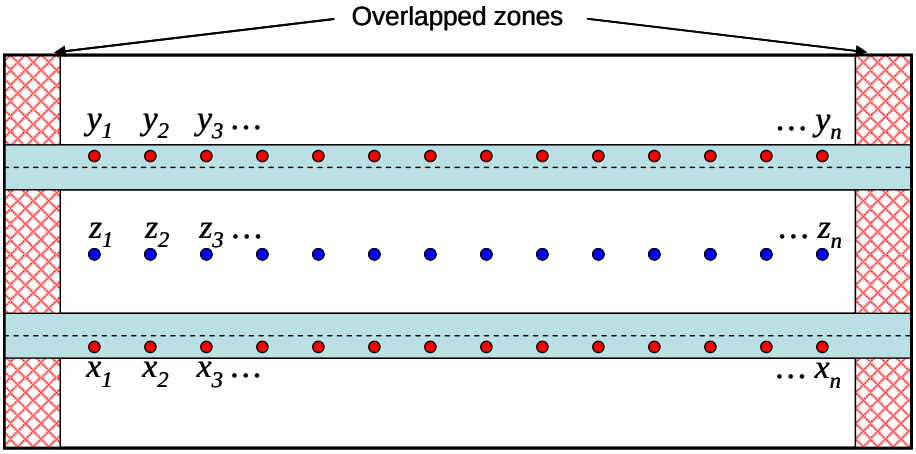

Figure 50. Example of typical test section rut measurement and averaging methodology.

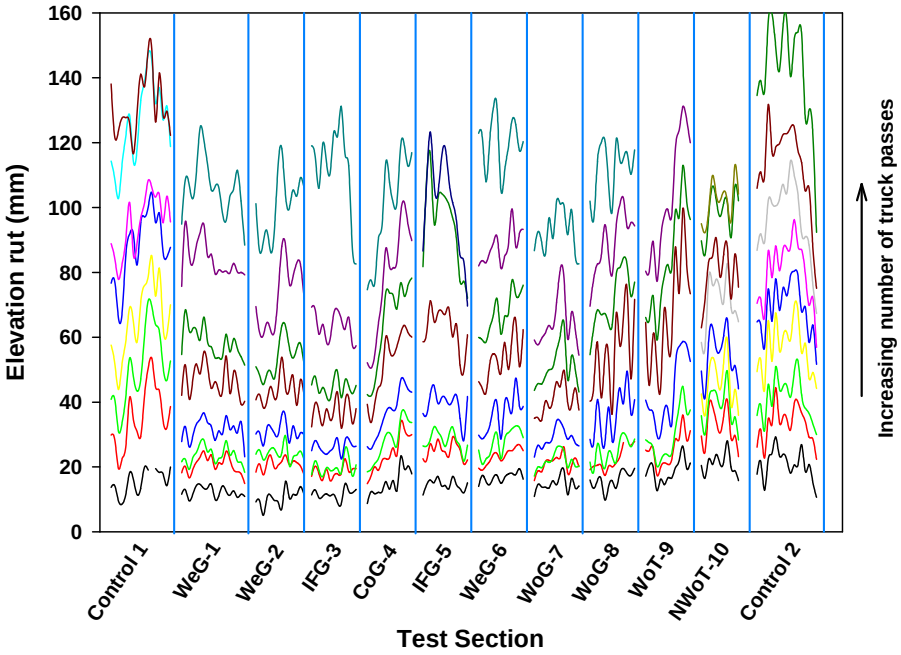

Figure 51. Averaged rut along the length of all test sections.

Fluctuations in rut within the test sections are attributed to natural variations in the strength of the test sections along their length. These variations made it difficult to make direct comparisons between test sections. Means and standard deviations were calculated for each test section for each truck pass to refine the results. The mean rut within each test section as a function of increasing test runs is shown in Figure 52.

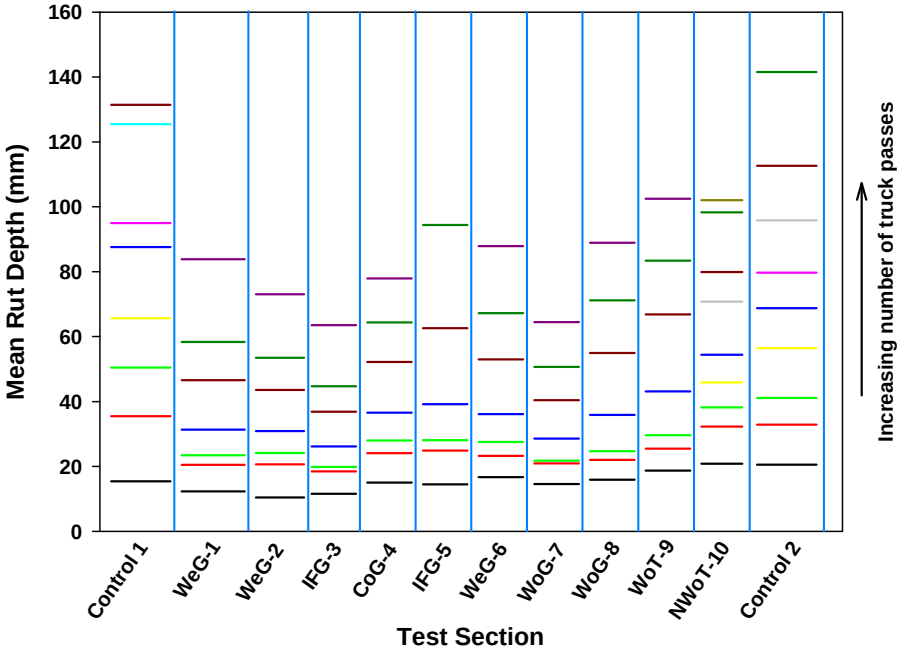

Figure 52. Mean rut depth for all test sections.

The data shown in Figure 52 is shown in Figure 53 as rut depth versus truck passes for each test section. This allows for a comparison of test sections while keeping in mind that average subgrade strength and aggregate thickness varied to some extent between test sections as demonstrated earlier. In Section 5.5, differences in subgrade strength and aggregate thickness are taken into account in an evaluation of relative performance of the test sections.

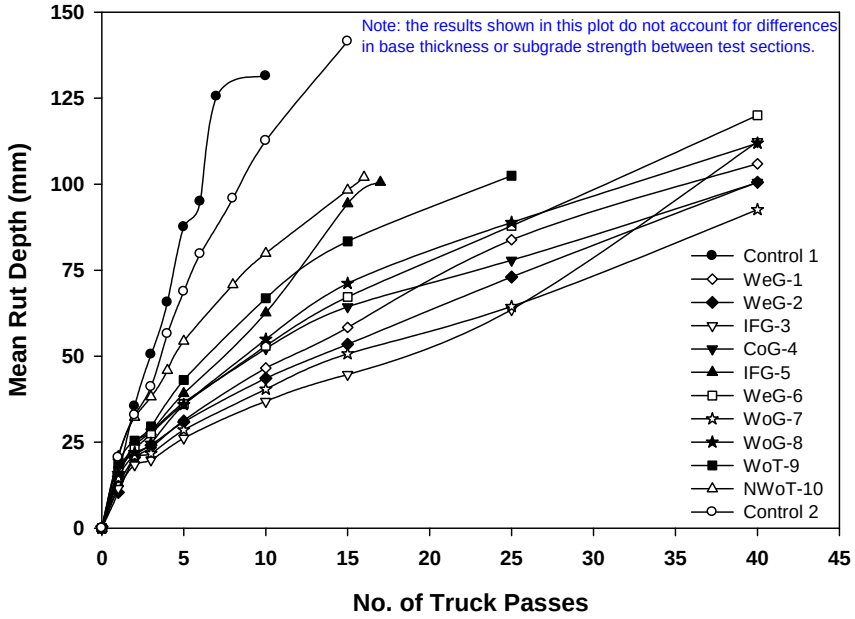

Figure 53. Mean rut depth as a function of the number of truck passes.

An alternative way to view the data presented in Figure 53 is to plot the number of traffic passes it took to reach a specific level of mean rut depth for each section. Recall that one truck pass equals 2.2 traffic passes (Section 2.3). Mean rut depths of 25, 50, 75 and 100 mm were chosen for this analysis; the results of which are shown in Figure 54 and tabulated in Table 15. In this case, lines that have lower slopes indicated poorer performance, while lines of greater slope indicate better performance. Concavity of the lines can be used to indicate the trend of rutting behavior in each of the materials. Lines that are concave up are improving in performance as truck passes increase; conversely, lines that are concave down are declining in performance. In general, most test sections showed a decrease in the rate of rutting as truck passes increased (i.e., lines exhibit concave upward trend) from 25 or more mm of rut. The trends associated with the two control sections were generally straight. Note that the final point for the WoG-7 test section was estimated by extending the curve in Figure 53 because it did not reach 100 mm of rut during testing. The two integrally-formed products (IFG-3 and IFG-5) exhibited concave down behavior indicating declining performance for increasing number of truck passes.

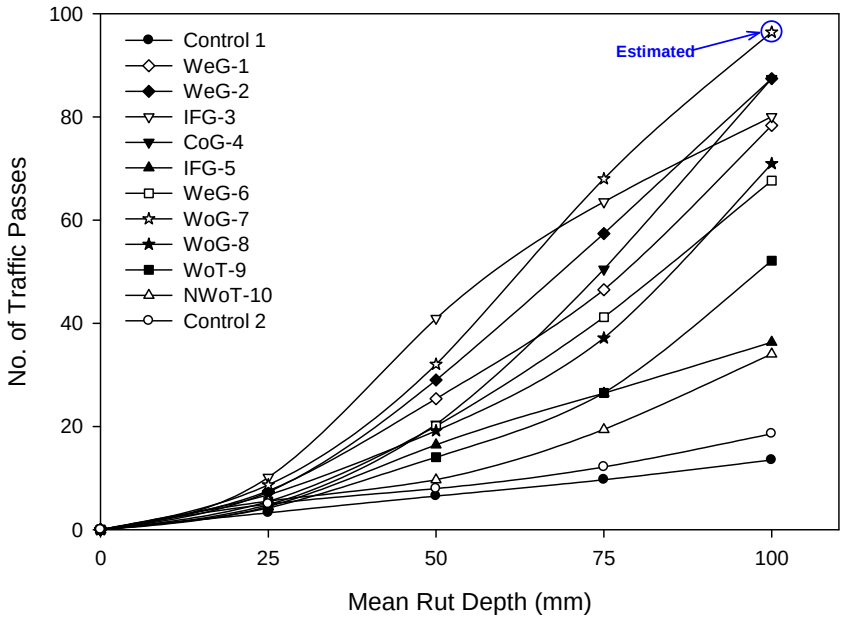

Figure 54. Traffic passes at given rut depths.

Table 15. Traffic Passes at Given Rut Depths

Test Section	25mm	50mm	75mm	100mm
Control 1	3.3	6.5	9.7	13.5
WeG-1	7.5	25.4	46.5	78.3
WeG-2	7.3	29.0	57.4	87.4
IFG-3	10.1	40.9	63.5	80.0
CoG-4	4.8	20.4	50.5	87.4
IFG-5	4.5	16.5	26.5	36.3
WeG-6	5.4	20.1	41.2	67.6
WoG-7	8.7	32.0	68.0	96.4†
WoG-8	6.8	19.2	37.1	70.9
WoT-9	4.2	14.0	26.5	52.1
NWoT-10	5.5	9.7	19.4	34.0
Control 2	5.0	8.0	12.2	18.6

† estimated value

While qualitative assessments are valuable in generally describing differences in performance between test sections, they are of limited use in situations when these differences are less pronounced. Additionally, data scatter may make it difficult to confidently state whether one test section clearly performed better than another, etc. Therefore, quantitative comparisons between test sections were made using a two sample t-test. This test evaluates the statistical significance of the differences in the means of two sample populations (in this case, the mean rut depth). The results of this test can be expressed in a variety of forms, and the decision was made to use the p-value for each comparison. The p-value for the test ranges between zero and one; values approaching zero indicate greater likelihood that the sample means are different, while values approaching one indicate greater likelihood that the means are the same.

The mean for each test section was compared to all other test sections for truck passes 1, 2, 3, 5, 10, 15, 25 and 40 using this methodology. Altogether, 528 comparisons were possible; however, because rut was not measured within certain sections during some truck passes (refer to Table 14 for details), only 434 valid comparisons were made. The degree of similarity and difference is arbitrary, and depends on how one chooses to consider the data being compared. For the purposes of this study, two means were considered more similar if the p-value was between 0 and 0.25; likewise, two means were considered more different if the p-value was between 0.75 and 1.00. Using these criteria, the results revealed that the comparisons of the means were different from one another 88.5 percent of the time. Conversely, the means were similar to one another 4.4 percent of the time. The remaining 7.1 percent of the values had p-values between 0.25 and 0.75. No trends were noticed and similarities between compared means were random. In conclusion, sufficient measurements were made within each test section during

trafficking to ensure that the mean rut values were directly comparable to one another. Therefore, measurements of longitudinal rut can be directly compared between test sections using the information provided in Figure 54. Appendix B shows the p-values for all the comparisons of the mean rut depths.

5.2 Transverse Rut Analysis

The rut bowl was also measured in the transverse direction (i.e., perpendicular to the direction of the test vehicle) to show rut formation during trafficking. These measurements were made using a rod and level and were taken after the third and final truck pass within each section as compared to the baseline shape of the road surface. An example of this is shown in Figure 55 for the WeG-2 test section. A complete set of results for all test sections are contained in Appendix C.

Transverse measurements of the surface profile of the gravel and subgrade were also made during the forensic evaluations by using the rod and level to make measurements along the north and south sides of each excavated trench. An example of this is shown in Figure 56 for the WeG-2 test section. A full photographic record of these areas was taken during the forensic investigations, and is contained in Appendix C.

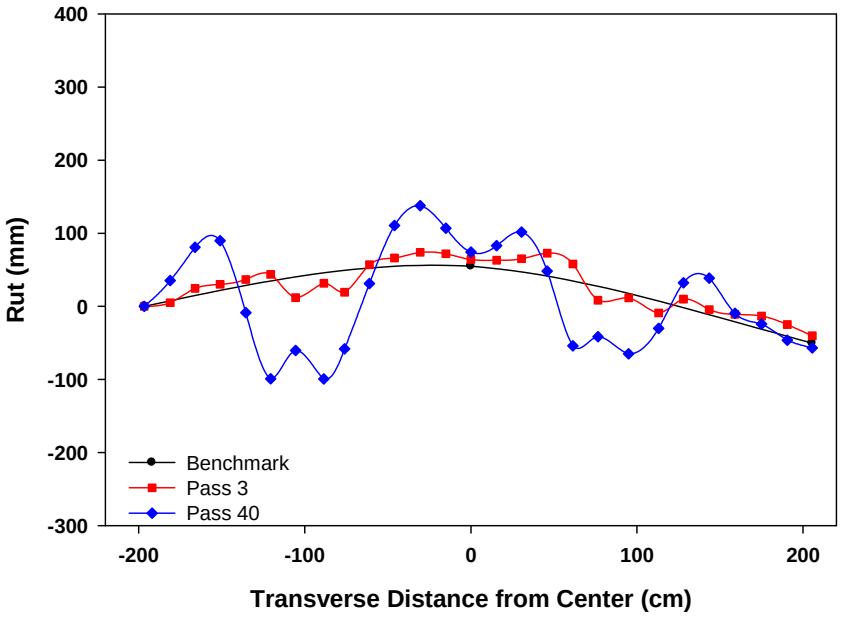

Figure 55. Transverse rut profiles of the road surface during trafficking (WeG-2).

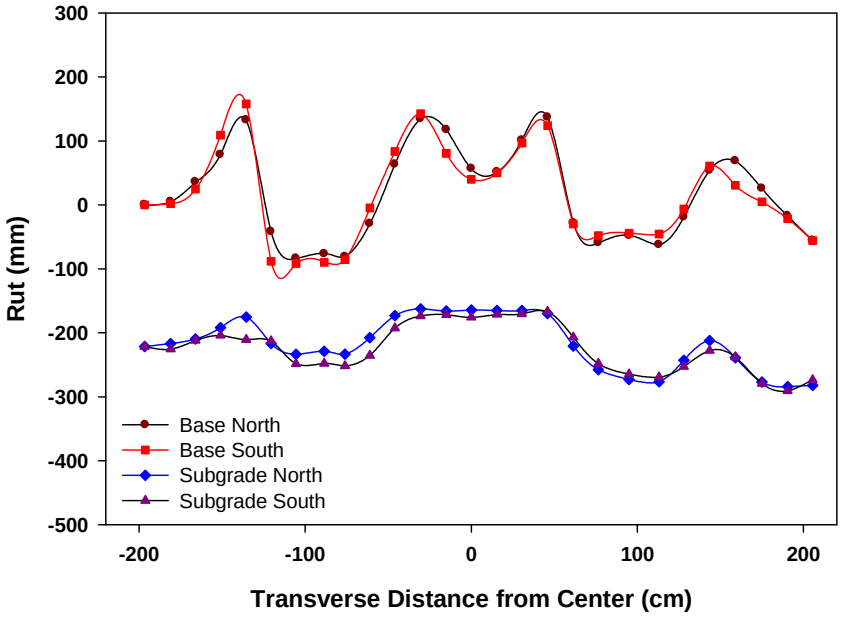

Figure 56. Transverse rut profiles of the base and subgrade during forensic excavations (WeG-2).

5.3 Geosynthetic Displacement and Strain Analysis

Transverse displacement of the geosynthetic was measured in each of the test sections using the LVDTs installed as described in Section 2.5 and illustrated in Figure 57. The points of measurement for each of the LVDTs was outside of the wheel path (LVDT 1 measurement), at the edge of the wheel path (LVDT 2 measurement), and directly under the outside tire of the dual wheel (LVDT 3 measurement). Three strain calculations were possible using these measurements and knowing the original distance between these points. Strain 1 is the strain between LVDT 1 and LVDT 2, Strain 2 is the strain between LVDT 2 and LVDT3, and Strain 3 is the overall strain between LVDT 1 and LVDT 3. The following sign convention was used: positive displacement moves to the left (westward) in Figure 57 and positive strain indicates tension.

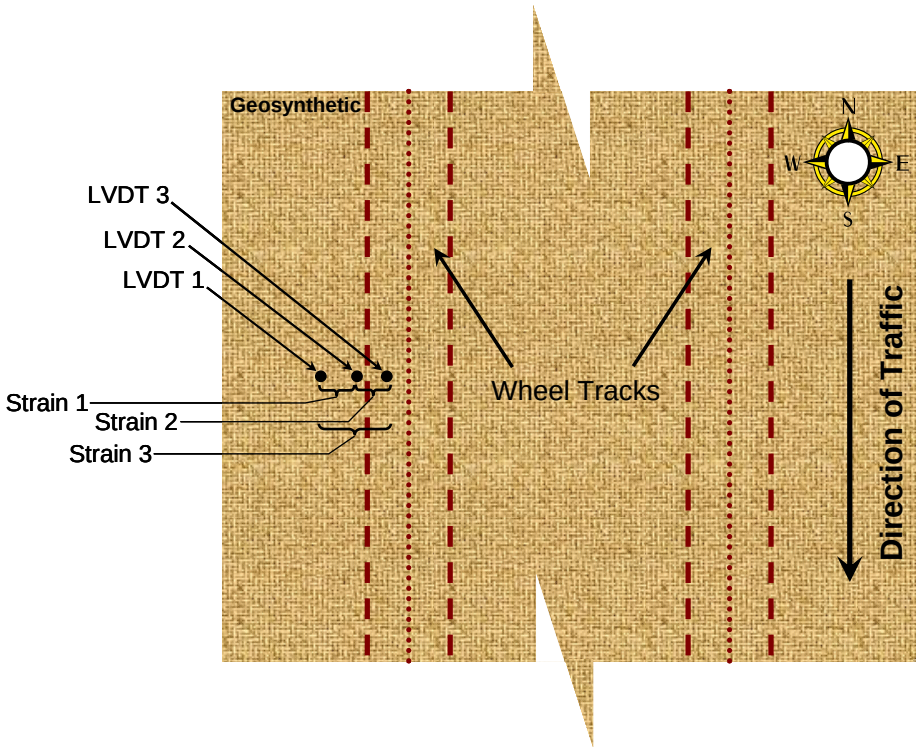

Figure 57. Illustration of displacement measurements and corresponding strain calculation.

Displacement in each of the test sections was generally similar with respect to the direction and initial magnitude of response. An example of the displacement response for the WeG-2 test section is provided in Figure 58. The first three truck passes are shown here to illustrate the dynamic displacement of the geosynthetic at each of the measurement points. For this type of plot, each truck pass accounts for about six to eight seconds of dynamic data taken at 200 Hz. Accumulated time between truck passes is removed to allow several truck passes to be shown on a single plot. The displacement record is the displacement at a single, stationary gage location when the truck is at various longitudinal positions along the test section. Thus, for example, the peaks corresponding to the tandem axles are later in the displacement history than the front axle (i.e., the front axle passes over the fixed gage location first, followed by the tandem axles). Three clearly defined peaks are produced as the truck passes over the instrumented area. The first peak corresponds to the front tire of the test vehicle and the two peaks that follow correspond to the tandem (dual) axles. For the example provided, all measured displacements were positive indicating that the geosynthetic was moving westward away from the side of the truck; however, some displacements were more positive than others thus indicating strain in the material.

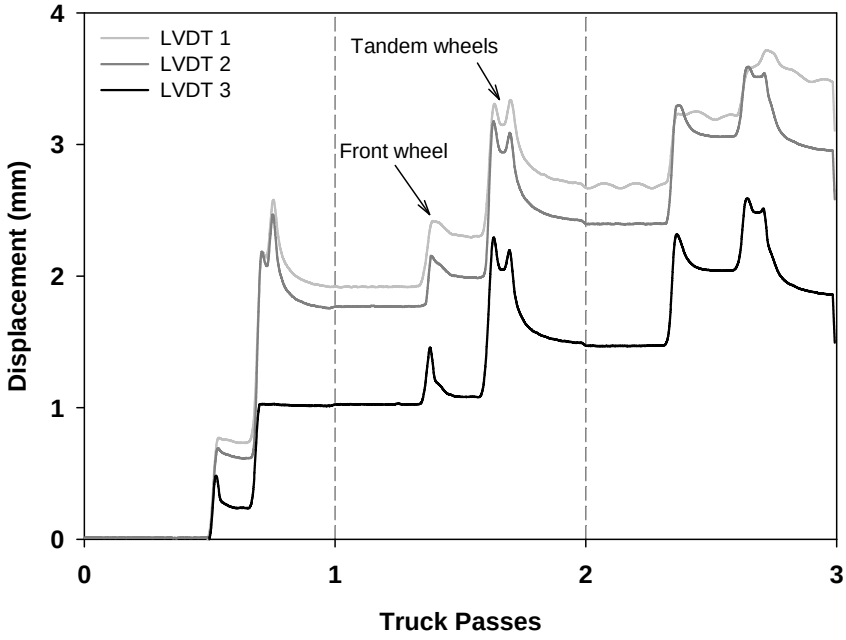

Figure 58. Displacement history of truck passes 1, 2 and 3 in the WeG-2 test section.

A complete history of the displacement of these points is provided in Figure 59. Early displacements generally accumulate in a positive direction indicating global movement of the geosynthetic to the west (away from the side of the test vehicle). After about five passes the sensors begin to move toward the truck as the geosynthetic is pulled down into the forming rut, as illustrated in Figure 60. This behavior is relatively similar between the test sections, with some sections making this transition after more truck passes. This indicates a transition between base reinforcement, involving the lateral movements of the base aggregate and the geosynthetic, to subgrade stabilization, involving deeper rutting and more of a tensioned-membrane effect. Appendix D shows the complete displacement history for all of the test sections. In most of the test sections, displacement measurements became erratic after about 20 passes. This is likely caused by the large deformations in the rut bowl which distorted the gaged area (Figure 60). Therefore, the erratic displacement measurements made after that point are suspect. Times when data was not collected during trafficking show up as straight line portions in the graph.

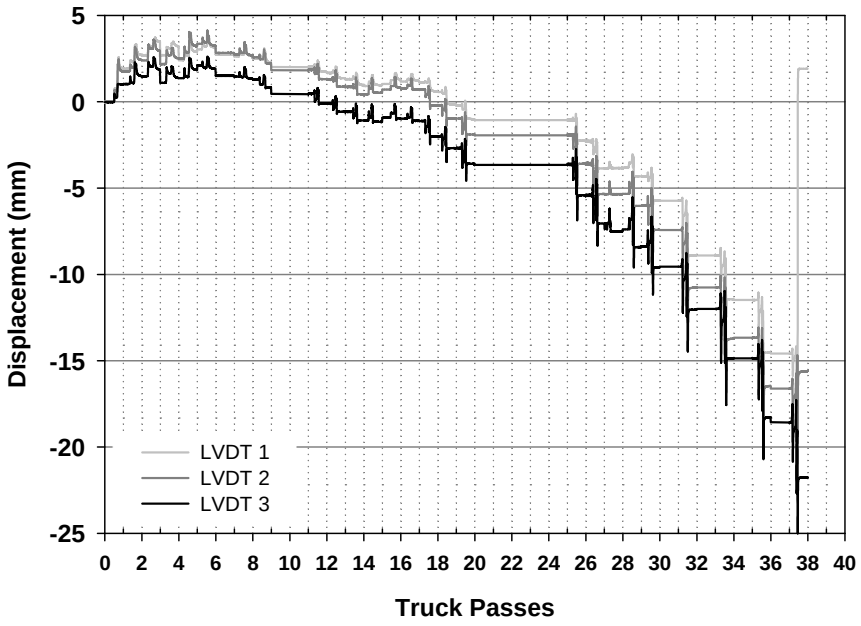

Figure 59. Entire displacement history of the WeG-2 test section.

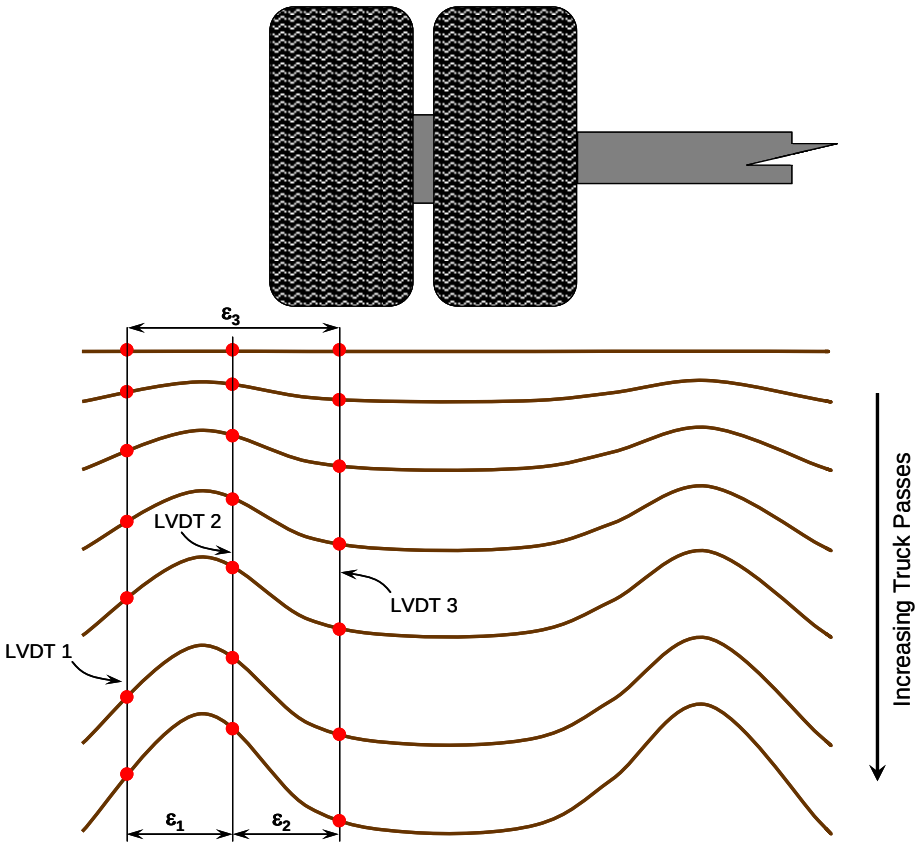

Figure 60. Distortion of the instrumented area due to rut formation.

A similar set of plots can be produced for the strains between the three displacement measurements, as described earlier. The development of positive or negatives strain depends on the position of the displacement measurement and the depth of rutting or gross deformation of the cross-section, as illustrated in Figure 60. For the example provided in Figure 61, strains were all positive, with the greatest strain occurring between LVDT measurements 2 and 3 (Strain 2 or ε_2) and the least strain occurring between displacement measurement points 1 and 2 (Strain 1 or ε_1). Strain 3 (ε_3) is the global strain between LVDT measurement points 1 and 3. In the example provided, ε_3 is not the average of ε_1 and ε_2, because the gage length between LVDTs 1 and 2 (80 mm) was not identical to the gage length between LVDTs 2 and 3 (195 mm). This is evident in Figure 61, since ε_3 is nearer in magnitude to ε_1 than it is to ε_2. Similar to the displacement measurements, individual axle passes are evident in the strain plot. As one may expect, ε_2 is the greatest since it is measuring the strain near the edge of the rut bowl where tension in the geosynthetic is the greatest. Likewise, ε_1 is the least since it is outside of this area.

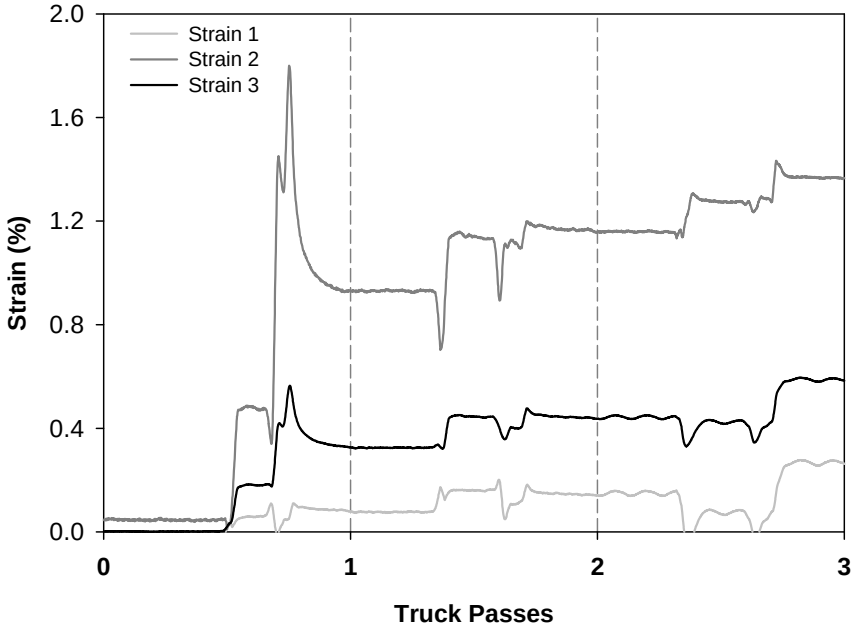

Figure 61. Strain history of truck passes 1, 2 and 3 in the WeG-2 test section.

The entire history of strain in the gaged area for the WeG-2 test section is shown in Figure 62. Accumulations of strain in the geosynthetic are evident from this plot as ε_2 increased from zero to a maximum of approximately 3 percent during truck pass 29. As expected, strain calculations depended on the displacement measurements, so when displacement measurements are erratic, the calculated strain is also erratic. Negative strains in Figure 62 are indicative of areas where the geosynthetic is being compressed. As the rut forms it is logical that materials near the edge of the rutted area will be shoved outward, thereby creating an apparent

compressive strain in the geosynthetic. True compressive strain in the material will most likely not be as pronounced since geosynthetics are not capable of sustaining large compressive forces. As mentioned before, the large movements in the rutted area, in many cases, caused significant distortions in the gaged area. These distortions were not necessarily in a single plane indicative of strains experienced by geosynthetics under pure tension. On the contrary, accumulated passes of the truck caused the subgrade and base course material to move upward and outward creating a large bulge in the gaged area (as illustrated in Figure 60). In addition, the torsional stresses applied by the truck tires during trafficking caused the geosynthetic to shear by as much as 9.2 cm out of plane along the bottom of the rut bowl, as measured during the forensic evaluations discussed in Section 4.1.5 of this report. In conclusion, the displacements and corresponding strains induced during trafficking were only useful up to the point when the rutted area became grossly distorted.

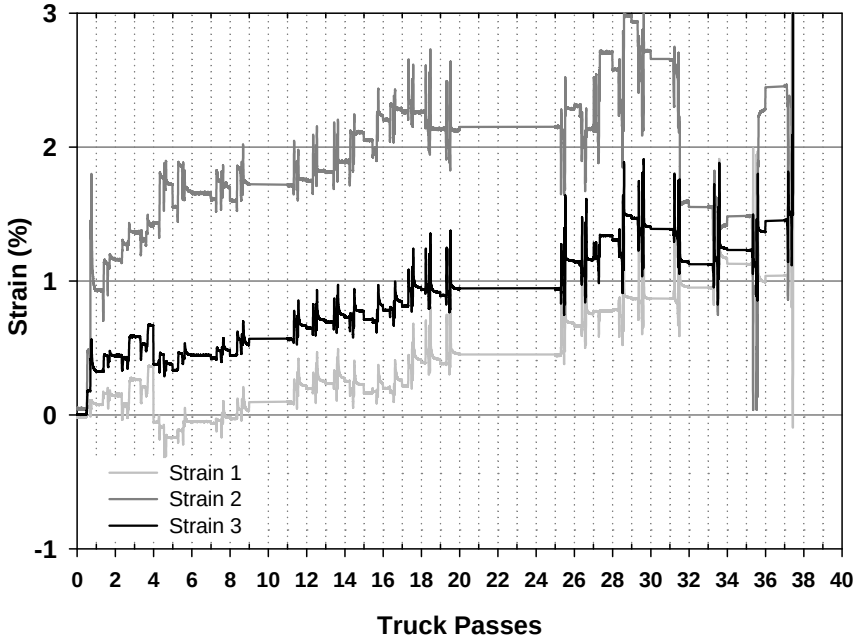

Figure 62. Entire strain history of the WeG-2 test section.

Dynamic strains were calculated for all truck passes for all of the test sections as the difference between the peak strain and the residual strain for a given truck pass. Figure 63, Figure 64 and Figure 65 show the dynamic strains for the ε_1, ε_2 and ε_3 measurements respectively, for all test sections as a function of truck passes. In general, peak strains increase in most test sections as truck passes increase. As expected, peak strains for ε_2 are the greatest and peak strains for ε_1 are the least. Test sections that performed well tend to correlate to low values of average dynamic strain in the geosynthetic, indicating that tensile stiffness is an important property for performance, as illustrated in Figure 66. The average dynamic strain was calculated

by taking the mean of the dynamic strain values within each test section prior to reaching gross distortion of the instrumented area (between 37 and 44 traffic passes).

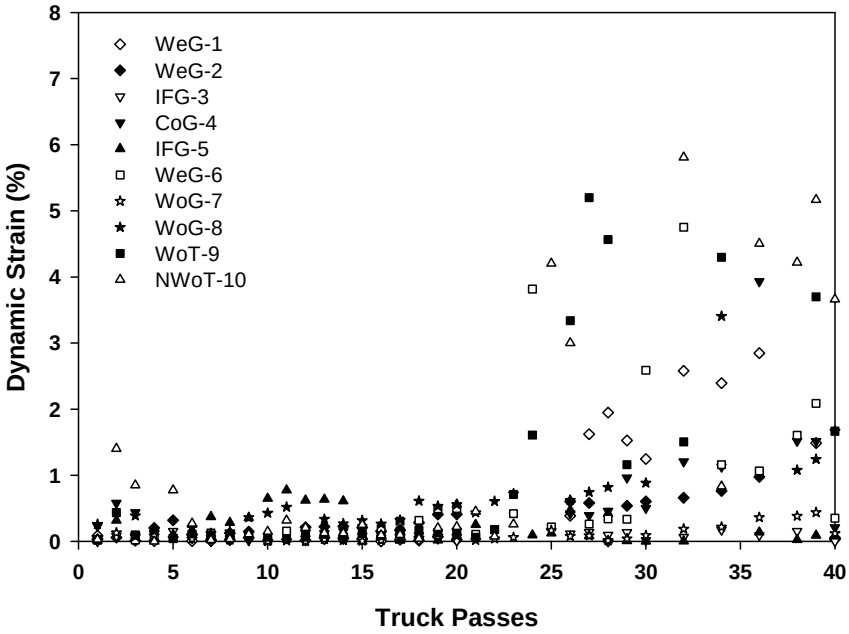

Figure 63. Dynamic ε_1 as a function of truck passes, for all test sections.

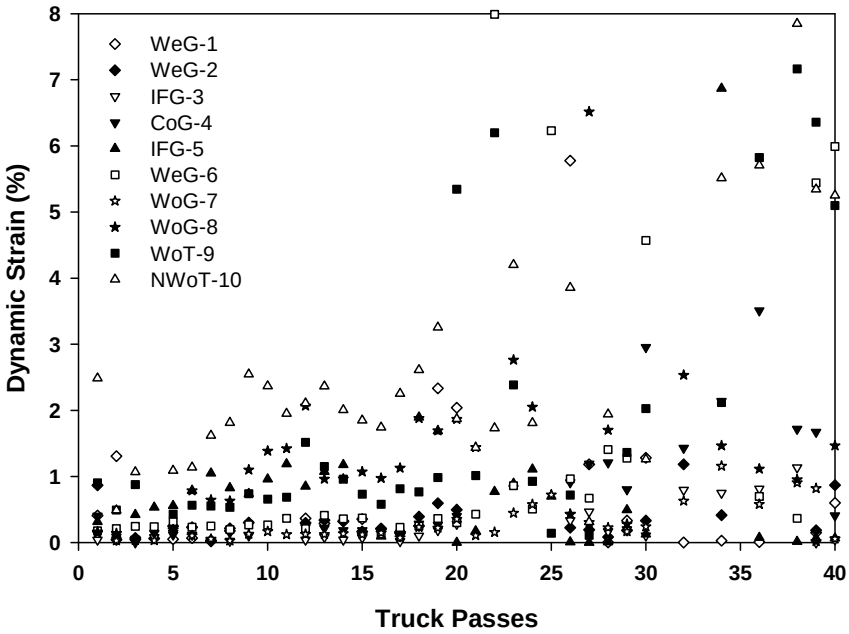

Figure 64. Dynamic ε_2 as a function of truck passes, for all test sections.

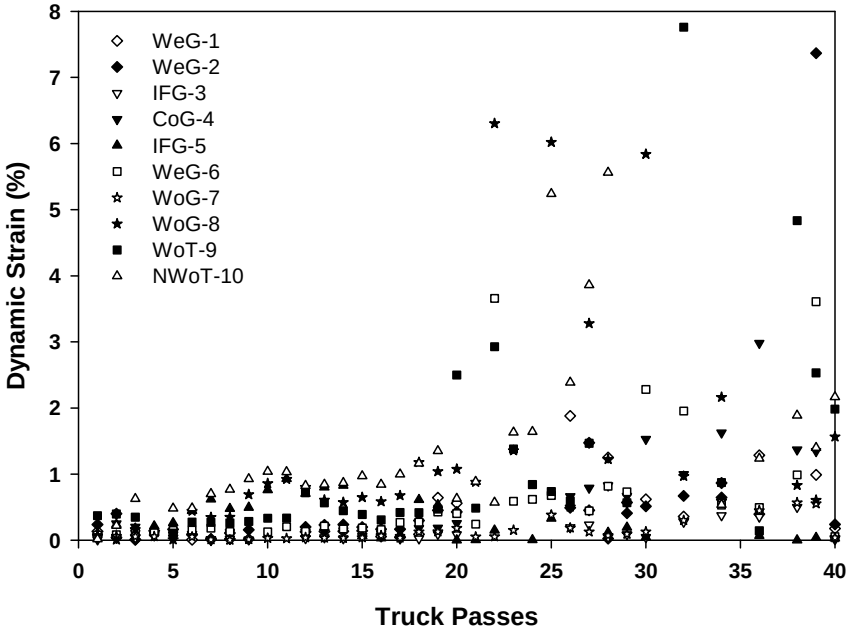

Figure 65. Dynamic ε_3 as a function of truck passes, for all test sections.

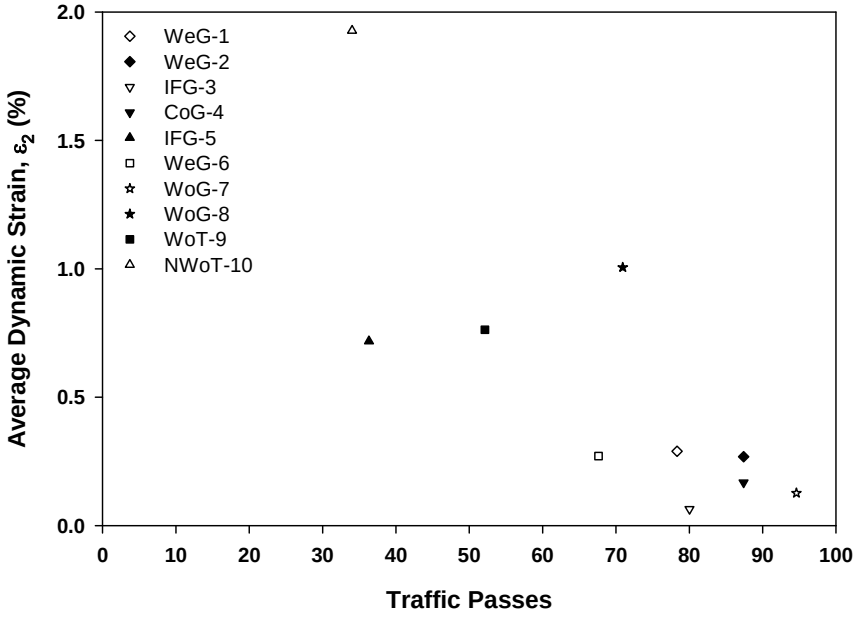

Figure 66. Average dynamic strain (ε_2) as a function of traffic passes to failure.

5.4 Pore Water Pressure Analysis

Pressure gages were used to measure pore-water pressure at a depth of 15 cm within the subgrade within the wheel path in all of the test sections, as described in Section 2.5 of this report. Dynamic measurements of pore pressure were made during trafficking and static levels of pore pressure were extracted from these measurements to show pore pressure trends over time for increasing traffic passes. Similar to measurements of displacement and strain, peaks associated with the passage of the truck are evident in the dynamic pore pressures data as illustrated in Figure 67. The data presented in this figure is from the WeG-2 test section and was taken from data sets when continuous truck passes were made (truck passes 12 through 15, which were approximately three minutes apart) followed by a rest period of 16 hours and another truck pass (truck pass 16). During the 16 hour rest period, pore-water pressure dissipated by about 3.7 kPa. Similar results are observed in all of the test sections, although not at always the same magnitude of dissipation. The dynamic pore water pressure increase, computed as the increase in pore water pressure due to the passage of a wheel, was calculated for each axle pass. Dynamic pore pressures were generally similar to one another and ranged between 0.2 and 1.5 kPa regardless of which axle was passing over the sensor, as seen in Figure 68, Figure 69, and Figure 70 for the front, first rear and second rear axles, respectively.

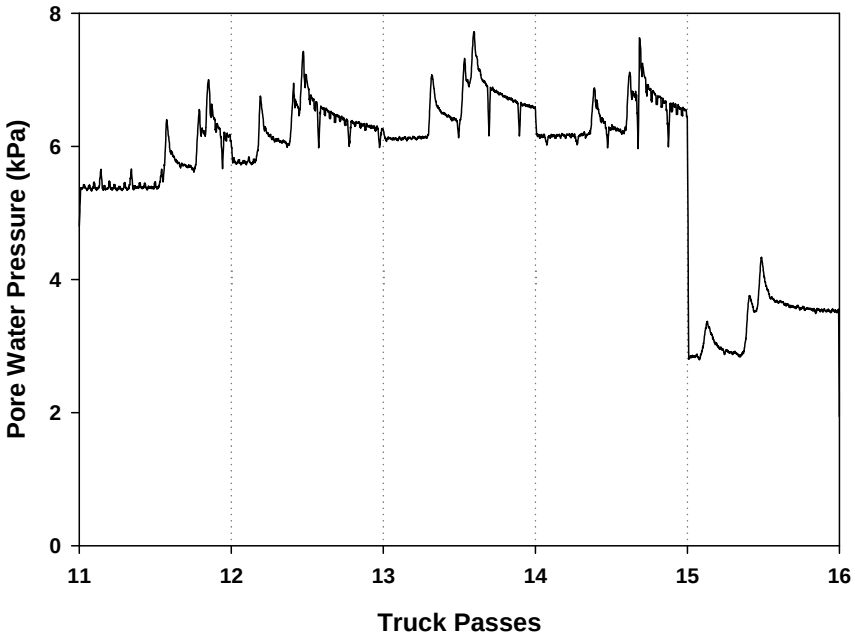

Figure 67. Pore water pressure history in Section WeG-2 for truck passes 12 through 16.

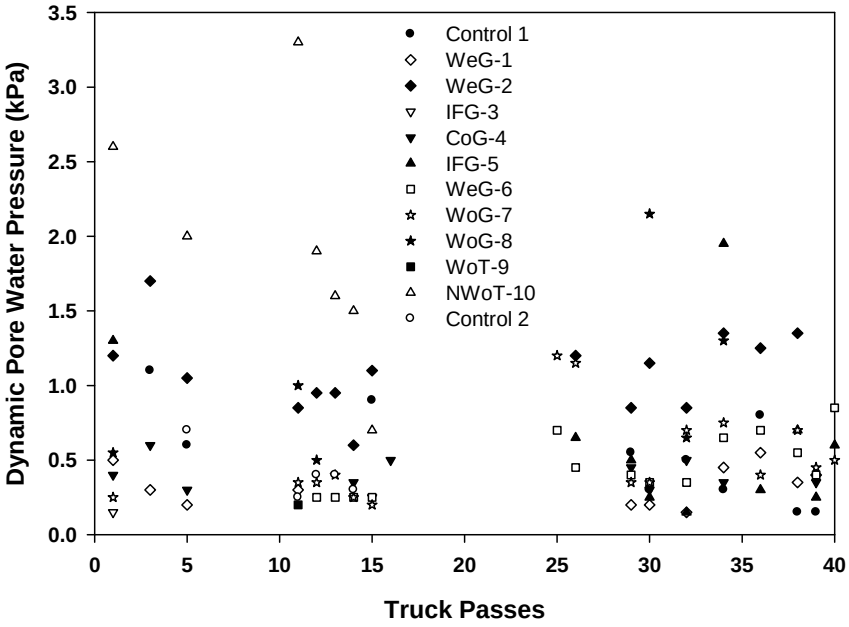

Figure 68. Dynamic pore water pressure caused by the front axle as a function of truck passes, for all test sections.

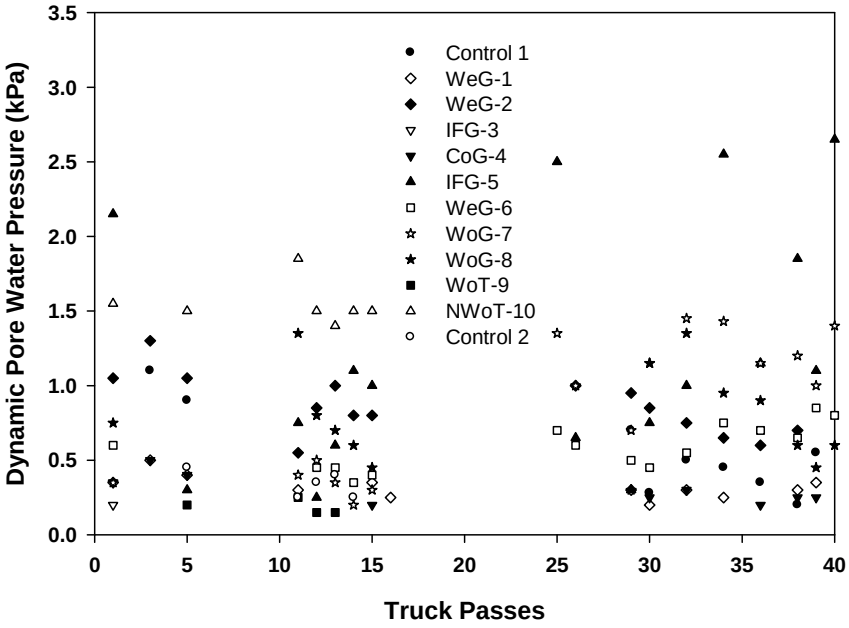

Figure 69. Dynamic pore water pressure caused by the first rear axle as a function of truck passes, for all test sections.

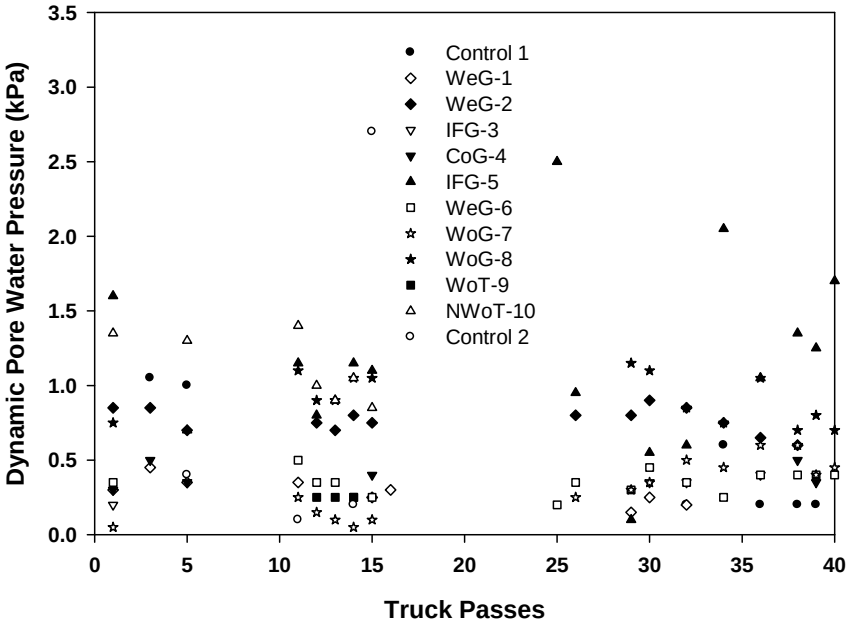

Figure 70. Dynamic pore water pressure caused by the second rear axle as a function of truck passes, for all test sections.

Static levels of pore pressure in all the test sections generally increased during trafficking of the test sections, as shown in Figure 71. Maximum levels of pore pressure were usually between 5.0 and 9.0 kPa. Differences between the static levels of pore pressure between test sections are basically within the sensitivity of the sensors. Christopher et al. (2009) also showed that static pore water pressure increases in the subgrade within large-scale box test sections to which a cyclic plate load is applied to the road surface. Using effective stress strength principles, Christopher et al. (2009) showed that the undrained shear strength of the subgrade reduced as excess pore water pressure increased according to Equation 7, where S_{uf} and S_{ui} are the final and initial subgrade undrained shear strengths after and before traffic loading and u_e is the static excess pore water pressure after traffic loading. This equation assumes a drained friction angle for the soil of 30 degrees and a value of the pore water pressure parameter A of 0.7. Undrained shear strength and subgrade CBR are related through the correlation equation between vane shear strength and CBR discussed earlier in this report and given below in Equation 8.

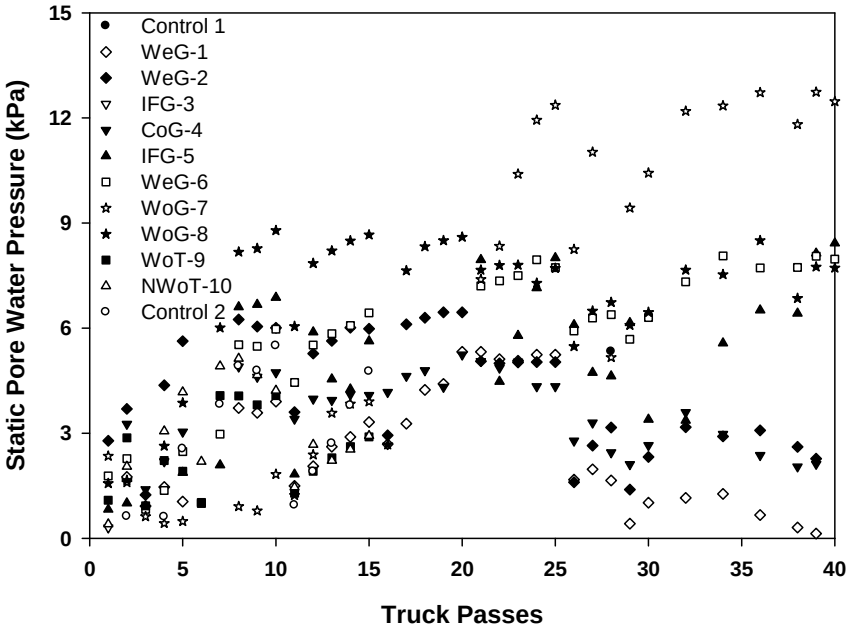

Figure 71. Static pore water pressure as a function of truck passes, for all test sections.

$$S_{uf} = S_{ui} - \frac{u_e}{1.4}$$ **Equation 7**

$$CBR = \frac{S_u + 9.5354}{39.418}$$ **Equation 8**

Using the maximum values of static pore water pressure from Figure 71, a prediction of the change in shear strength of the subgrade was made using the relationships outlined above. Values of static pore water pressure and the results of this analysis are listed in Table 16 along with the predicted change in subgrade strength in terms of CBR. Overall, the predicted decreased of the subgrade strength was approximately 0.1 CBR, which amounts to about a 6.5 percent decrease from the original strength measurement. The greatest decrease occurred in the WoG-7 test section (decrease of 0.23 CBR). In Section 4.2, results from measurements of subgrade CBR during forensic excavations were presented, which showed an overall decrease in subgrade strength due to trafficking. The pore water pressure increase and its impact on subgrade strength are partly responsible for this observation.

Table 16. Static Pore Water Pressure after Trafficking and Predicted and Composite Subgrade CBR

Geosynthetic Test Section	Composite Subgrade CBR after Construction	Composite Subgrade CBR after Trafficking	Static Pore Water Pressure (kPa)	Predicted Decrease in Subgrade CBR
Control 1	1.80	1.31	5.0	0.09
WeG-1	1.96	1.20	5.2	0.09
WeG-2	1.72	1.25	6.3	0.11
IFG-3	1.69	1.32	0.3	0.01
CoG-4	1.69	1.30	5.1	0.09
IFG-5	1.82	1.25	8.2	0.15
WeG-6	1.79	1.16	8.0	0.14
WoG-7	1.99	1.46	12.5	0.23
WoG-8	1.88	1.31	8.5	0.15
WoT-9	1.72	1.30	4.0	0.07
NWoT-10	1.66	1.29	5.0	0.09
Control 2	2.11	1.40	5.0	0.09

5.5 Performance Evaluation

One of the primary objectives of this study was to evaluate and compare the ability of various geosynthetics to stabilize weak subgrade soils. Direct comparisons between test sections can only be accomplished if the conditions between each of the individual test sections are identical. Accordingly, during construction every effort was made to maintain a tight level of control within each of the main design components, most importantly, the subgrade strength and the thickness of the base course layer. Because of the relatively similar rutting performance between the test sections, small differences in these components along the testing area were more influential than anticipated. Therefore, a direct comparison of performance of the test sections was not possible because of small but important differences in aggregate thickness and subgrade strength. Nevertheless, empirical performance comparisons between the test sections were made using the subgrade strength data collected after trafficking. This data was used for three main reasons: 1) the collection method and the total number of data points were more consistent between all of the test sections (the standard deviation of the subgrade strength after construction was 0.14 CBR, while the standard deviation of the subgrade after trafficking was 0.08 CBR), 2) the subgrade had an opportunity to coalesce during the two week period after construction but prior to trafficking making it more uniform, and 3) loading of the subgrade during trafficking helped amalgamate the subgrade. The average aggregate thickness, composite subgrade CBR after construction, composite subgrade CBR after trafficking (from Section 4.2) and number of standard axle passes to reach 100 mm of rut (N_{field}) for each test section is summarized in Table 17.

Table 17. Summary of Test Section Properties and Relative Rutting Performance

Geosynthetic Test Section	Average Base Thickness (mm)	Composite Subgrade CBR after Construction	Composite Subgrade CBR after Trafficking	N_{field}
Control 1	211	1.80	1.31	13.5
WeG-1	216	1.96	1.20	78.3
WeG-2	215	1.72	1.25	87.4
IFG-3	211	1.69	1.32	80.0
CoG-4	206	1.69	1.30	87.4
IFG-5	199	1.82	1.25	36.3
WeG-6	192	1.79	1.16	67.6
WoG-7	184	1.99	1.46	96.4
WoG-8	178	1.88	1.31	70.9
WoT-9	173	1.72	1.30	52.1
NWoT-10	171	1.66	1.29	34.0
Control 2	172	2.11	1.40	18.6

5.5.1 Comparison of Rutting Results to Existing Design Solutions

The test sections were originally designed for a target base thickness of 200 mm and a subgrade CBR of 1.7 using the FHWA (1995) method for unpaved roads, as previously discussed in Section 2.3. Based on this design, it was expected that the control test sections would reach 100 mm of rut in a number of traffic passes less than 100 and the geosynthetic-stabilized test sections would require more than 1000 passes. On average, the sections failed more rapidly than that predicted by FHWA (1995). Reasons for this premature failure are somewhat uncertain; however, two items that possibly influenced this were: 1) the in-place strength of the base course aggregate, and 2) the air pressure in the test vehicle tires. Although the base course aggregate met the required specification as outlined in the FHWA design methodology (CBR was greater than 100 % which is greater than the required 80 %), the quantity and size of the rounded particles may have weakened the stone matrix in the compacted aggregate layer. The specification for CBR tests conducted on this material required that stones larger than 19 mm be replaced with stones between 4.75 and 19 mm, in this case a 22 percent replacement. In other words, the in-field CBR strength could have been less than the laboratory determined value, which would have influenced overall performance. In-field CBR tests were not conducted on the compacted base course. Secondly, and perhaps more importantly, the tire pressures on the test vehicle were 690 kPa, while the FHWA design methodology is based on tire pressures of 550 kPa. The higher tire pressures likely contributed to more rapid failures of the test sections in this study. Together, these two items may have contributed (at least partially) to premature failure of the test sections when compared to design expectations; however, inadequacies in the design may also be responsible.

The FHWA (1995) design method does not have the ability to refine the calculation for the number of traffic passes to reach 100 mm of rut based on differences in aggregate thickness and subgrade strength from section to section. An alternative and more sophisticated design method recently developed by Giroud and Han (2004) contains a mathematical model (shown in Equation 9) that quantitatively accounts for a number of variables thought to affect the rutting performance of geosynthetics used as subgrade stabilization. Using these design inputs, the number of traffic passes to cause failure in each of the test sections was used to predict the required aggregate thickness, which was then compared to the constructed aggregate thickness.

$$h = \frac{0.868 + (0.661 - 1.006\ J^2)\left(\frac{r}{h}\right)^{1.5} \log N}{\left[1 + 0.204\ (R_E - 1)\right]} \left[\sqrt{\frac{\frac{P}{\pi r^2}}{\frac{s}{fs}\left[1 - 0.9e^{-\left\{\frac{r}{h}\right\}^2}\right] N_c S_{u-sg}}} - 1 \right] r \qquad \textbf{Equation 9}$$

where:

$(0.661\text{-}1.006J^2)>0$ ($J<0.81$)

h = required base course thickness

J = aperture stability modulus {N-m/degree} – values listed in Table 18

P = wheel load in {kN} (P = 38.1 kN)

r = radius of tire print {m} (r = 0.133 m)

N = number of traffic passes

R_E = modulus ratio = $E_{bc}/E_{sg} \leq 5$ (R_E = 5)

E_{bc} = base course resilient modulus {MPa}

E_{sg} = subgrade resilient modulus {MPa}

f_s = rut depth factor {mm} (f_s = 75 mm)

s = maximum rut depth {mm} (s = 75 mm)

N_c = bearing capacity factor (3.14 for unreinforced roads, 5.14 for geotextile roads, 5.71 for geogrid reinforced roads)

$S_{u\text{-}sg}$ = undrained shear strength of the subgrade {kPa}

Values for the aperture stability modulus (J) were available for the majority of the geogrids and are listed in Table 18; however, missing values were assumed (as indicated in Table 18); J is taken as zero for the geotextiles. For materials CoG-4 and WeG-6, the limiting value of J of 0.81 was used in the analysis. Table 18 also lists the number of traffic passes to reach a depth 100 mm of rut observed in the test sections and the composite subgrade CBR after trafficking for each test section. Equation 9 was used to predict the required base thickness, which is compared to the constructed base thickness which led to the N_{field} values observed (Figure 72). Comparison of the required base thickness predicted by the Giroud and Han (2004) method to the constructed base thickness shows that, overall, this method significantly underpredicts the amount of aggregate needed to support the observed traffic. This amount of underprediction is most significant for the geogrid sections and for those sections with larger values of aperture stability

modulus. For the two sections with the greatest values of aperture stability modulus, the solution produces illogical results.

Table 18. Summary of Test Section Properties and Performance for the Giroud and Han Method

Geosynthetic Test Section	*J* (N-m/degree)	N_{field}	Composite Subgrade CBR after Trafficking	Required Base Thickness (mm)
Control 1	0	13.5	1.31	166
WeG-1	0.5†	78.3	1.20	174
WeG-2	0.526	87.4	1.25	124
IFG-3	0.650	80.0	1.32	95
CoG-4	2.00	87.4	1.30	33
IFG-5	0.320	36.3	1.25	144
WeG-6	1.82	67.6	1.16	39
WoG-7	0.15†	96.4	1.46	145
WoG-8	0.15†	70.9	1.31	156
WoT-9	0	52.1	1.30	141
NWoT-10	0	34.0	1.29	132
Control 2	0	18.6	1.40	168

† value of aperture stability modulus (*J*) was assumed

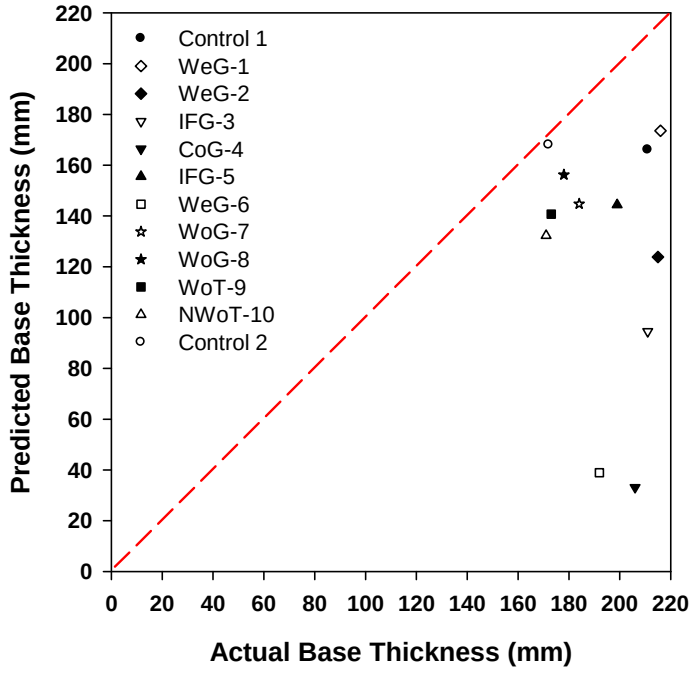

Figure 72. Comparison of actual and predicted base thickness using the Giroud and Han method.

5.5.2 Empirical Performance Comparisons

In this section, engineering judgment involving simple and empirical comparisons between test sections are made to correct for differences in aggregate thickness and subgrade strength such that product performance can be more directly compared. The three variables that dictated performance in these test sections were subgrade strength, base course thickness and the properties of the geosynthetic. For purposes of making corrections for differences in aggregate thickness and subgrade strength by simple and empirical comparisons, it is necessary to have at least two sections that can be viewed as duplicates of each other and where differences in aggregate thickness and subgrade CBR exist. These two sets of test sections are the two control sections and the WeG-2 and WeG-6 test sections, which used a welded geogrid from the same manufacturer that had approximately the same tensile strength properties, manufacturing process and aperture size (see Table 5, page 11).

Three equations (Equation 10, 11 and 12) were developed to adjust the number of traffic passes seen in the field (N_{field}) for small differences in aggregate thickness and subgrade strength as these values deviated from the target values of 200 mm and 1.7 CBR, respectively. In Equation 10 and Equation 11, the variables ΔN_{agg} and ΔN_{sub} are the change in the number of traffic passes that a particular test section would experience based on differences of base course aggregate thickness and subgrade strength, respectively. The variables C_{agg} and C_{sub} are correction factors for aggregate thickness and subgrade CBR and have units of traffic pass per mm of aggregate and traffic passes per subgrade CBR, respectively, and T_i and CBR_i are the measured aggregate thickness and subgrade CBR of each test section. The corrected number of traffic passes (N_{corr}) that would have occurred in each of the test sections based on their base course aggregate thickness and subgrade strength was calculated using Equation 12. Equation 10 and Equation 11 were simultaneously solved by varying values of C_{agg} and C_{sub} using a numerical solver while assuming that the N_{corr} values in the two control sections were the same and the N_{corr} values in WeG-2 and WeG-6 test sections were also the same. This resulted in values of C_{agg} and C_{sub} of 0.22 traffic passes per mm of base course aggregate and 122.5 traffic passes per subgrade CBR, respectively.

$$\Delta N_{agg} = C_{agg}(200 - T_i) \qquad \textbf{Equation 10}$$

$$\Delta N_{sub} = C_{sub}(1.7 - CBR_i) \qquad \textbf{Equation 11}$$

$$N_{corr} = N_{field} + \Delta N_{agg} + \Delta N_{sub} \qquad \textbf{Equation 12}$$

Values of N_{corr} were then used to compute the additional number of traffic passes that each reinforced section carried as compared to the control sections, hereby referred to as N_{add}. This

analysis was carried out using N_{field} values corresponding to mean rut depths of 25, 50, 75 and 100 mm. Results from this analysis are tabulated in Table 19 and shown graphically in Figure 73.

Table 19. Summary of Additional Traffic Passes, N_{add} at Various Rut Depths

Geosynthetic Test Section	N_{add} at various rut depths			
	25 mm	50 mm	75 mm	100 mm
WeG-1	6.4	25.7	49.2	81.5
WeG-2	5.2	26.0	54.1	82.9
IFG-3	6.7	33.6	52.4	65.2
CoG-4	1.8	15.2	43.1	77.1
IFG-5	2.4	15.4	26.7	35.3
WeG-6	5.2	26.0	54.1	82.9
WoG-7	2.5	18.5	45.7	65.8
WoG-8	3.6	16.6	34.6	65.6
WoT-9	1.2	12.7	26.3	49.4
NWoT-10	2.8	9.3	21.0	33.3

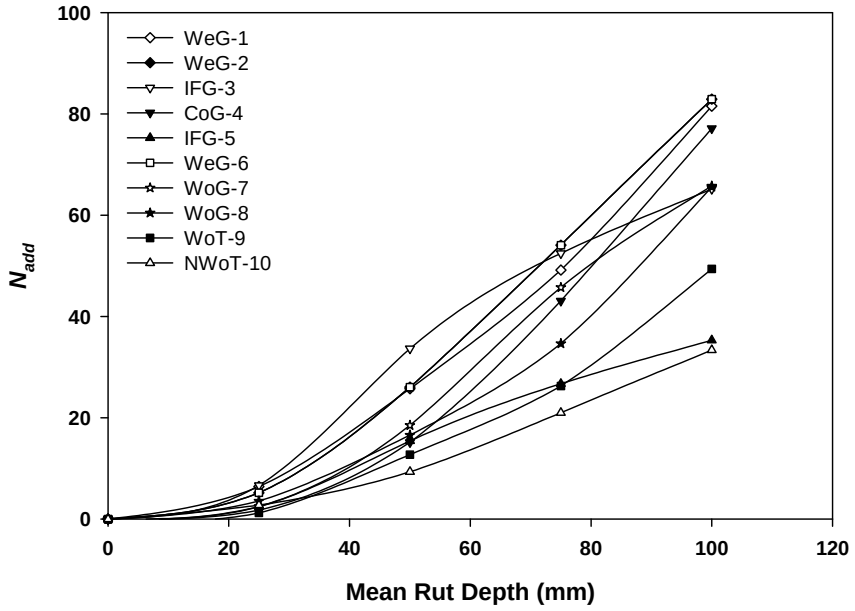

Figure 73. Relationship of N_{add} to mean rut depth at given rut depths.

Differences in the relative performance between the various test sections are most prominent at larger mean rut depths. Similar to the raw results shown in Figure 54 (page 53), lines that have lower slopes indicate poorer performance, whereas lines of greater slope indicate better performance. The shape of the line (i.e., concave up versus concave down) indicates improving

performance versus declining performance, respectively. In general, most test sections show a concave up trend indicating that performance is improving as the mean rut depth increases. Nevertheless, the IFG-3, IFG-5 and WoG-7 test sections showed a concave down trend, indicating that as the rut depth increased, the benefit of the geosynthetic was decreasing. Damage sustained in the two integrally-formed geogrids during the forensic excavations substantiated this trend (see Section 4.1.3). This trend was somewhat less pronounced in the WoG-7 test section. Broad categories were assigned based on a visual interpretation of the trends in Figure 73 to help make general distinctions between the overall performance of the various products with respect to mean rut depth. When considering the performance at 50 mm of rut, the IFG-3 product performed the best, the welded geogrids WeG-1, WeG-2 and WeG-6 performed average and the remaining products performed worse than these. When considering the performance at 75 mm of rut, several products make a dramatic shift to indicate better performance. In this case, the welded geogrid test sections (WeG-1, WeG-2, CoG-4 and WeG-6), the IFG-3 test section and the WoG-7 test sections performed the best, the WoG-8 performed average and the remaining products (WoT-9, IFG-5 and NWoT-10) performed the worst. Lastly, when considering the performance at 100 mm of rut, there seems to be four distinct categories. The welded geogrids (WeG-1, WeG-2, CoG-4 and WeG-6) were in the first category which performed the best overall. The second category performed slightly worse than these and included the two woven geogrids (WoG-7 and WoG-8) and the stronger integrally formed geogrid (IFG-3). Next, the woven geotextile test section (WoT-9) performed somewhat below average, while the integrally-formed geogrid (IFG-5) and the non-woven geotextile (NWoT-10) performed the worst overall. In conclusion, the welded geogrids, woven geogrids and the stronger integrally formed geogrid seemed to provide the best overall performance, while the two geotextile products and the weaker integrally formed geogrid provided significantly less stabilization benefit.

The reasons for poorer performance can be partly explained considering the evidence collected during the forensic investigations. The main reason the woven geotextile performed poorly is because it pulled out from the edges during trafficking. This product had a relatively smooth texture which required that it have more development length to ensure that it was anchored in the soil adjacent to the rutted area. The non-woven geotextile performed relatively poorly because it has significantly less tensile strength in the cross-machine direction than the other products, which made it less effective at reinforcing the rutted area through the membrane effect. The reason the weaker integrally-formed geogrid performed the poorly is because it ruptured in the machine direction in both ruts which significantly reduced its ability to carry load in the cross-machine direction during trafficking.

Regardless of the fact that a number of geosynthetic properties may be working together to stabilize the weak subgrade, it is believed that the majority of the benefit derived from these products was due to their ability to support loads in a direction transverse to the applied load, i.e.,

the cross-machine direction of the geosynthetic. As previously discussed, early loading within the test sections involves lateral restraint of the aggregate, while later loading involves a tensioned-membrane effect. Therefore, tensile stiffness and tensile strength are most likely key material properties. A direct comparison between tensile strength in the cross-machine direction (at 2 and 5 percent tensile strain) and N_{add} (at 75 mm and 100 mm of mean rut depth) was made to investigate whether rutting performance was related to tensile strength in the cross-machine direction. Plots of tensile strength in the cross-machine direction with respect to N_{add} at 75 mm and 100 mm of mean rut depth are shown in Figure 74 and Figure 75, respectively. These plots show a relatively good correlation between the 2 percent tensile strength in the cross-machine direction and N_{add}, and a fair correlation between the 5 percent tensile strength in the cross-machine direction and N_{add}, as indicated by the R^2 values shown in these figures. A y-intercept value of zero was used in this linear regression analysis because the absence of geosynthetic tensile strength should result in a value of N_{add} equal to zero. Various other comparisons were made using 2 percent, 5 percent and ultimate tensile strength in the cross-machine direction, and N_{add} at 25 mm and 50 mm of rut, but produced significantly poorer correlations.

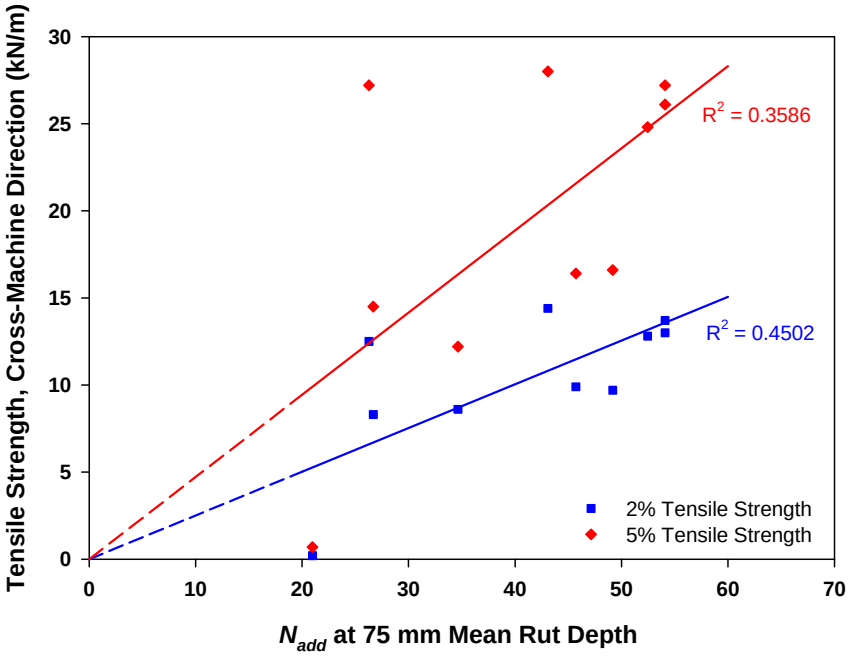

Figure 74. Relationship between geosynthetic tensile strength in the cross-machine direction and N_{add} at 75 mm of mean rut depth.

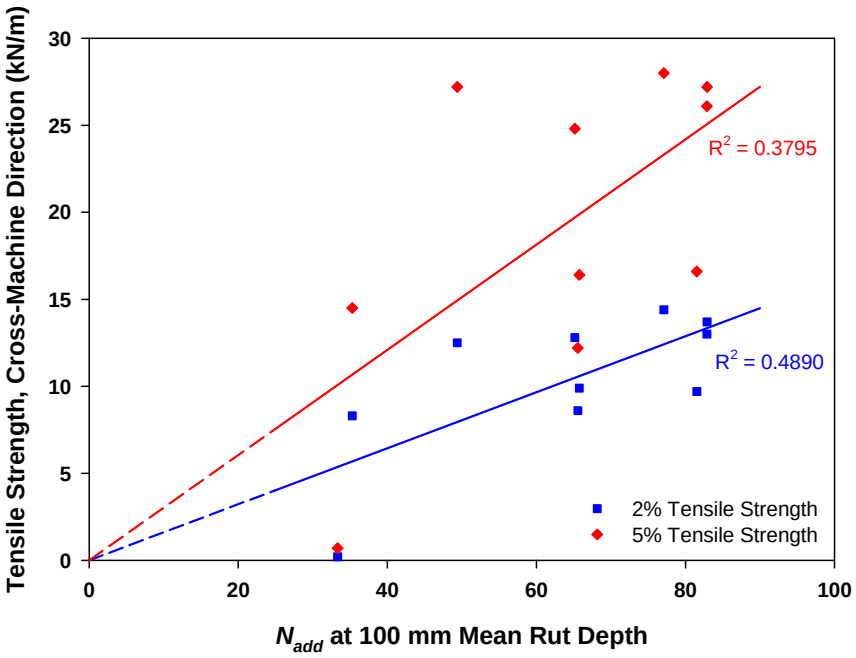

Figure 75. Relationship between geosynthetic tensile strength in the cross-machine direction and N_{add} at 100 mm of mean rut depth.

6 SUMMARY, CONCLUSIONS AND RECOMMENDATAIONS

This research was initiated to gain a greater understanding of which geosynthetic material properties are most relevant when they are used as subgrade stabilization as the Montana Department of Transportation seeks to update its specifications to more broadly encompass materials with which they have had good experience, as well as open up the application to other suitable materials. This is particularly important since new geosynthetics and manufacturing processes are regularly introduced into the market.

6.1 Summary

To achieve these objectives, a full-scale field test section was constructed, trafficked, and monitored at TRANSCEND, a full-scale transportation research facility managed by the Western Transportation Institute, to compare the relative performance of 12 test sections – ten with geosynthetics and two without geosynthetics. Existing pavement and base materials were excavated from the site to create a trench where an artificial subgrade (A-2-6 material) was placed in a weak condition. In-field measurements of vane shear, moisture content and DCP were primarily used to monitor subgrade strength during construction and after trafficking. Results from these tests showed that the subgrade soil was indeed weak and generally similar between test sections, especially for the upper layers which were primarily responsible for carrying the vehicle loads. After installation of the geosynthetics on top of the subgrade, displacement and pore water pressure sensors were installed at a single location along the length of each of the test sections. Approximately 20 centimeters of crushed base course aggregate (A-1-a material) was placed in a single lift as a structural layer and driving surface. The depth of the base course was determined using the FHWA U.S. Forest Service method (FHWA, 1995). Once the subgrade material was placed, all construction equipment was prevented from driving on the test area, and the base course layer was placed, leveled and graded from the side of the test area.

A fully loaded, three-axle dump truck was used to traffic the test sections. Measurements of longitudinal rut, transverse rut, displacement of the geosynthetic and pore pressures within the subgrade were taken during trafficking. Longitudinal ruts measurements were made within each of the two ruts at 1-meter increments along the entire length of the test sections for given truck passes, more frequently in the beginning and less frequently in the end. Displacement and pore water pressure was collected at 200 Hz to capture dynamic responses due to the passage of the test vehicle. Individual axle passes were evident in both the displacement and pore pressure data traces. Most displacement measurements were reasonable up to about 22 or more passes of the truck. After that time, many of the test sections experienced large ruts which distorted the gaged area and thus made the displacement measurements meaningless. Dynamic strain measurements made in the sidewall of the rut during trafficking were generally the greatest and had a magnitude less than 2 percent. Static strain measurements were around 3 to 5 percent in most

materials; the greatest strain was in the non-woven geotextile (14 or more percent at 100 mm average rut depth). Dynamic pore pressure measurements during trafficking were generally less than 2 kPa, and static levels of pore pressure were generally less than 9 kPa for all test sections. These changes in pore pressure decreased the strength only slightly (0.1 CBR on average).

Failure, defined as 100 mm of elevation rut, occurred in each of the test sections at or before 40 truck passes (88 traffic passes) of a fully-loaded, three-axle dump truck, which was much less than the 1000 design traffic passes expected from the geosynthetic-stabilized sections. The two control sections failed earliest, followed successively by sections NWoT-10, IFG-5 and WoT-9. The ruts in these sections were filled in to facilitate additional traffic on the remaining test sections. Following stringent guidelines to ensure equality in the subgrade strength and base thickness between the test sections, the test sections were similar, yet small differences did exist in the finished construction characteristics, namely, subgrade strength and base course thickness. Although these differences were small, they may have accounted for larger differences in performance between test sections, given the fact that most test sections performed relatively similarly. An empirical approach was used to normalize these differences so that a more direct comparison between test sections could be made. The empirical approach normalized the thickness of the base course and the strength of the subgrade using test plots that had similar properties. Soil subgrade strength values determined during the post-trafficking forensic evaluations were used in this analysis. The result of this procedure was the number of additional traffic passes (N_{add}) necessary to fail the test section as compared to what was needed to fail the control test sections.

In light of the fact that the FHWA design method grossly overestimated the number of traffic passes that actually occurred on site, a comparative analysis was conducted using the design method developed by Giroud and Han (2004). This analysis was used to compare the actual and predicted base course layer thickness using information from each of the test sections (subgrade strength, number of traffic passes and aperture stability modulus of the geosynthetic). The results revealed that this method also significantly underpredicted the base thickness.

Post-trafficking forensic excavations were conducted in areas containing similar rut depth at failure (100 mm average rut over a two-meter length of test section) to assess damage to the geosynthetics from trafficking. Vane shear, moisture content and DCP measurements were also taken to evaluate soil strength in the excavated areas after trafficking. Compressed air and a large vacuum truck were used to excavate the base course aggregate from the surface of the geosynthetics to minimize damage to the reinforcement during the forensic investigations. After removal of the base material, approximately 6 square meters of geosynthetic were extracted from these areas to be qualitatively evaluated for junction and rib intactness. As expected, the majority of the damage occurred in rutted area, and damage outside of these areas was minimal. The junctions in the welded and woven geogrids were mostly intact (range of 72.7 to 93.2 percent intact). Rib damage in these same geogrids was minimal (93.1 to 99.9 percent intact).

Rupture damage occurred in the integrally-formed geogrids within the rut bowl. Approximately 90 percent of the IFG-3 product (the stronger of the two integrally-formed geogrids) was ruptured and the IFG-5 material was entirely ruptured in the longitudinal direction in both ruts. Reverse excavations were also conducted to evaluate whether or not damage was induced in the welded geogrids during the forensic excavations. Samples that were excavated from underneath did not show significant difference in junction damage.

Soils strength in the excavated areas was generally similar yet, according to the results of the vane shear, had lower strength than after construction. The DCP did not show significant difference in shear strength. Moisture contents collected during construction and after trafficking did not change significantly.

6.2 Conclusions

From the work performed in this project, the following conclusions can be made:

- To be able to more directly evaluate a geosynthetic's ability to stabilize weak subgrades, it is important to minimize differences in the subgrade strength and base course thickness between test sections. Despite arduous efforts made on this behalf during the construction phase, even small differences between test sections created some difficulty in making these direct comparisons. Nevertheless, defensible conclusions as to which geosynthetics performed better than others were made using a simple empirical analysis. Based on the normalized rutting performance at 50, 75 and 100 mm of rut, the welded geogrids, woven geogrids and the stronger integrally formed geogrid product seemed to provide the best overall performance, while the two geotextile products and the weaker integrally formed geogrid provided significantly less stabilization benefit. These test sections failed rapidly (< 40 truck passes); therefore, it is probable that different results may be seen for sections that do not fail as quick.
- The FHWA design method underpredicts the depth of base aggregate needed to support the loads applied during this study as evidenced by the reduced number of traffic passes sustained by any of the test sections. Outside of inherent design limitations, two other possible reasons for premature failure may be the quality and/or in-place strength of the base course aggregate and the increased tire pressures in the test vehicle when compared to the tire pressures used to formulate the design methodology. Using the material properties of the actual test sections as inputs, the Giroud and Han (2004) design method also grossly underpredicted the depth of base material needed to support the loads applied during trafficking.
- This research project attempted to relate readily-available geosynthetic properties to field performance when these materials were used as subgrade stabilization. An

exhaustive comparison of which material parameters dictated the performance of each test section was beyond the scope of this project; however, based on the empirically-derived comparative analysis conducted during this study, tensile strength at 2 percent axial strain (indicative of the stiffness of the geosynthetic) in the cross-machine direction of the geogrids likely plays a significant role in suppressing rut formation under these conditions. In addition, tensile strength in the cross-machine direction at 5 percent axial strain is also related to performance, although to a lesser extent. It is unclear as to which material or interaction properties are most relevant for geotextiles; however, the function of separation likely aided the non-woven geotextile and composite welded geogrid stabilize the weak subgrade. Further research is needed to pinpoint which geosynthetic material properties most directly relate to stabilization of weak subgrade soils.

- Displacement of the geosynthetics in each of the test sections was generally similar with respect to the direction and initial magnitude of response. Initially, the wheel loads pushed the geosynthetic away from the side of the vehicle toward the outer edge of the test sections. As the rut bowl began to form, these measurements showed that the geosynthetic began to move in the opposite direction (toward the rutted area). Therefore, using the displacement measurements, it was possible to perceive the primary reinforcement mechanism of the geosynthetics shift from lateral restraint of the base course to the membrane effect. This effect was perceptible in all of the test sections, regardless of their rate of failure. Dynamic strain during trafficking in the geosynthetic was relatively small (~2 percent), and static strain measurements were around 3 to 5 percent in most materials, and greatest in the non-woven geotextile (14+ percent at 100 mm rut).
- Limited static and dynamic pore pressure measurements made during trafficking yielded low values of pore pressure which only slightly reduced the overall strength of the subgrade. Pore pressure development in the subgrade, however, depends on the material composition of the soils that make up this layer.
- The majority of junction and rib damage occurred in the rutted area. Junction damage was greatest in the WeG-1 material (27.4 percent damage) and least in the WoG-7 material (6.8 percent). Rib damage was minimal in the welded and woven products. Both of the integrally-formed grids sustained rupture damage during trafficking, which was seen to directly impact their ability to support the traffic loads, and this phenomenon had a more profound affect on the IFG-5 test section than in the IFG-3 test section. Reverse excavations were successful in showing that very little damage was induced in the geosynthetics while being excavated during the forensic investigations.

- The vane shear showed a good correlation to CBR and was a quick and simple method of quality control during construction of the test sections.
- The apparent rut (measured as the vertical distance between the crest of the rut bowl to the bottom of the trough) is much greater than the elevation rut (measured as the change in vertical elevation of a point at the center of the wheel path).

6.3 Recommendations for Future Work

The results of this study indicated that tensile strength at 2 percent axial strain correlated to performance for the majority of the geosynthetics used. Other properties may also be important as indicators of performance for those materials that did not seem to fit this trend. Additional research is needed to determine other material tests and to relate these results to field performance. Tensile stiffness appears to be the most pertinent material property (based on the results found during this research); therefore, additional properties such as cyclic tensile modulus and Poisson's ratio may be combined together to reflect a single indicator of tensile stiffness that relates well to field performance.

The test sections constructed in this project failed under a relatively small number of traffic passes. While this work provided useful information on performance of geosynthetics under loads producing gross failure, additional work is recommended to study conditions pertinent to operating conditions of a greater number of passes. These conditions will show differences in products for safe operating conditions, while the results from this project will provide information to help avoid gross and rapid failure. It is also recommended that new test sections constructed for operating conditions be used for a second stage of testing, which would involve regrading the rutted base layer and surfacing with asphalt concrete. This would mimic the entire process of subgrade stabilization and base reinforcement and would provide valuable information on how these two functions work together.

To better understand the reasons why various geosynthetics perform differently under the same conditions, the relationship between several geosynthetic material properties and performance needs to be more thoroughly investigated. To facilitate this, a new series of controlled test sections need to be constructed that are less likely to fail as rapidly as those in this study, which can be accomplished simply by increasing the depth of the base course aggregate. The performance data from these new test sections can be used as the basis to create models which are better suited to relate various geosynthetic material properties to their field performance. This will provide a more complete assessment of which geosynthetic properties (or combinations thereof) directly relate to their ability to reinforce or stabilize weak subgrades. Increased instrumentation in the field will also help understand the behavior of the geosynthetics, subgrade and base course aggregate as they are subjected to traffic loading. Small scale laboratory tests may also be necessary to more fully control and understand these behaviors.

7 REFERENCES

Benson, C.H., Edil, T.B., Tanyu, B.F., and Kim, W.-H. (2005) Equivalency of Crushed Rock with Industrial By-Products and Geosynthetic-Reinforced Aggregates Used for Working Platforms During Pavement Construction. Wisconsin Highway Research Program, Final Report No. 0092-00-12, 100pp.

Christopher, B.R., Perkins, S.W., Lacina, B.A., and Marr, W.A. (2009) "Pore Water Pressure Influence on Geosynthetic Stabilized Subgrade Performance." Proceedings: Geosynthetics 2009, February 25-27, Salt Lake City, UT, pp.215-221.

Cuelho, E.V., Christopher, B.R., Perkins, S.W. (2008) "Small Strain and Displacement Monitoring Methods for Geosynthetics under Monotonic and Cyclic Loading" Proceedings: Geoamericas 2008 Conference, IFAI, March 2-5, Cancun, Mexico.

Edil, T.B., Benson, C.H., Senol, A., Bin-Shafique, M.S., Tanyu, B.F., and Kim, W.-H. (2002) Field Evaluation of Construction Alternatives for Roadway Over Soft Subgrade. Wisconsin Highway Research Program, Interim Report, 65pp.

Fannin, R.J. and Sigurdsson, O. (1996) "Field Observations on Stabilization of Unpaved Roads with Geosynthetics." Journal of Geotechnical Engineering. vol 122, no. 7, pp.544-553.

FHWA (1995) Geosynthetic Design and Construction Guidelines, Federal Highway Administration, Report No. FHWA-HI-95-038, 417pp.

Gabr, M (2001) Cyclic Plate Loading Tests on Geogrid Reinforced Roads. Research Report to Tensar Earth Technologies, Inc., NC State Univ., 43pp.

Gabr, M.H., Robinson, B., Collin, J.G., and Berg, R.R. (2006) Promoting Geosynthetics Use on Federal Lands Highway Projects. Central Federal Lands Highway Division, Final Report No. FHWA-CFL/TD-06-009, 116pp.

Giroud, J.P., Ah-Line, C., and Bonaparte, R. (1985) "Design of Unpaved Roads and Trafficked Areas with Geogrids.'' Proceedings of a Conference Sponsored by the Science and Engineering Research Council, *Polymer Grid Reinforcement*, London: Thomas Telford Ltd, pp.116–127.

Giroud, J.P. and Han, J. (2004) "Design Method for Geogrid-Reinforced Unpaved Roads. Parts I and II." Journal of Geotechnical and Geoenvironmental Engineering. vol 130, no. 8, pp.775-797.

Giroud, J.P. and Noiray, L. (1981) "Geotextile-Reinforced Unpaved Road Design." Journal of Geotechnical Engineering. vol. 107, no.9, pp.1233–1254.

Hammitt, G. M (1970) Thickness Requirement for Unsurfaced Roads and Airfields, Bare Base Support, Project 3782-65. U.S. Army Engineer Waterways Experiment Station, Technical Rep. S-70-5, CE, Vicksburg, Miss, 139pp.

Holtz, R.D., Christopher, B.R. and Berg, R.R. (2008) Geosynthetic Design and Construction Guidelines. U.S. Department of Transportation, Federal Highway Administration, Washington DC, Report No. FHWA-NHI-07-092, 592 pp.

Hufenus, R., Rueegger, R., Banjac, R., Mayor, P., Springman, S.M., and Bronnimann, R. (2006) Full-Scale Field Tests on Geosynthetic Reinforced Unpaved Roads on Soft Subgrade. Geotextiles and Geomembranes. vol. 24, no. 1, pp. 21–37.

Leng, J. (2002) Characteristics and Behavior of Geogrid-Reinforced Aggregate Under Cyclic Load. PhD Thesis. North Carolina State University, 164pp.

Maxwell, S., Kim, W.-H., Edil, T.B., and Benson, C.H. (2005) Geosynthetics in Stabilizing Soft Subgrades with Breaker Run. Wisconsin Highway Research Program, Final Report No. 0092-45-15, 88pp.

NHI – National Highway Institute (2008) "Chapter 5: Geosynthetics in Roadways and Pavements" Geosynthetics Engineering, National Highway Institute, Report No. FHWA-NHI-07-092, 92pp.

Perkins, S.W. (2002) Evaluation of Geosynthetic Reinforced Flexible Pavement Systems Using Two Pavement Test Facilities. Montana Department of Transportation, Final Report No. FHWA/MT-02-008/20040, 136pp.

Perkins, S.W., Bowders, J.J., Christopher, B.R., and Berg, R.R. (2005) "Geosynthetic-Reinforcement for Pavement Systems: US Perspectives." Proceedings: Geo-Frontiers 2005, ASCE Geotechnical Special Publications 130-142, American Society of Civil Engineers, Reston, VA, pp.3039-3063.

Santoni, R.L., Smith, C.J., Tingle, J.S., and Webster, S.L. (2001) Expedient Road Construction Over Soft Soils. U.S. Army Corps of Engineers, Final Report No. ERDC/GSL TR-01-7, 107pp.

Steward, J., Williamson, R. and Mohney, J. (1977) Guidelines for Use of Fabrics in Construction and Maintenance of Low-Volume Roads. USDA, Forest Service, Portland, OR. Also reprinted as Report No. FHWA-TS-78-205, Federal Highway Administration, Washington, D.C.

Tingle, J.S. and Webster, S.L. (2003) "Corps of Engineers Design of Geosynthetic-Reinforced Unpaved Roads" Transportation Research Record 1849, pp.193-201.

Watn, A., Eiksund, G., Jenner, C., and Rathmayer, H. (2005) "Geosynthetic Reinforcement for Pavement Systems: European Perspectives." Proceedings: Geo-Frontiers 2005, ASCE Geotechnical Special Publications 130-142, American Society of Civil Engineers, Reston, VA, pp.3019-3037.

Yoder, E.J. and Witczak, M.W. (1975) *Principles of Pavement Design*. New York: Wiley.

Appendix A

Geosynthetic Properties from Manufacturers' and Wide-Width Test Results from WTI Laboratory

Table A-1. Geosynthetic Material Properties for Rolls Used in This Study as Provided by Manufacturers

Geosynthetic Test Section[a]	Generic Specifications Published by Manufacturers: Strength[b] @ 2% (kN/m) MD	XMD	Strength[b] @ 5% (kN/m) MD	XMD	Ultimate[b] Strength (kN/m) MD	XMD	Actual Test Information from Production Lot Tested by Manufacturers: Strength[b] @ 2% (kN/m) MD	XMD	Strength[b] @ 5% (kN/m) MD	XMD	Ultimate[b] Strength (kN/m) MD	XMD	Junction Strength[c] (kN/m) MD	Production Lot (Roll) Information	Test Date
WeG-1	11	NP	22	NP	30	NP	NP		NP		NP		NP		
WeG-2	8	8	16	16	20	20	13.5	13.4	27.1	27.4	39.3	40.2	11.85	0013209113	06/04/08
IFG-3	6.0	9.0	11.8	19.6	19.2	28.8	6.9	12.0	13.3	23.6	21.4	32.0	21.2	111353 (#031)	05/17/08
CoG-4	12	12	24	24	30[d]	30[d]	15.2	14.8	30.3	30.2	42.5	45.2	12.2	0013220898	06/05/08
IFG-5	4.1	6.6	8.5	13.4	12.4	19.0	6.8	5.8	10.1	17.1	14.3	21.3	14.4	39522 (#088)	05/17/08
WeG-6	12	12	24	24	30	30	14.4	14.0	29.2	28.7	43.8	41.7	14.0	0013221988	06/05/08
WoG-7	7.3	7.3	13.4	13.4	29.2	29.2	11.9	11.1	21.3	18.4	41.6	60.1		033072629	
WoG-8	7.7	8.4	11.5	15.2	34.9	56.5	NP		NP		35.5	62.7	NP	28/103/02-171	
WoT-9	8.8	8.8	21.9	21.9	52.5	47.3	8.8	8.8	21.9	21.9	52.5	47.3		953294549	
NWoT-10	NP		NP		912[e]		NP		NP		NP		NP		

a = Acronym meanings: WeG = welded grid, IFG = integrally-formed grid, CoG = composite grid, WoG = woven grid, WoT = woven textile, NWoT = non-woven textile; numbers represent position along length of test site

b = ASTM D 6637

c = GRI-GG2

d = Non-woven portion of this material increases the ultimate strength by 6 kN/m in the MD and by 10 kN/m in the XMD

e = Grab tensile strength (ASTM D-4632) in Newtons at 50% elongation

NP - information was not provided by the manufacturer

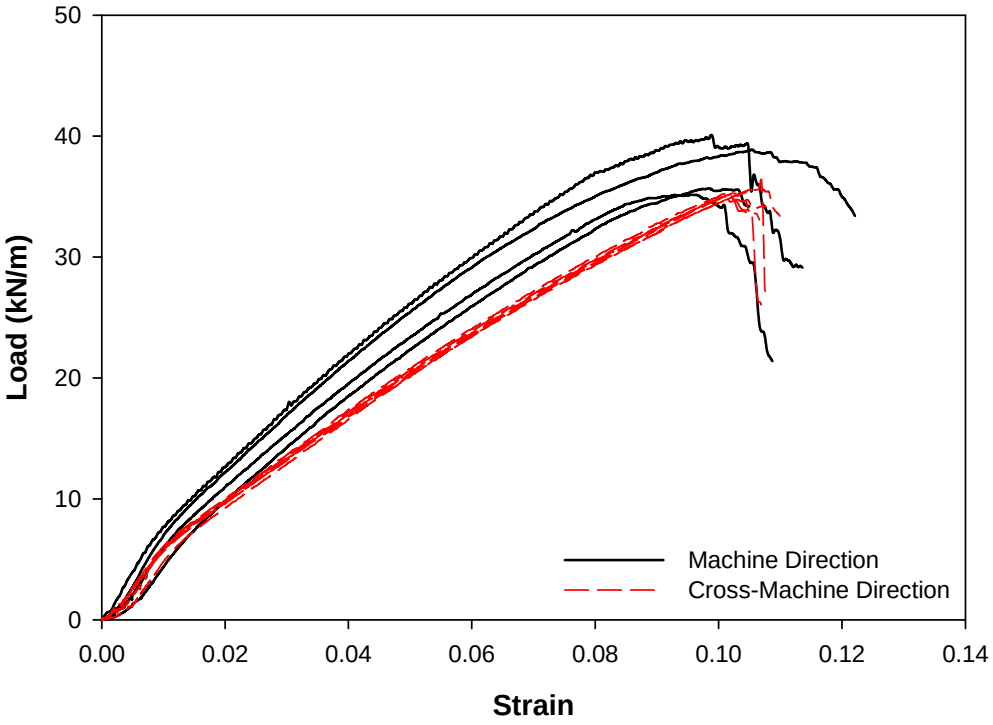

Figure A-1. WTI wide-width tension results for the WeG-1 geogrid.

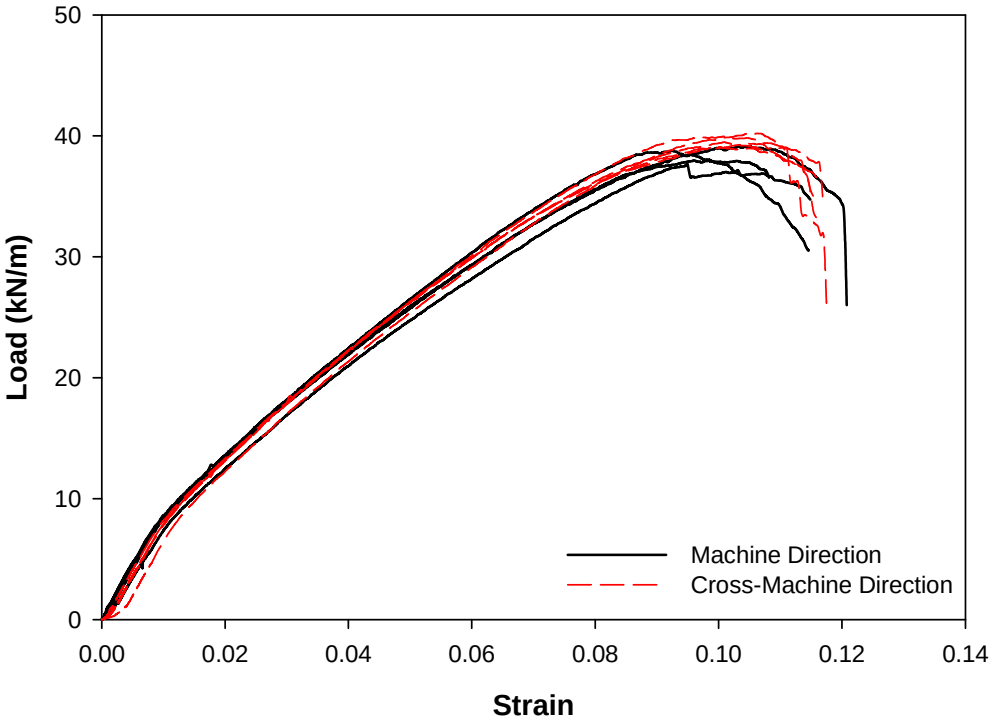

Figure A-2. WTI wide-width tension results for the WeG-2 geogrid.

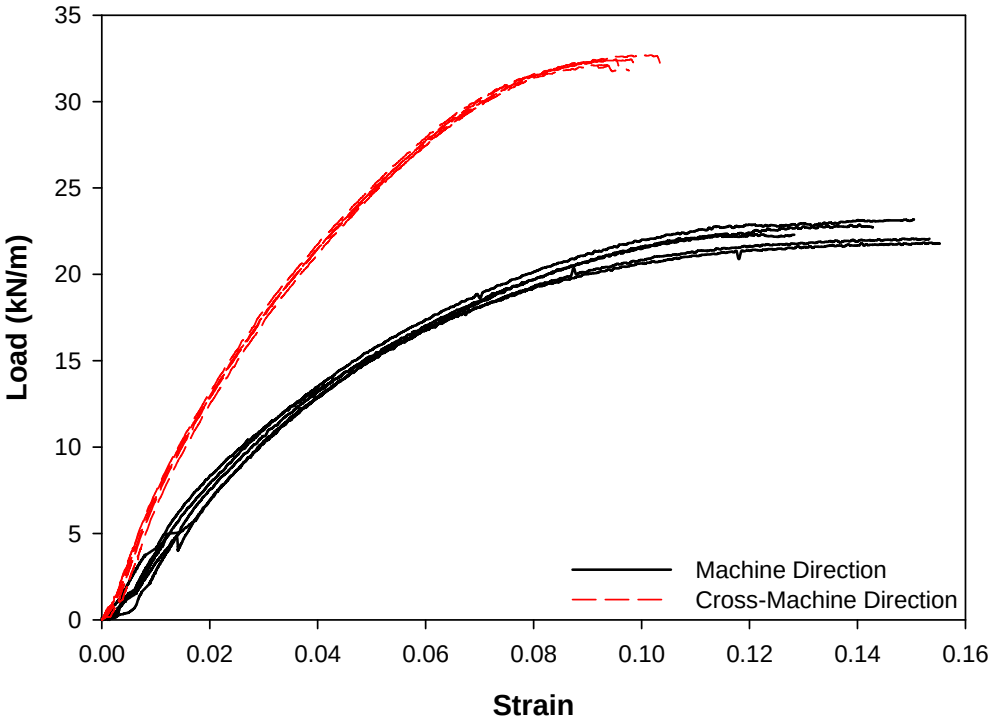

Figure A-3. WTI wide-width tension results for the IFG-3 geogrid.

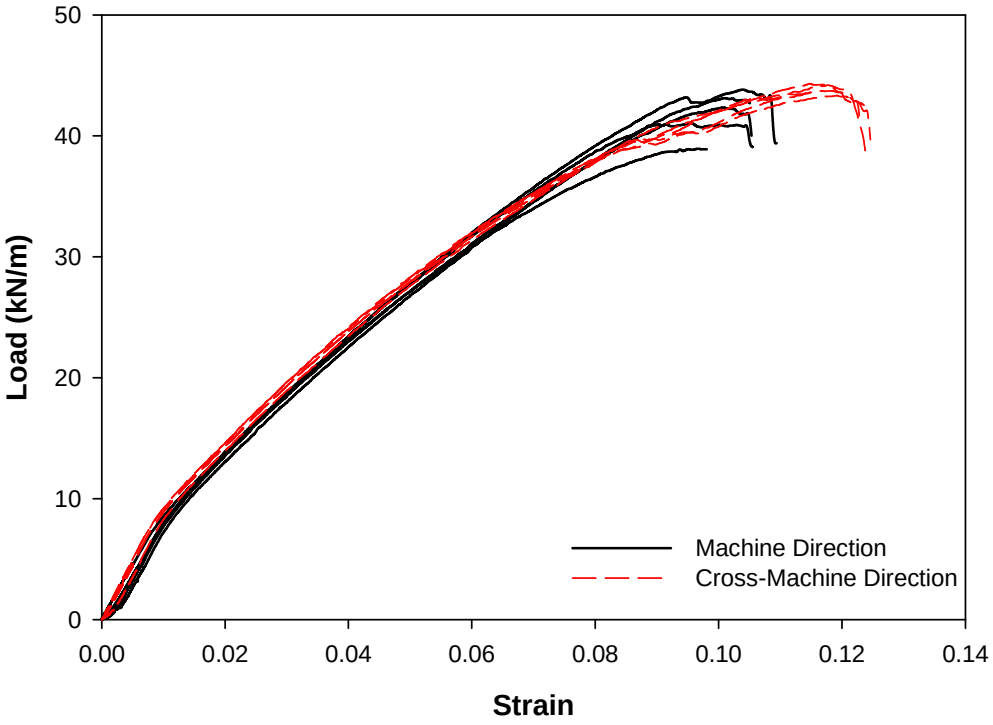

Figure A-4. WTI wide-width tension results for the CoG-4 geogrid.

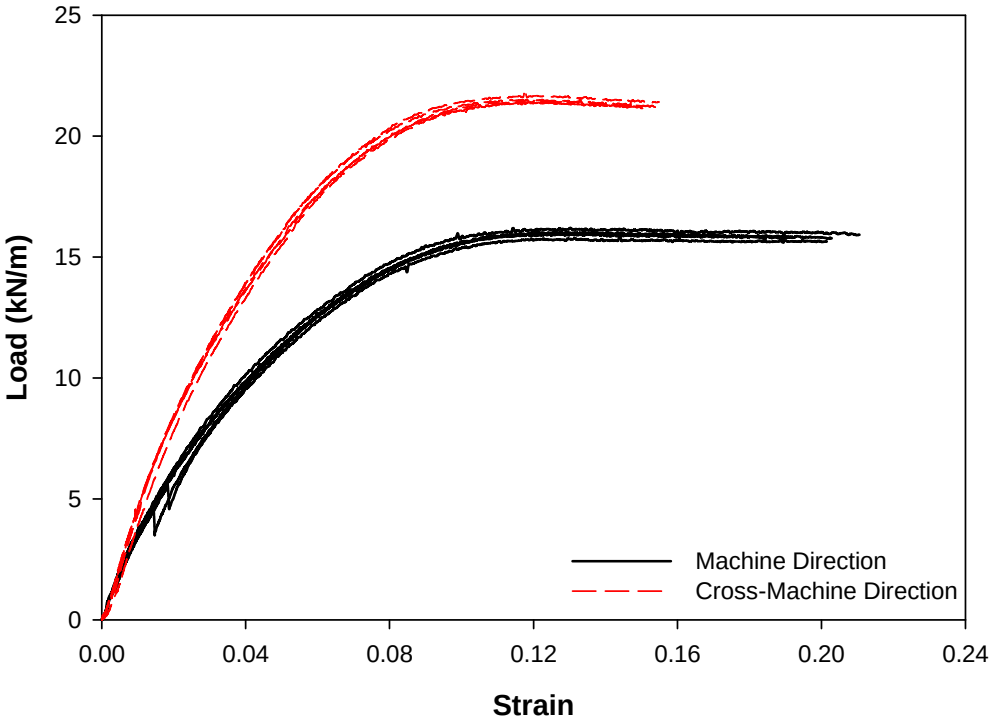

Figure A-5. WTI wide-width tension results for the IFG-5 geogrid.

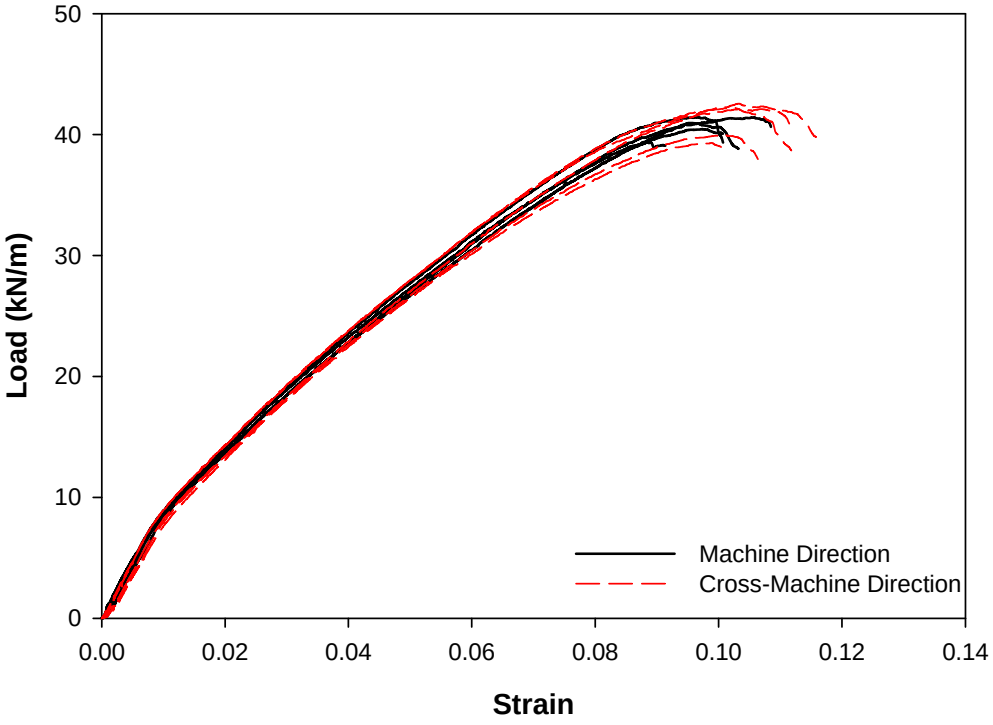

Figure A-6. WTI wide-width tension results for the WeG-6 geogrid.

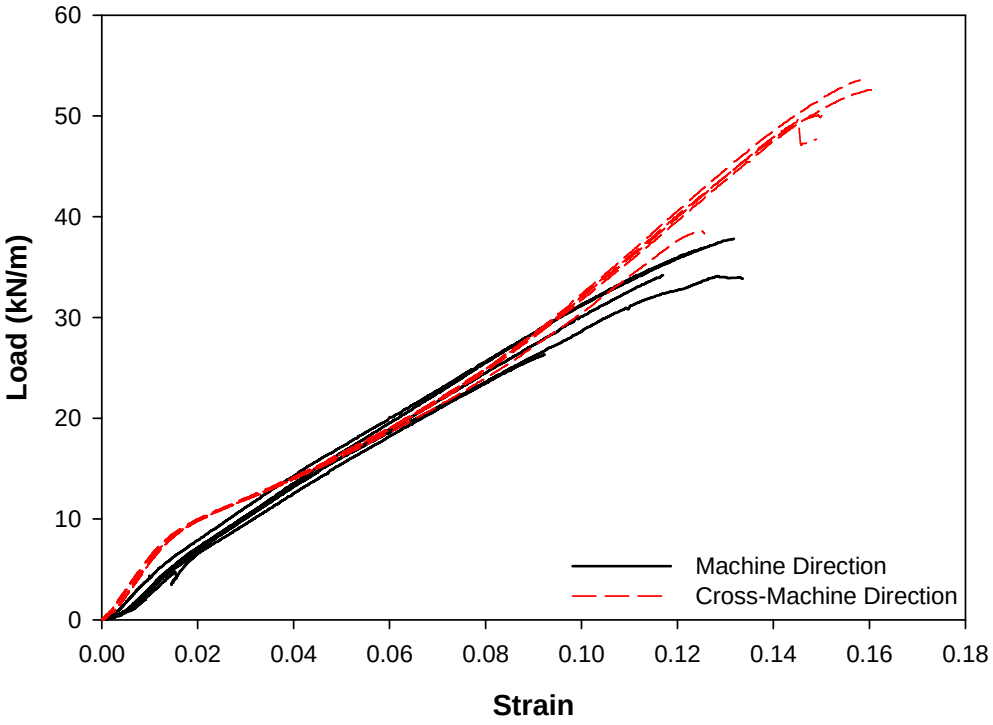

Figure A-7. WTI wide-width tension results for the WoG-7 geogrid.

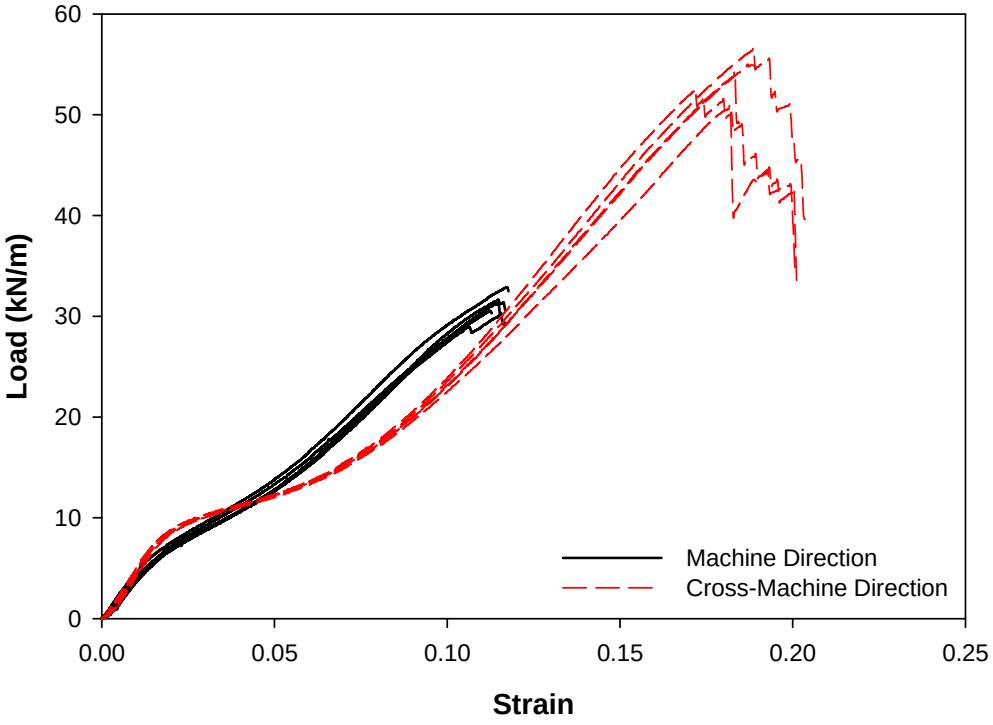

Figure A-8. WTI wide-width tension results for the WoG-8 geogrid.

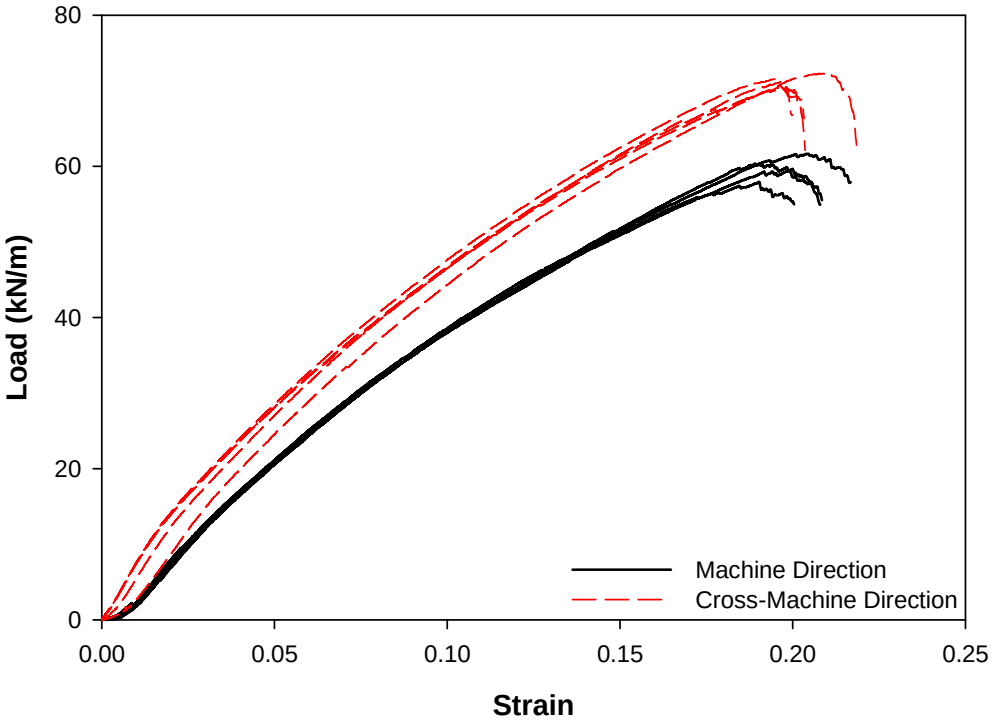

Figure A-9. WTI wide-width tension results for the WoT-9 geotextile.

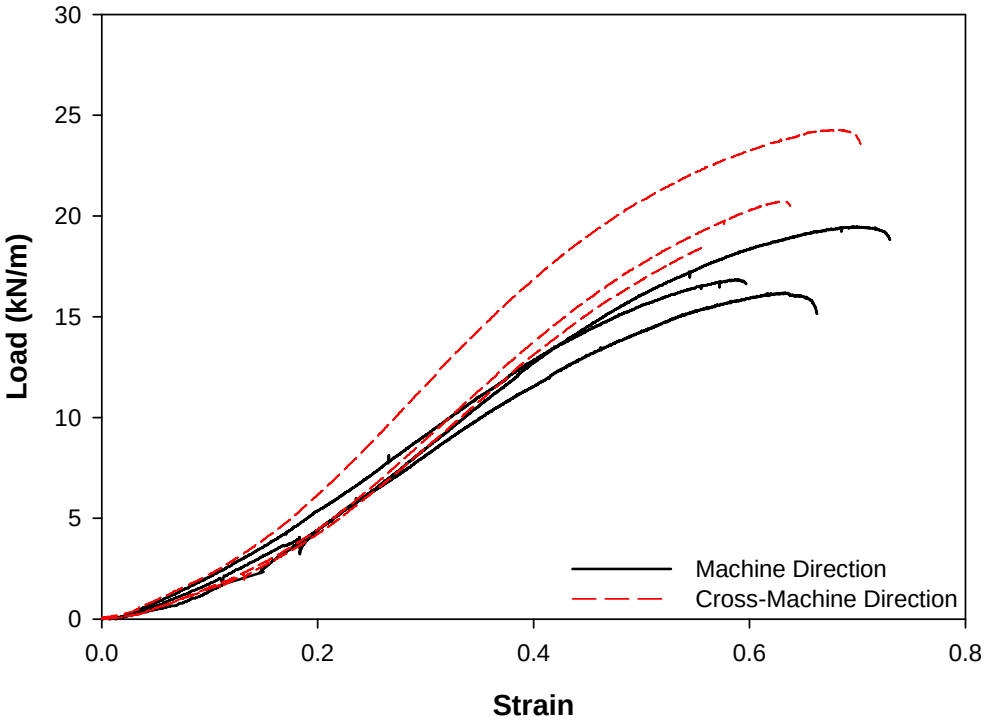

Figure A-10. WTI wide-width tension results for the NWoT-10 geotextile.

Appendix B

Statistical Summary of Longitudinal Rut Data

Key:

similar (p > 0.75)
between (0.25 < p < 0.75)
different (p <0.25)

Comparison	Run 1	Run 2	Run 3	Run 5	Run 10	Run 15	Run 25	Run 40
C1 to WeG-1	0.0049	0.0000	0.0000	0.0000	0.0000	N/A	N/A	N/A
C1 to WeG-2	0.0003	0.0000	0.0000	0.0000	0.0000	N/A	N/A	N/A
C1 to IFG-3	0.0011	0.0000	0.0000	0.0000	0.0000	N/A	N/A	N/A
C1 to CoG-4	**0.8174**	0.0004	0.0000	0.0000	0.0000	N/A	N/A	N/A
C1 to IFG-5	0.3889	0.0002	0.0000	0.0000	0.0000	N/A	N/A	N/A
C1 to WeG-6	0.2287	0.0000	0.0000	0.0000	0.0000	N/A	N/A	N/A
C1 to WoG-7	0.4826	0.0000	0.0000	0.0000	0.0000	N/A	N/A	N/A
C1 to WoG-8	0.6760	0.0000	0.0000	0.0000	0.0000	N/A	N/A	N/A
C1 to WoT-9	0.0233	0.0010	0.0000	0.0000	0.0000	N/A	N/A	N/A
C1 to NWoT-10	0.0010	0.2800	0.0014	0.0000	0.0000	N/A	N/A	N/A
C1 to C2	0.0016	0.3486	0.0077	0.0000	0.0001	N/A	N/A	N/A
WeG-1 to WeG-2	0.0249	**0.8269**	0.4390	0.6893	0.0706	0.0155	0.0012	0.1205
WeG-1 to IFG-3	0.2249	0.0199	0.0008	0.0000	0.0000	0.0000	0.0000	0.1510
WeG-1 to CoG-4	0.0328	0.0494	0.0236	0.0288	0.0746	0.1470	0.2523	0.2888
WeG-1 to IFG-5	0.0017	0.0002	0.0002	0.0000	0.0000	0.0000	N/A	N/A
WeG-1 to WeG-6	0.0000	0.0082	0.0049	0.0134	0.0086	0.0004	0.0506	0.0001
WeG-1 to WoG-7	0.0048	0.6509	0.0957	0.0295	0.0015	0.0012	0.0000	0.0001
WeG-1 to WoG-8	0.0004	0.2090	0.3322	0.0469	0.0313	0.0001	0.1078	0.0658
WeG-1 to WoT-9	0.0000	0.0046	0.0109	0.0012	0.0004	0.0000	0.0027	N/A
WeG-1 to NWoT-10	0.0000	0.0000	0.0000	0.0000	0.0000	0.0000	N/A	N/A
WeG-1 to C2	0.0000	0.0000	0.0000	0.0000	0.0000	0.0000	N/A	N/A
WeG-2 to IFG-3	0.1885	0.0049	0.0001	0.0000	0.0001	0.0000	0.0037	0.0177
WeG-2 to CoG-4	0.0025	0.0545	0.0478	0.0172	0.0087	0.0151	0.3898	**0.9906**
WeG-2 to IFG-5	0.0001	0.0001	0.0006	0.0000	0.0000	0.0000	N/A	N/A
WeG-2 to WeG-6	0.0000	0.0063	0.0135	0.0064	0.0003	0.0000	0.0001	0.0000
WeG-2 to WoG-7	0.0002	**0.7664**	0.0171	0.0523	0.0772	0.2472	0.0208	0.0210
WeG-2 to WoG-8	0.0000	0.2372	0.6517	0.0283	0.0049	0.0000	0.0004	0.0035
WeG-2 to WoT-9	0.0000	0.0045	0.0200	0.0007	0.0001	0.0000	0.0001	N/A
WeG-2 to NWoT-10	0.0000	0.0000	0.0000	0.0000	0.0000	0.0000	N/A	N/A
WeG-2 to C2	0.0000	0.0000	0.0000	0.0000	0.0000	0.0000	N/A	N/A
IFG-3 to CoG-4	0.0100	0.0029	0.0003	0.0001	0.0000	0.0001	0.0089	0.0581
IFG-3 to IFG-5	0.0002	0.0000	0.0000	0.0000	0.0000	0.0000	N/A	N/A
IFG-3 to WeG-6	0.0000	0.0000	0.0000	0.0000	0.0000	0.0000	0.0000	0.0947
IFG-3 to WoG-7	0.0008	0.0108	0.0772	0.0314	0.0412	0.0051	0.7097	0.0001
IFG-3 to WoG-8	0.0001	0.0043	0.0010	0.0001	0.0001	0.0000	0.0000	**0.9217**
IFG-3 to WoT-9	0.0000	0.0001	0.0003	0.0000	0.0000	0.0000	0.0000	N/A
IFG-3 to NWoT-10	0.0000	0.0000	0.0000	0.0000	0.0000	0.0000	N/A	N/A
IFG-3 to C2	0.0000	0.0000	0.0000	0.0000	0.0000	0.0000	N/A	N/A
CoG-4 to IFG-5	0.6450	0.6617	**0.9497**	0.2852	0.0050	0.0000	N/A	N/A
CoG-4 to WeG-6	0.1975	0.6377	**0.8325**	**0.8586**	**0.8194**	0.5079	0.0625	0.0008
CoG-4 to WoG-7	0.7275	0.0889	0.0033	0.0019	0.0010	0.0039	0.0194	0.1227
CoG-4 to WoG-8	0.5390	0.2893	0.1214	**0.8197**	0.5483	0.1528	0.0618	0.0358
CoG-4 to WoT-9	0.0242	0.5388	0.5569	0.0853	0.0127	0.0045	0.0026	N/A
CoG-4 to NWoT-10	0.0015	0.0030	0.0009	0.0000	0.0000	0.0000	N/A	N/A
CoG-4 to C2	0.0022	0.0004	0.0000	0.0000	0.0000	0.0000	N/A	N/A
IFG-5 to WeG-6	0.0024	0.1226	0.6871	0.1315	0.0014	0.0000	N/A	N/A
IFG-5 to WoG-7	**0.8821**	0.0010	0.0000	0.0000	0.0000	0.0000	N/A	N/A
IFG-5 to WoG-8	0.1236	0.0317	0.0178	0.1723	0.0615	0.0000	N/A	N/A
IFG-5 to WoT-9	0.0009	0.7310	0.5109	0.2367	0.4016	0.0798	N/A	N/A
IFG-5 to NWoT-10	0.0000	0.0011	0.0001	0.0000	0.0000	0.3760	N/A	N/A
IFG-5 to C2	0.0000	0.0000	0.0000	0.0000	0.0000	0.0000	N/A	N/A
WeG-6 to WoG-7	0.0119	0.0332	0.0003	0.0004	0.0000	0.0000	0.0000	0.0000
WeG-6 to WoG-8	0.3895	0.3281	0.0803	**0.9392**	0.6307	0.2199	0.7492	0.0184
WeG-6 to WoT-9	0.0713	0.1828	0.3948	0.0492	0.0111	0.0037	0.0147	N/A
WeG-6 to NWoT-10	0.0012	0.0002	0.0002	0.0000	0.0000	0.0000	N/A	N/A
WeG-6 to C2	0.0039	0.0000	0.0000	0.0000	0.0000	0.0000	N/A	N/A
WoG-7 to WoG-8	0.1949	0.3903	0.0325	0.0030	0.0007	0.0000	0.0000	0.0000
WoG-7 to WoT-9	0.0020	0.0103	0.0020	0.0002	0.0000	0.0000	0.0000	N/A
WoG-7 to NWoT-10	0.0001	0.0000	0.0000	0.0000	0.0000	0.0000	N/A	N/A
WoG-7 to C2	0.0001	0.0000	0.0000	0.0000	0.0000	0.0000	N/A	N/A
WoG-8 to WoT-9	0.0344	0.0636	0.0488	0.0570	0.0499	0.0292	0.0328	N/A
WoG-8 to NWoT-10	0.0010	0.0001	0.0000	0.0000	0.0000	0.0000	N/A	N/A
WoG-8 to C2	0.0023	0.0000	0.0000	0.0000	0.0000	0.0000	N/A	N/A
WoT-9 to NWoT-10	0.1488	0.0074	0.0073	0.0081	0.0226	0.0086	N/A	N/A
WoT-9 to C2	0.2389	0.0010	0.0002	0.0000	0.0000	0.0000	N/A	N/A
NWoT-10 to C2	**0.8454**	**0.7858**	0.2539	0.0001	0.0000	0.0000	N/A	N/A

Appendix C

Transverse Rut Profiles and
Photographic Record of Forensic Investigations

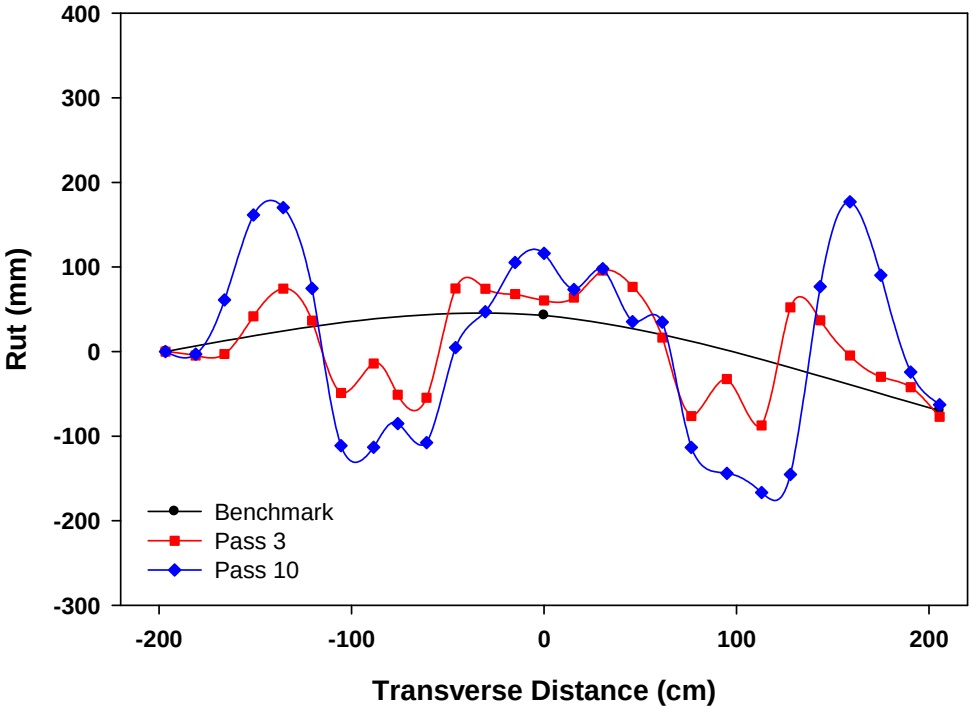

Figure C-1. Transverse rut profiles of the Control 1 test section during trafficking.

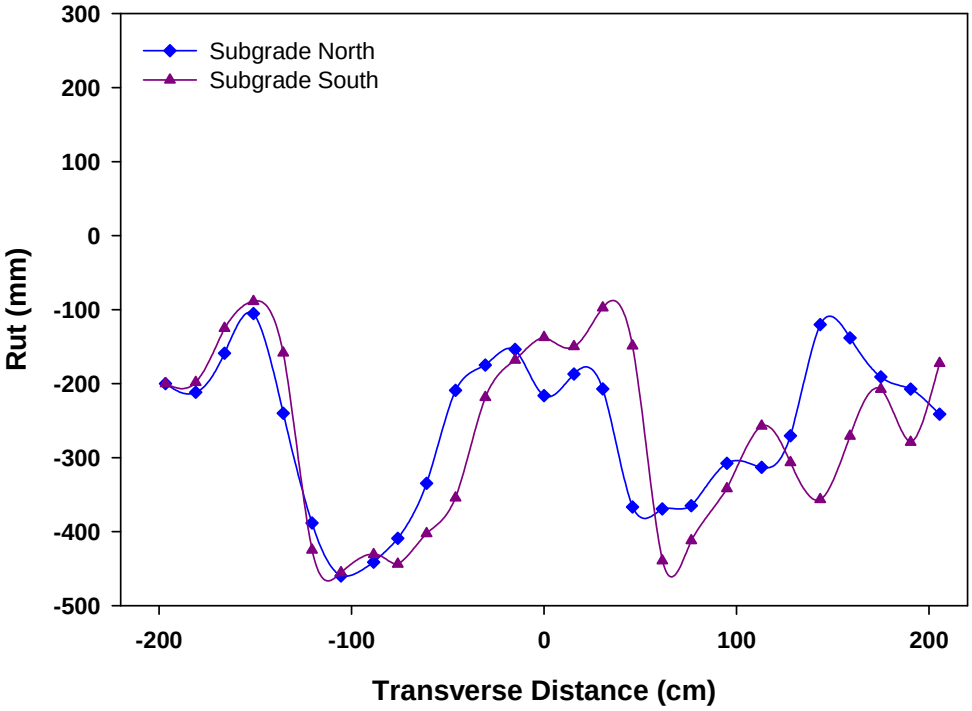

Figure C-2. Transverse rut profiles of the Control 1 test section during forensic excavations.

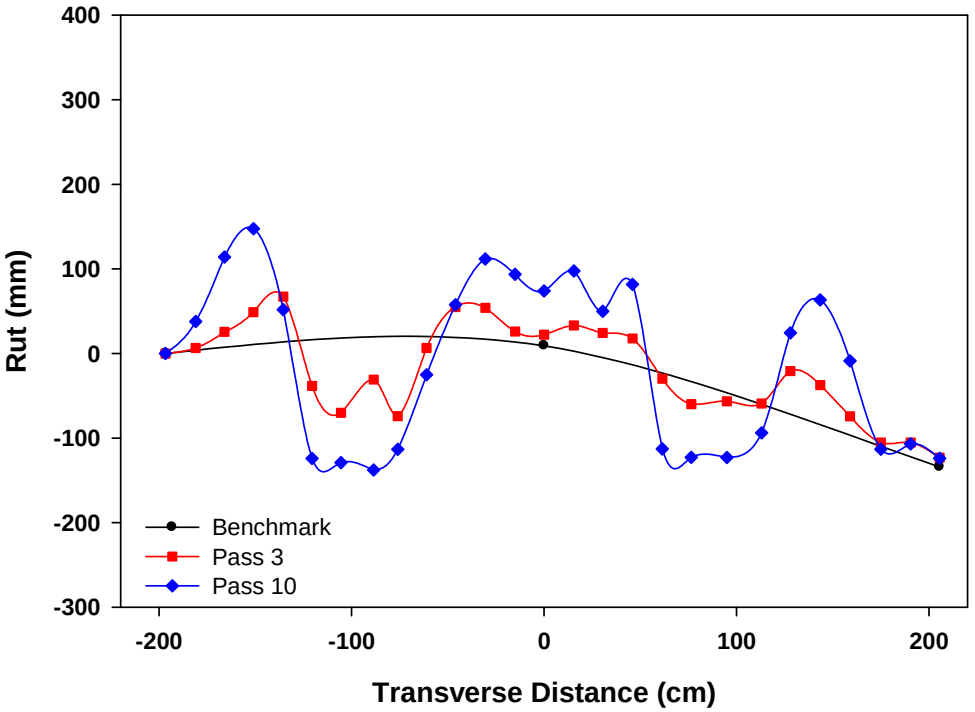

Figure C-3. Transverse rut profiles of the Control 2 test section during trafficking.

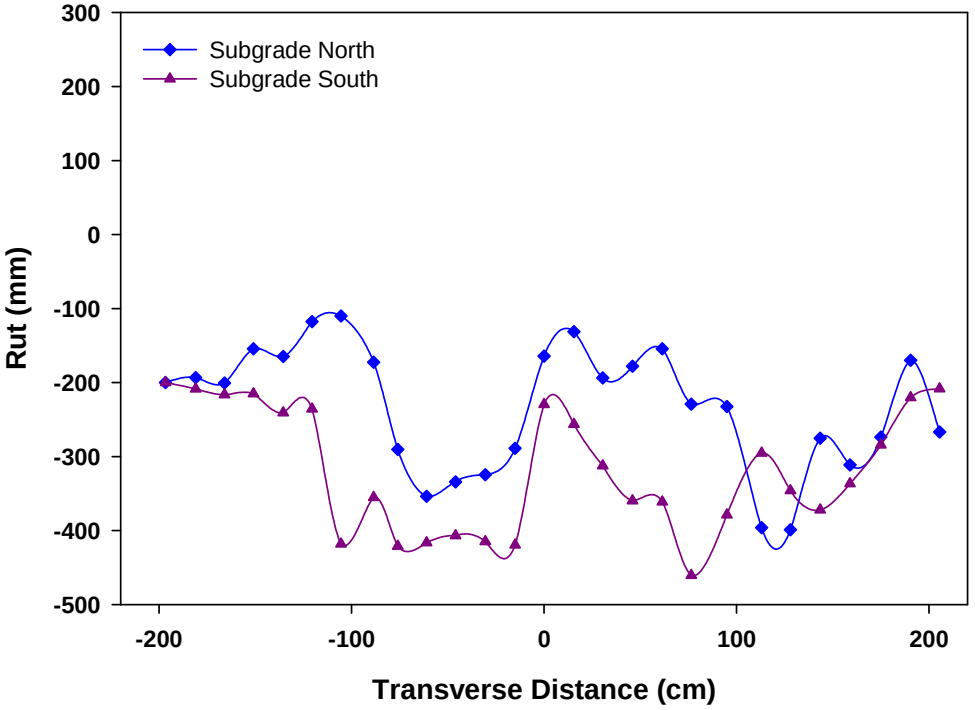

Figure C-4. Transverse rut profiles of the Control 2 test section during forensic excavations.

Figure C-5. Photos of the forensic excavations of the Control sections: a) and b) excavation of Control 1, c) and d) rut profile of Control 1, e) and f) rut profile of Control 2.

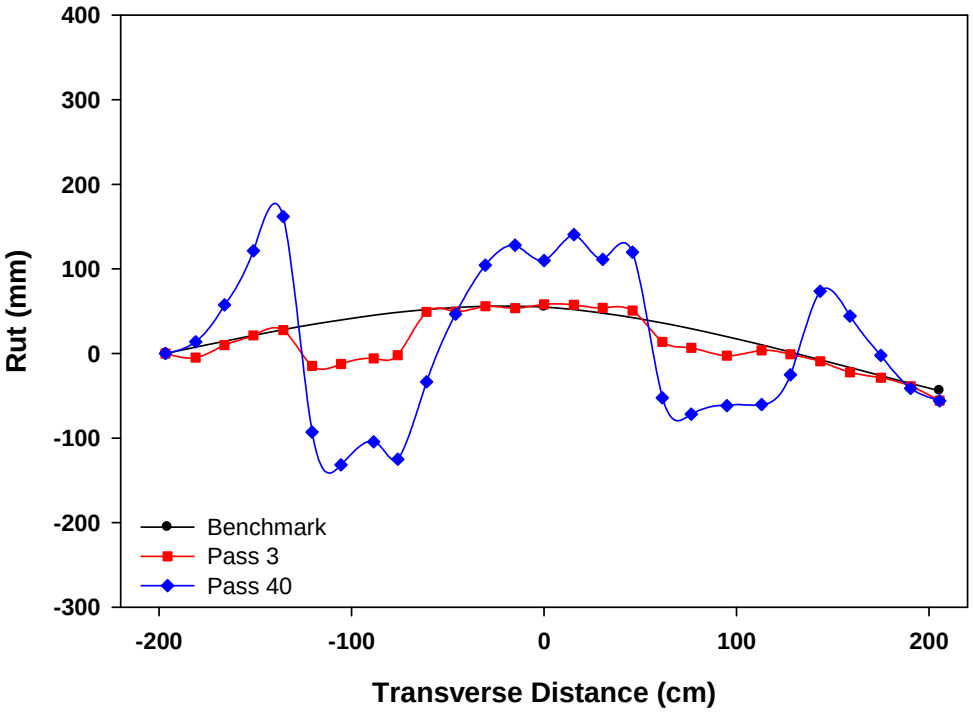

Figure C-6. Transverse rut profiles of the WeG-1 test section during trafficking.

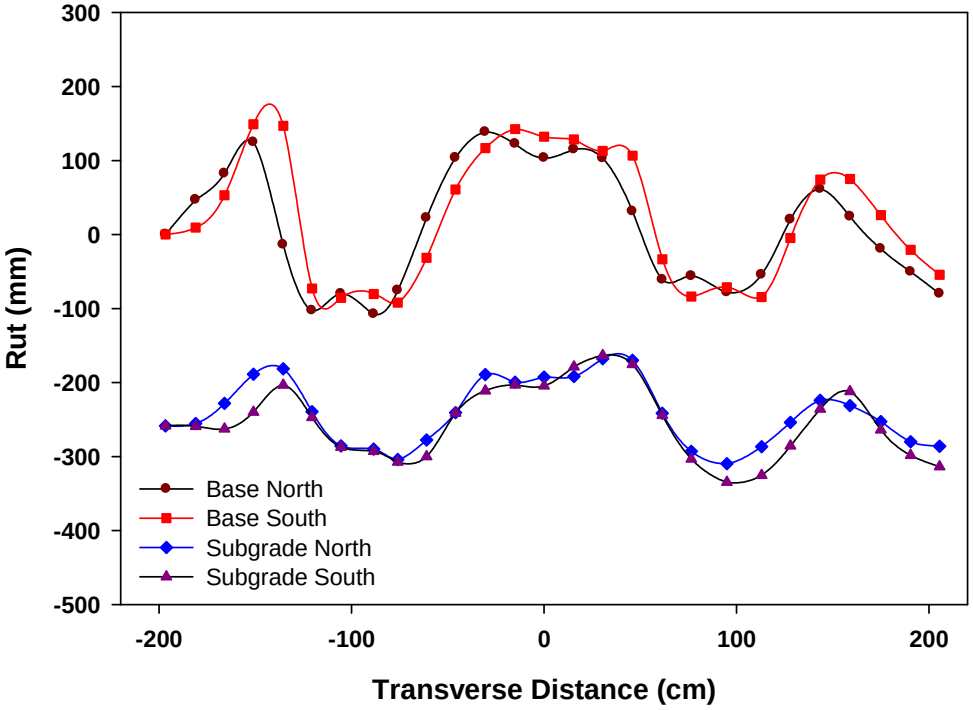

Figure C-7. Transverse rut profiles of the WeG-1 test section during forensic excavations.

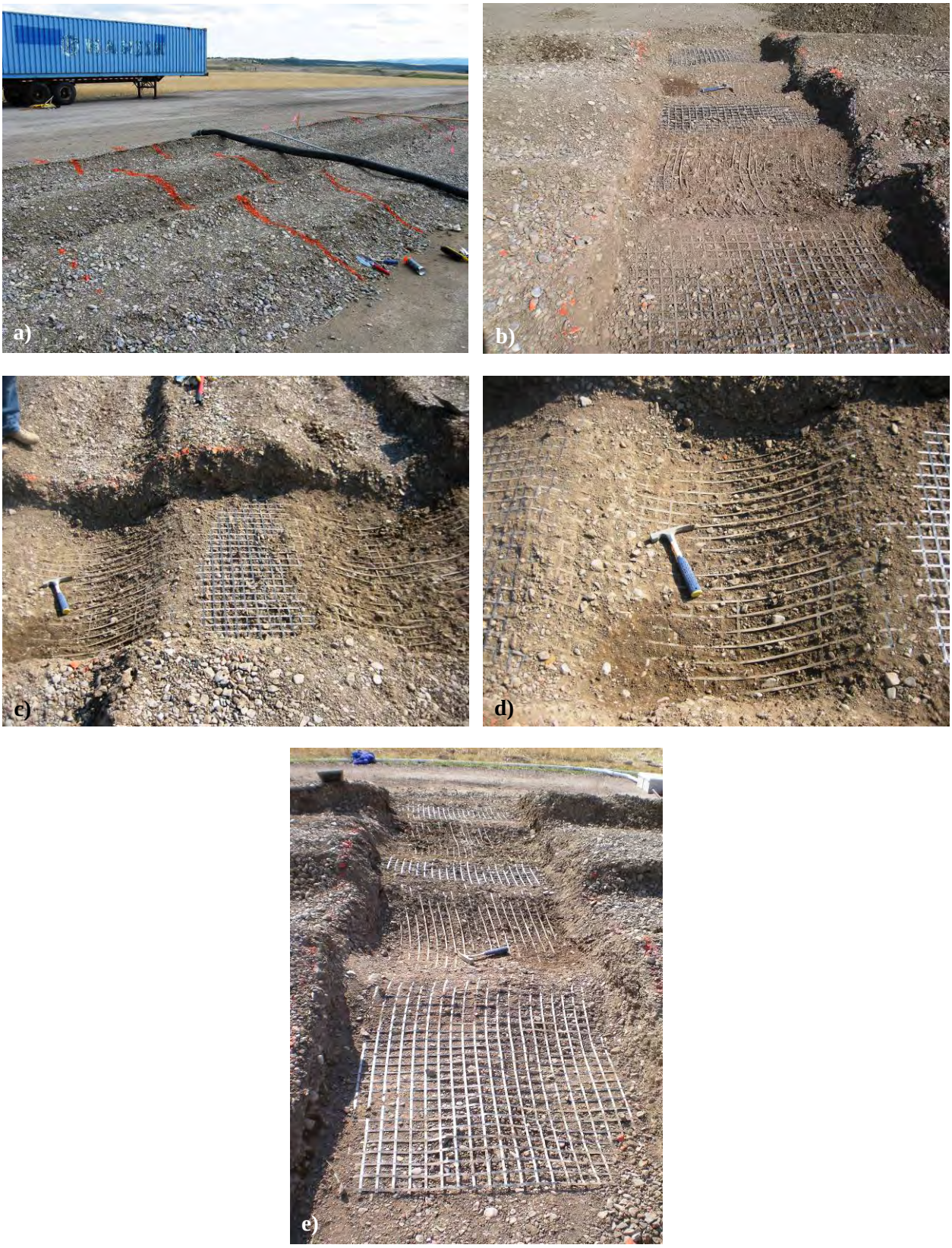

Figure C-8. Photos of the forensic excavations of the WeG-1 test section: a) excavation area, b) looking east, c) rut profile, d) close-up of rut, and e) looking west.

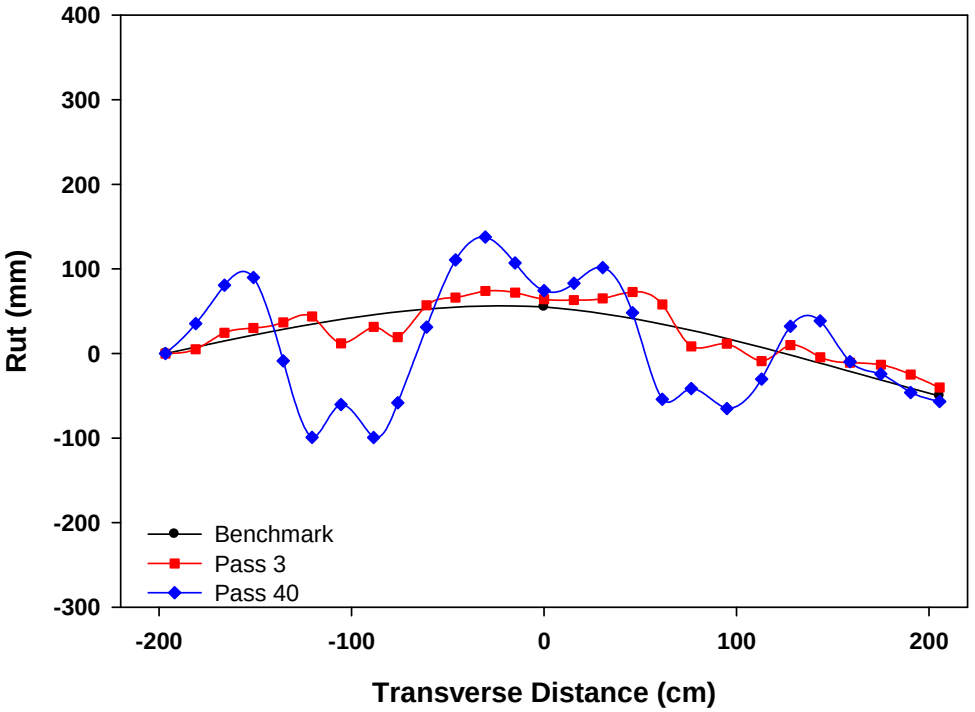

Figure C-9. Transverse rut profiles of the WeG-2 test section during trafficking.

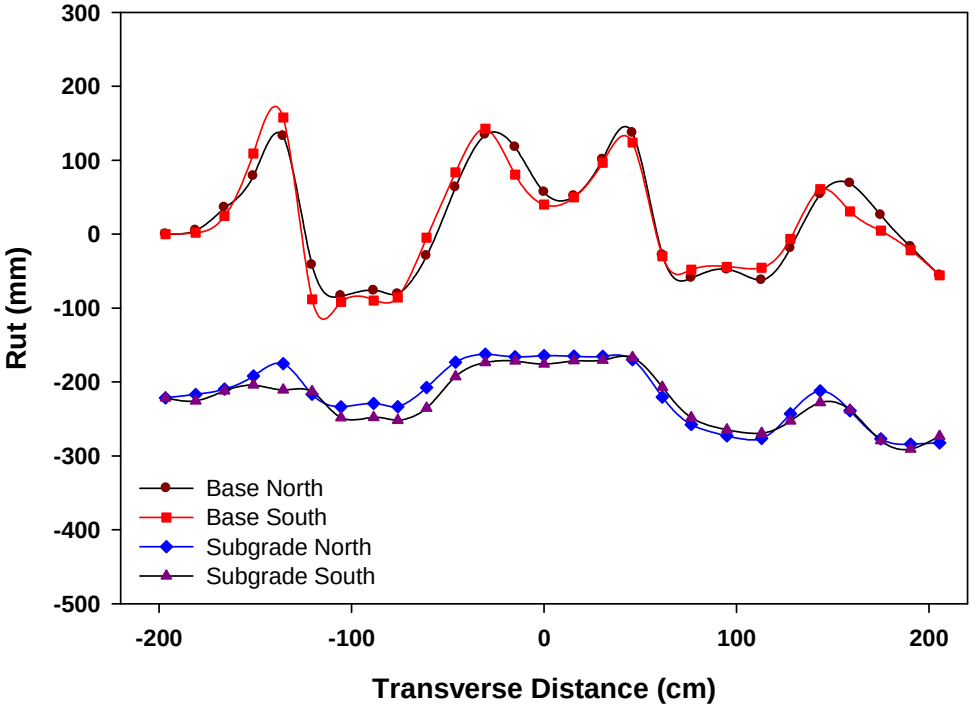

Figure C-10. Transverse rut profiles of the WeG-2 test section during forensic excavations.

Figure C-11. Photos of the forensic excavations of the WeG-2 test section: a) looking east, b) rut bowl, c) close-up of rut bowl, d) overhead view of rut, e) close-up of rut, and f) looking west.

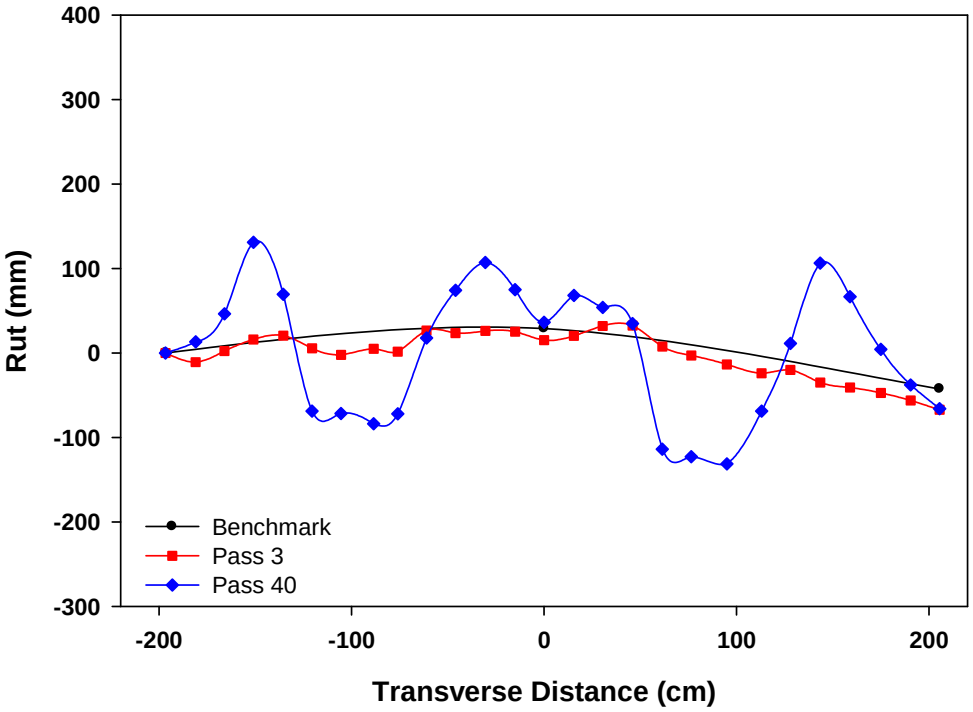

Figure C-12. Transverse rut profiles of the IFG-3 test section during trafficking.

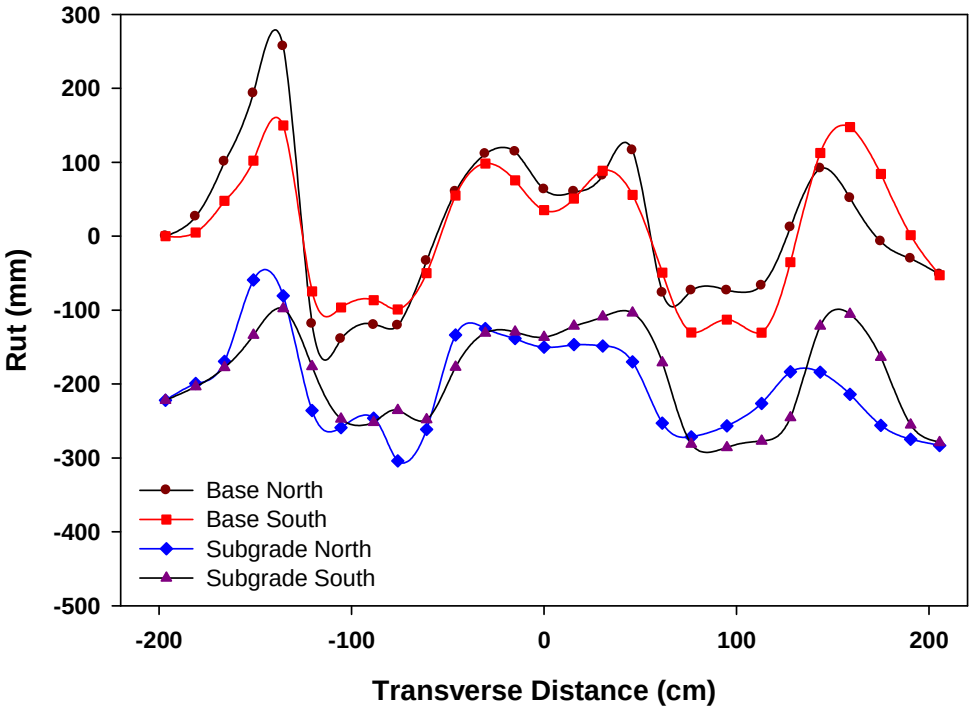

Figure C-13. Transverse rut profiles of the IFG-3 test section during forensic excavations.

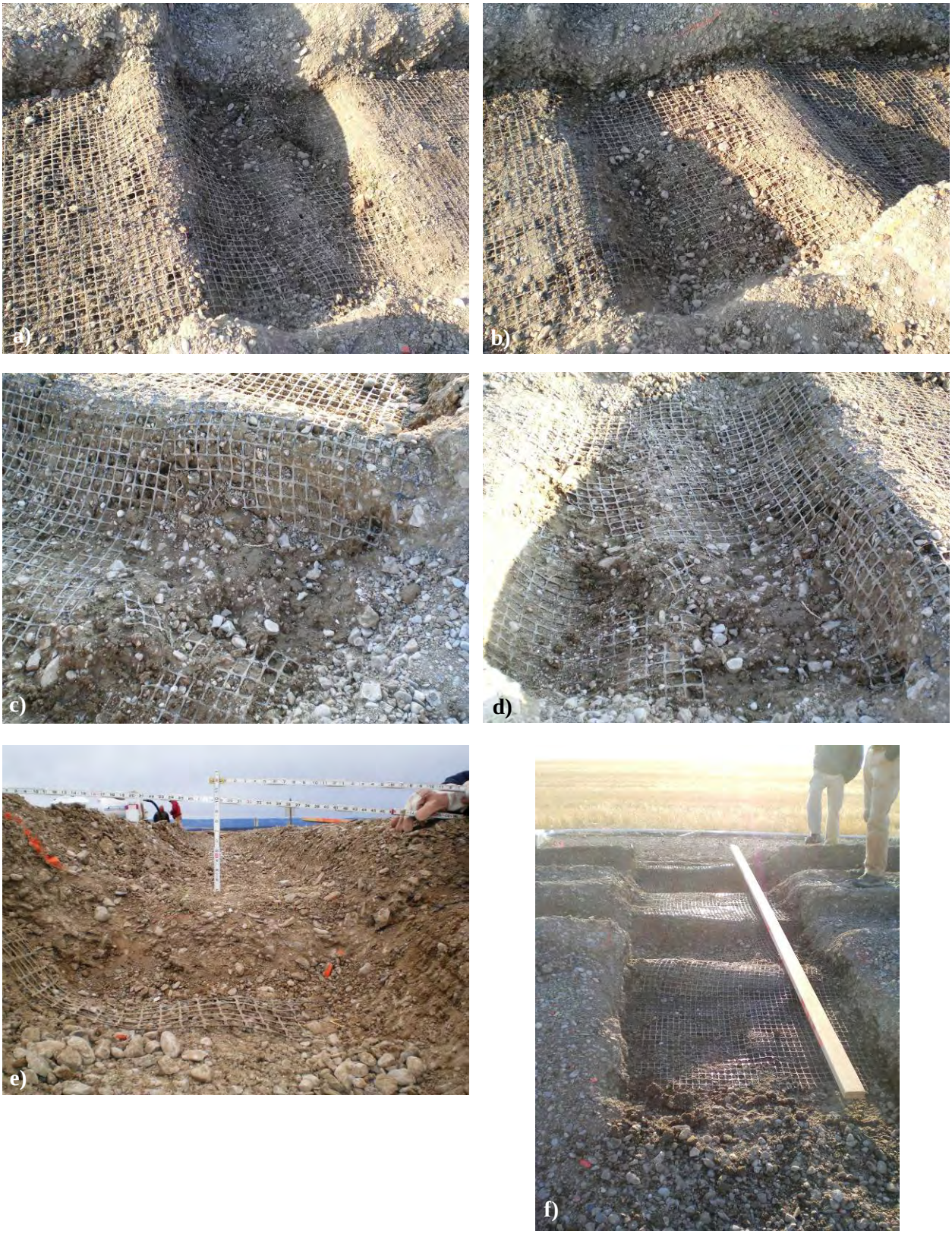

Figure C-14. Photos of the forensic excavations of the IFG-3 test section: a) rut bowl, b) rut bowl, c) close-up of side of rut bowl, d) close-up of rut, e) rut profile and f) looking west.

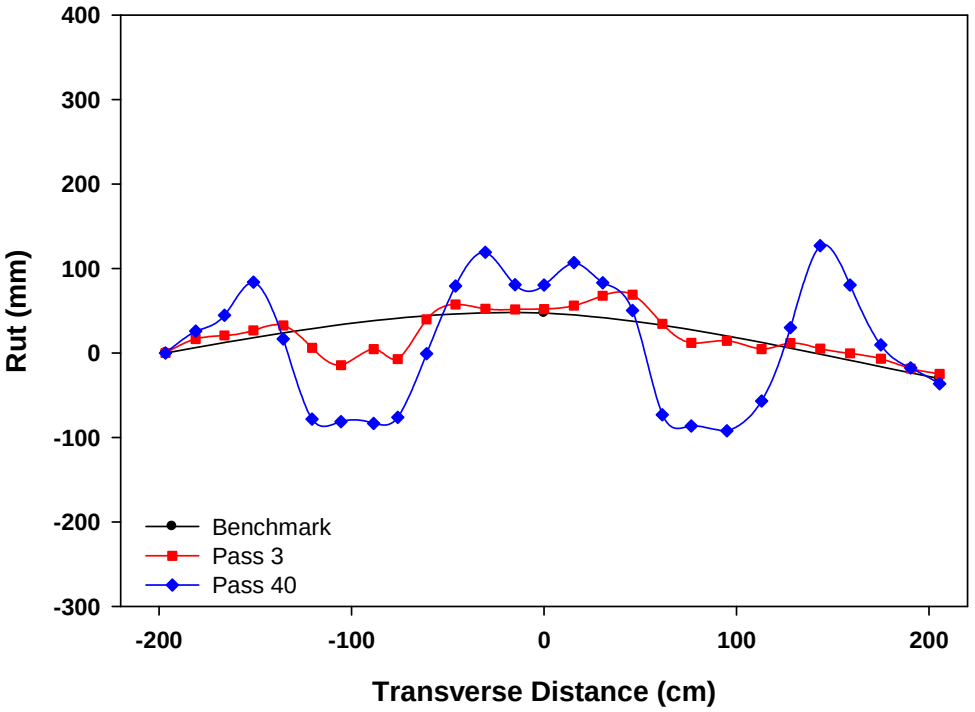

Figure C-15. Transverse rut profiles of the CoG-4 test section during trafficking.

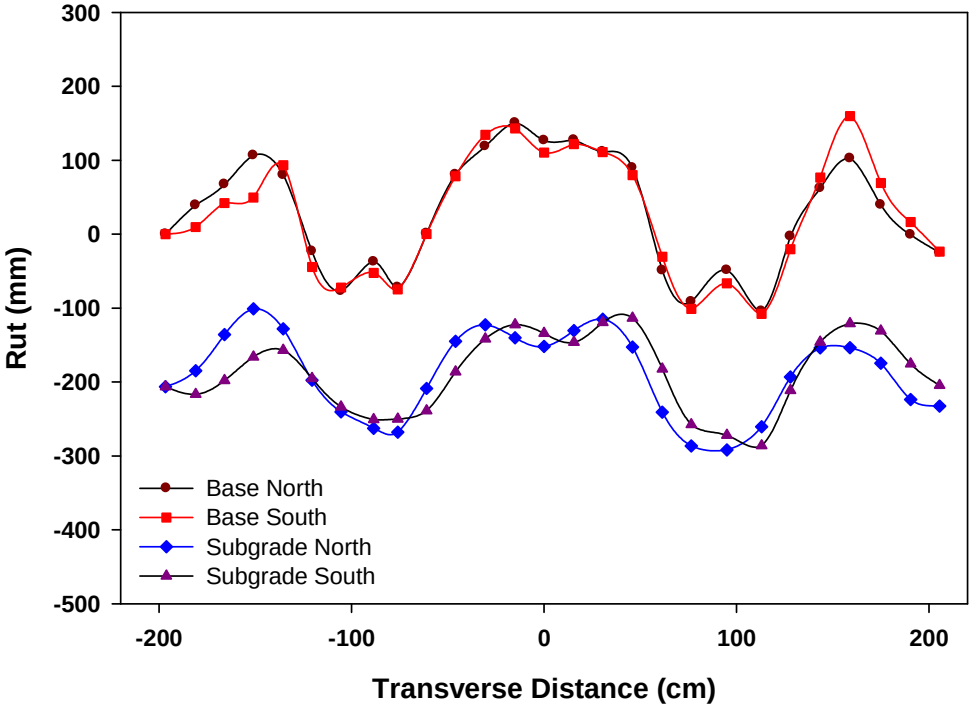

Figure C-16. Transverse rut profiles of the CoG-4 test section during forensic excavations.

Figure C-17. Photos of the forensic excavations of the CoG-4 test section: a) looking west, b) rut bowl, c) base rut profile, d) subgrade rut profile, e) close-up of rut and f) layering of base and subgrade.

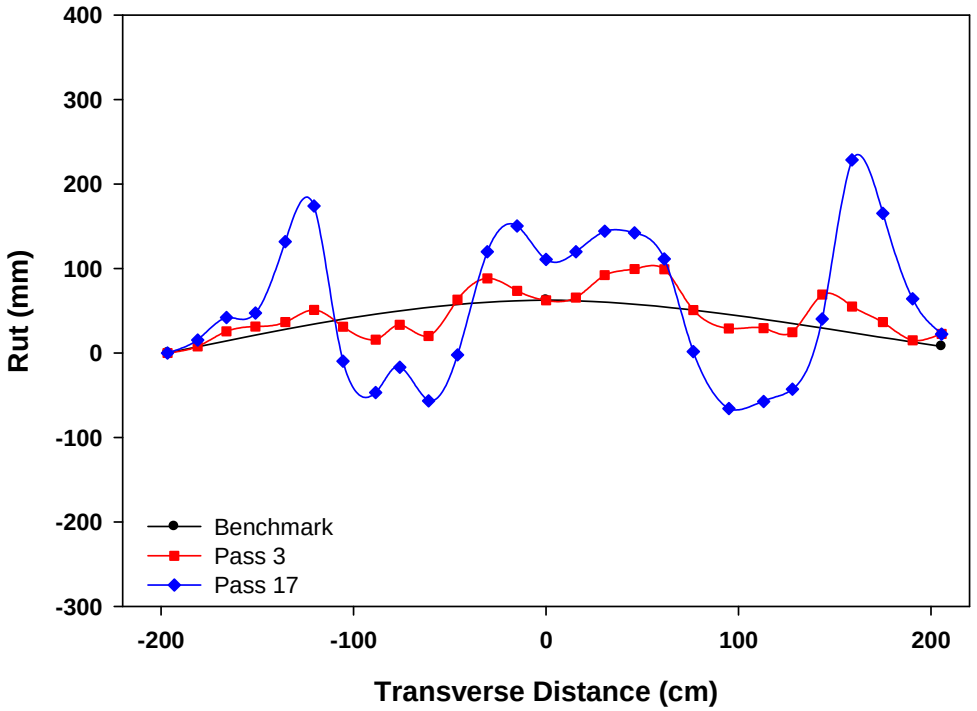

Figure C-18. Transverse rut profiles of the IFG-5 test section during trafficking.

Note: No transverse rut profiles of the IFG-5 test section were taken during the forensic excavations.

Figure C-19. Photos of the forensic excavations of the IFG-5 test section: a) base rut profile, b) subgrade rut profile, c) close-up of rut, d) close-up of damage, e) rut bowl and f) looking east.

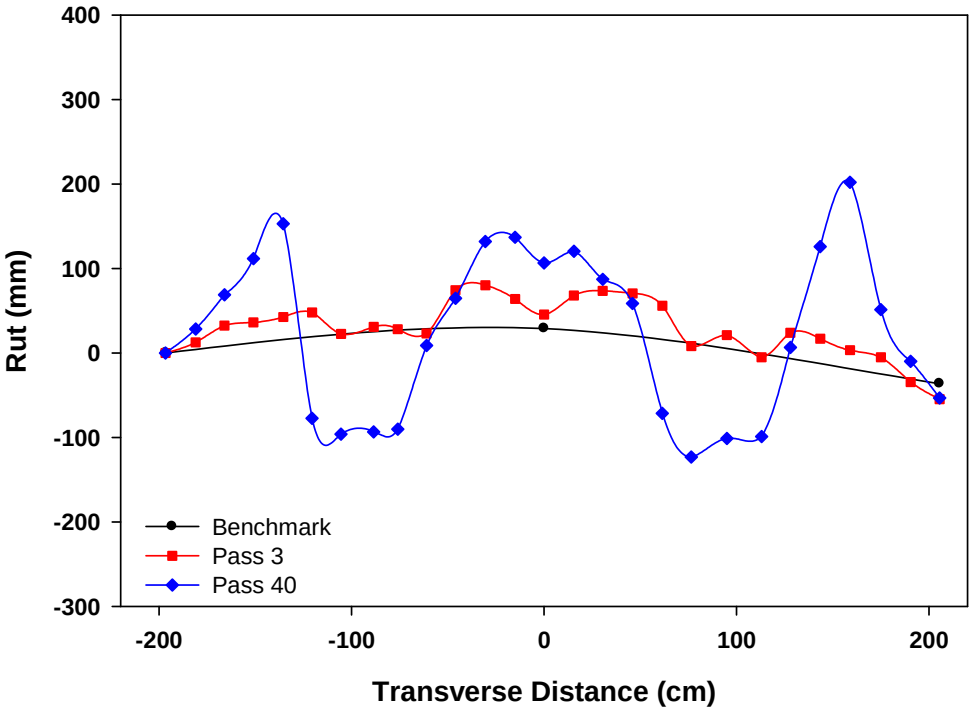

Figure C-20. Transverse rut profiles of the WeG-6 test section during trafficking.

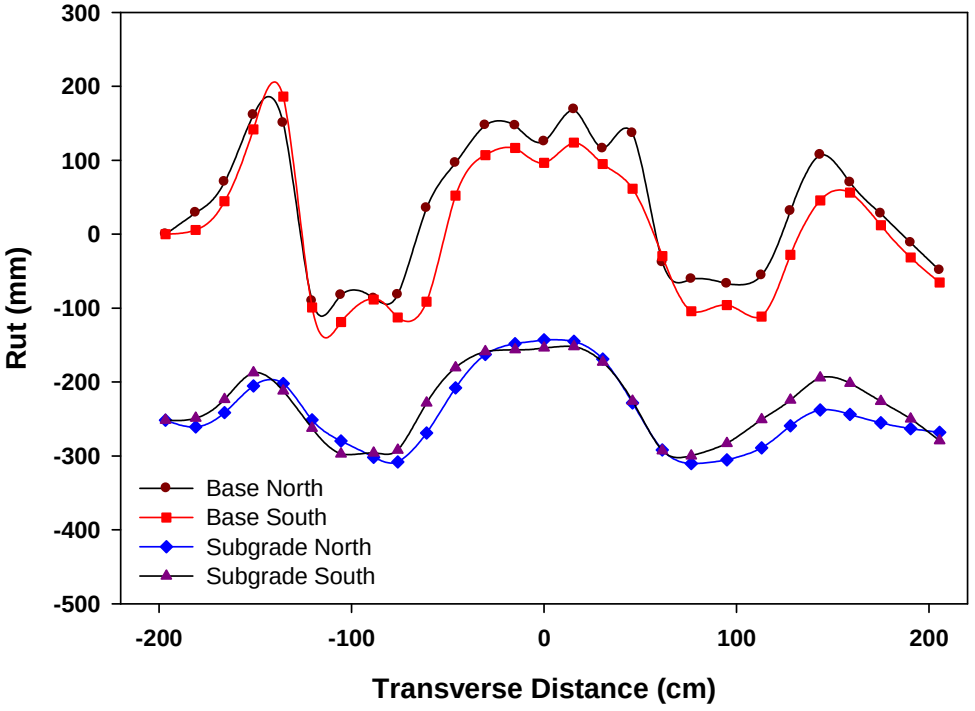

Figure C-21. Transverse rut profiles of the WeG-6 test section during forensic excavations.

Figure C-22. Photos of the forensic excavations of the WeG-6 test section: a) looking west, b) base rut profile, c) subgrade rut profile, d) rut bowl, e) view from the side and f) layering of base and subgrade.

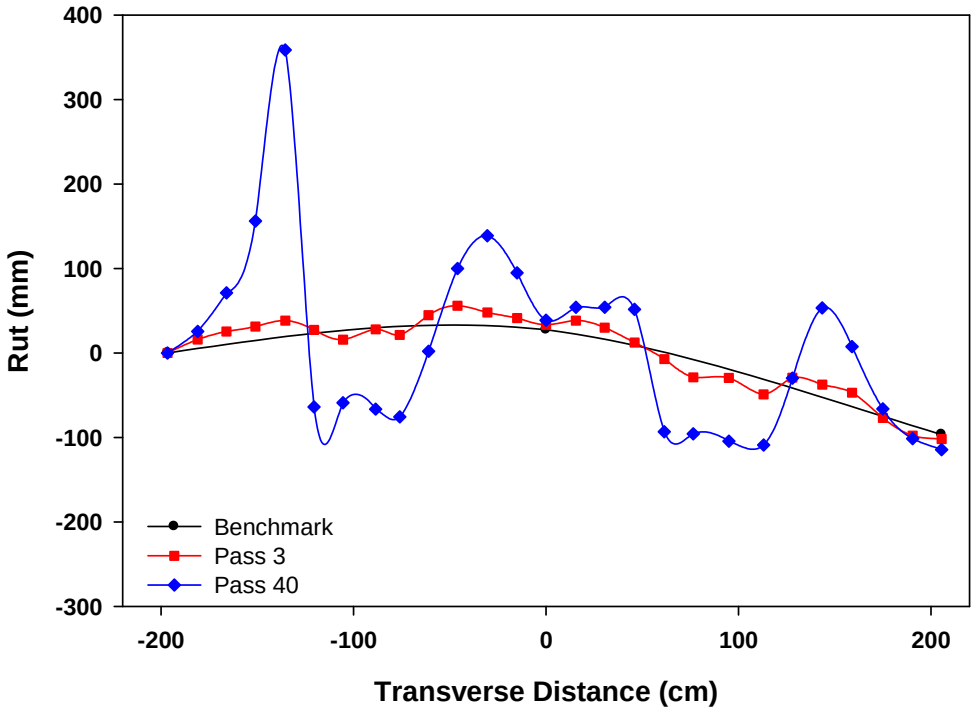

Figure C-23. Transverse rut profiles of the WoG-7 test section during trafficking.

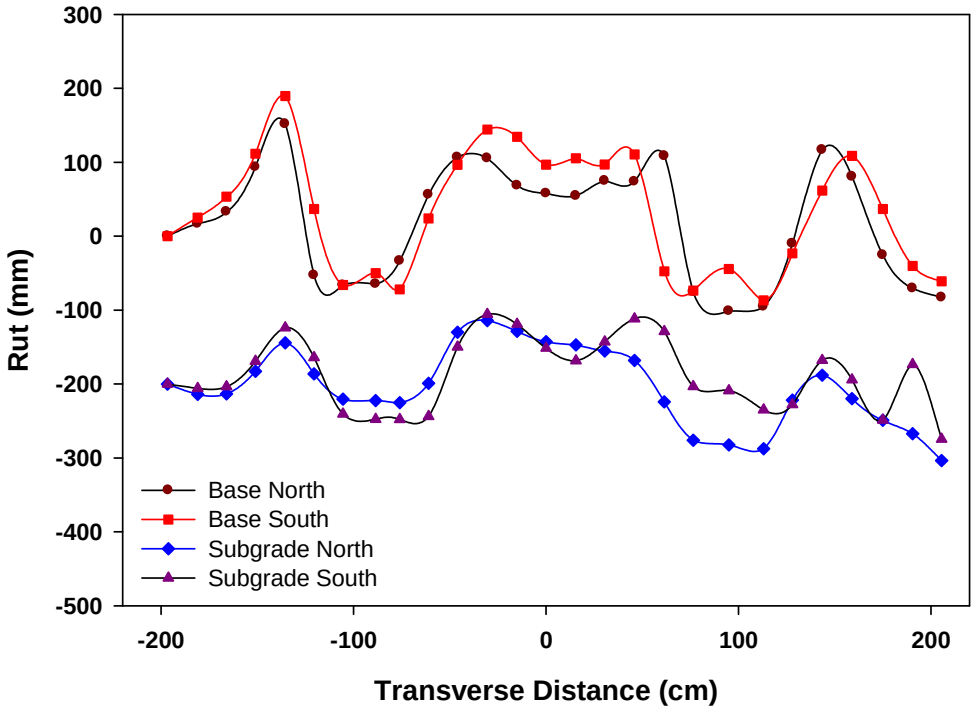

Figure C-24. Transverse rut profiles of the WoG-7 test section during forensic excavations.

Figure C-25. Photos of the forensic excavations of the WoG-7 test section: a) excavation area, b) looking west, c) rut bowl, d) subgrade rut profile, e) subgrade rut profile and f) base rut profile.

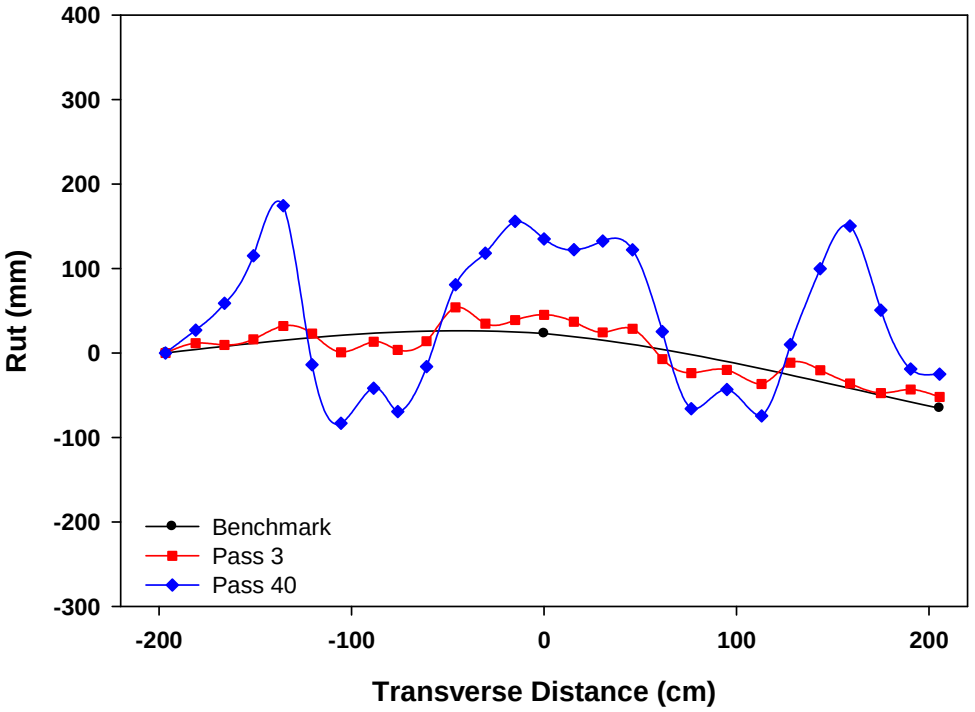

Figure C-26. Transverse rut profiles of the WoG-8 test section during trafficking.

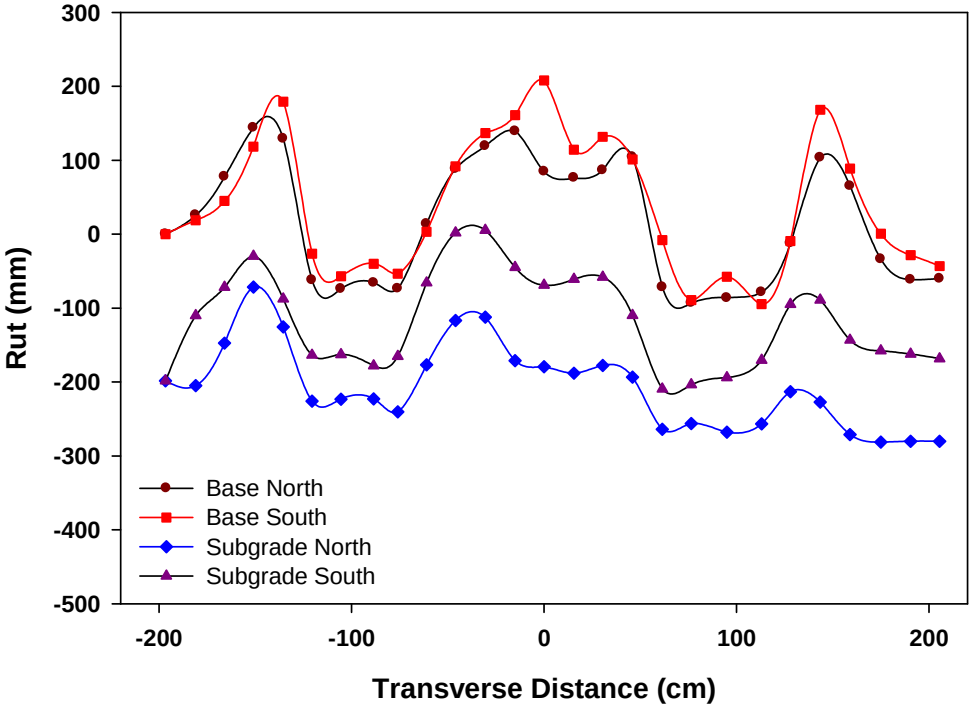

Figure C-27. Transverse rut profiles of the WoG-8 test section during forensic excavations.

Figure C-28. Photos of the forensic excavations of the WoG-8 test section: a) excavation area, b) looking west, c) rut bowl, d) base rut profile, e) subgrade rut profile and f) close-up of rut.

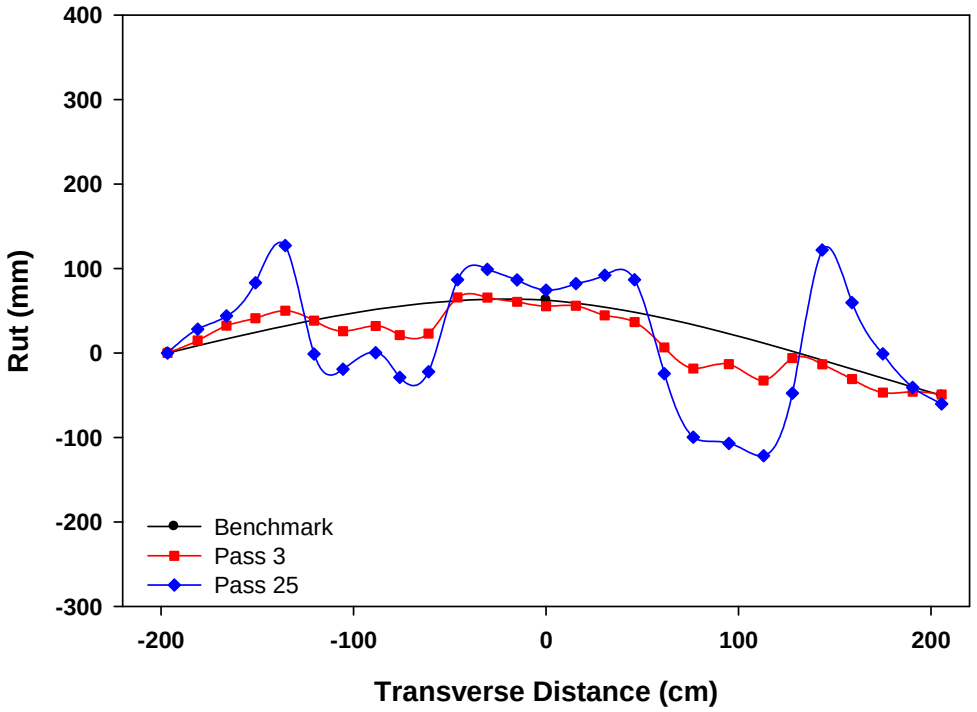

Figure C-29. Transverse rut profiles of the WoT-9 test section during trafficking.

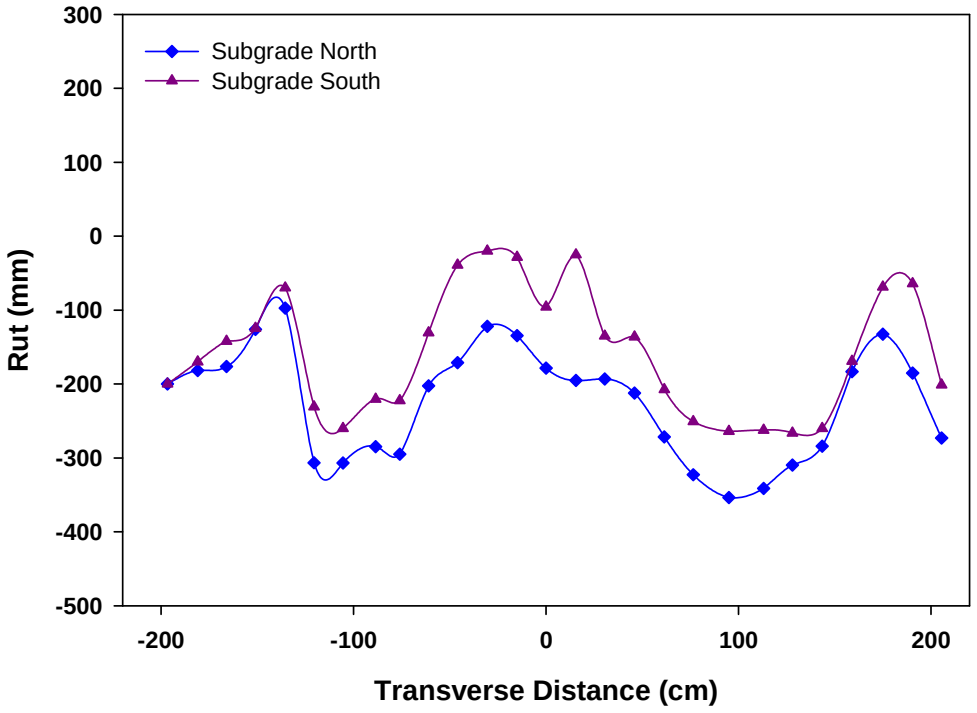

Figure C-30. Transverse rut profiles of the WoT-9 test section during forensic excavations.

Figure C-31. Photos of the forensic excavations of the WoT-9 test section: a) rut bowl, b) base rut profile, c) subgrade rut profile, d) subgrade surface, e) looking east and f) pullout failure.

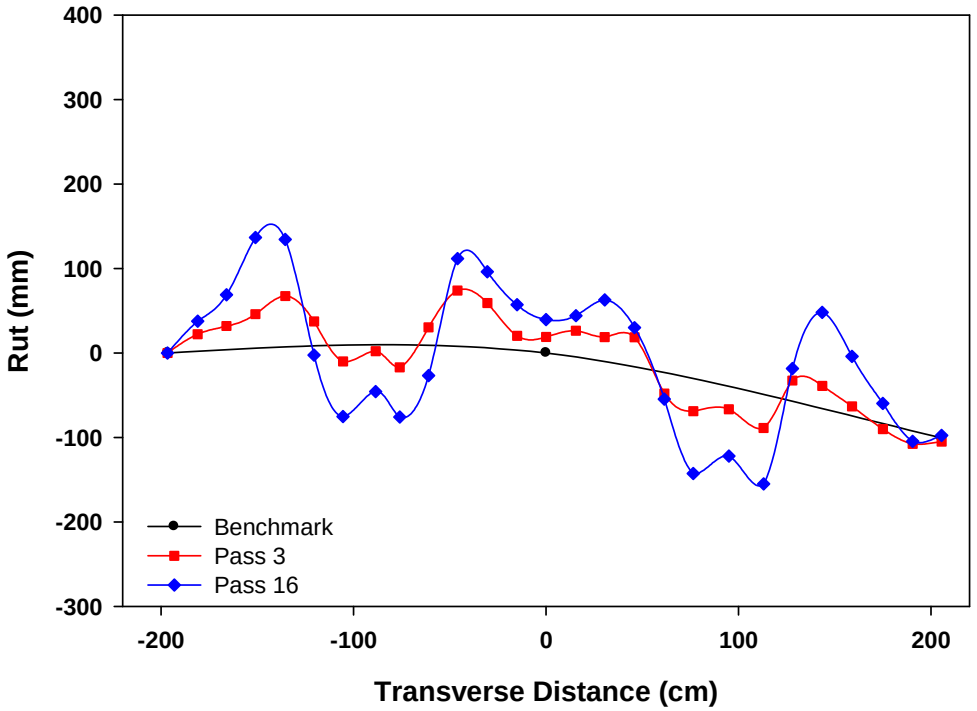

Figure C-32. Transverse rut profiles of the NWoT-10 test section during trafficking.

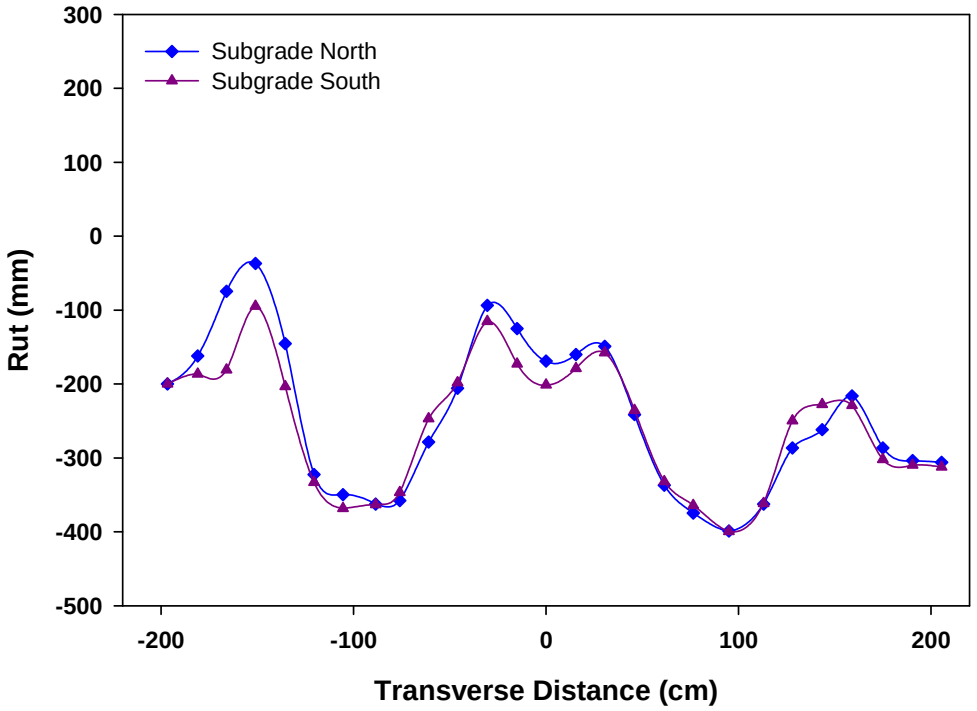

Figure C-33. Transverse rut profiles of the NWoT-10 test section during forensic excavations.

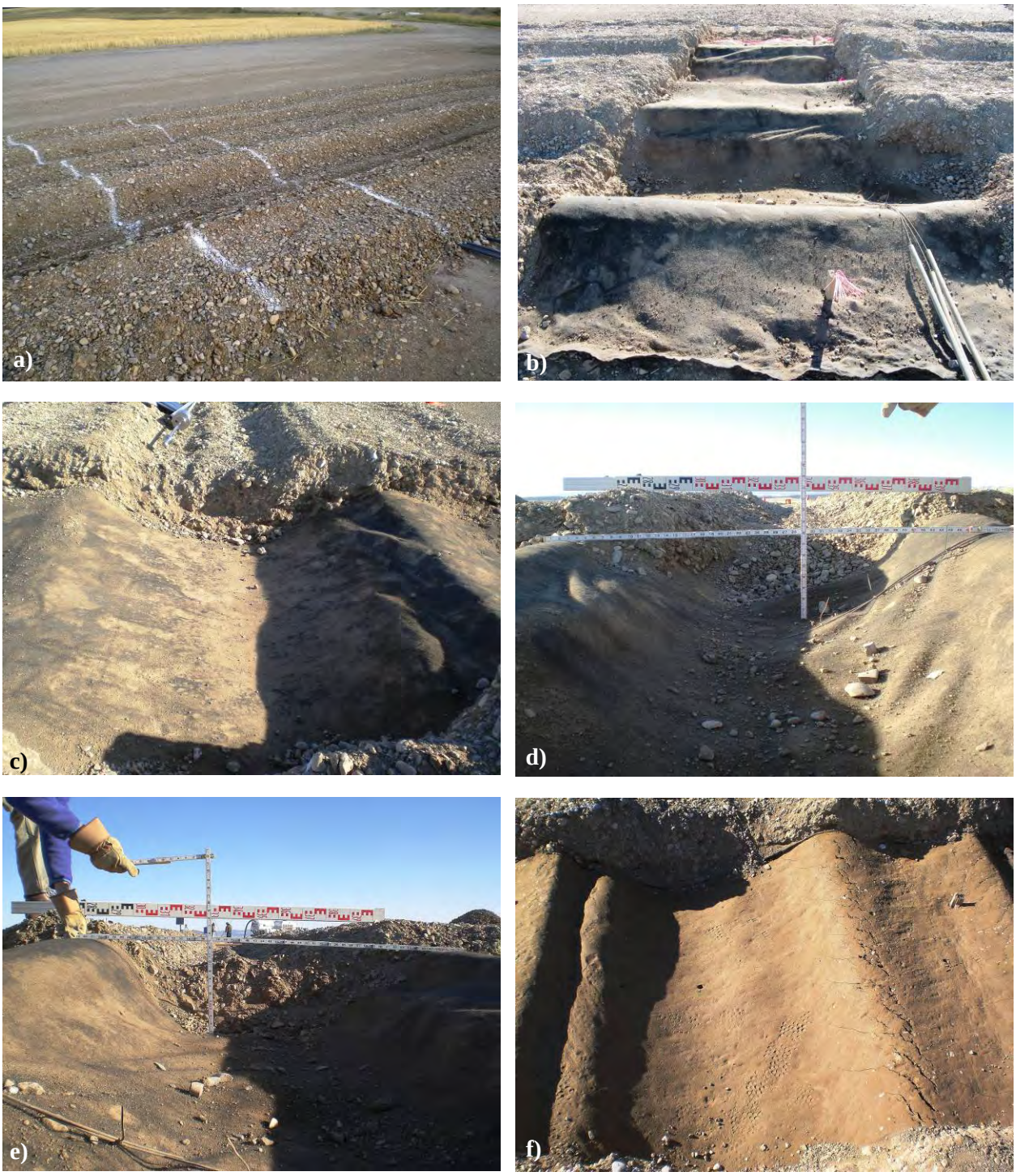

Figure C-34. Photos of the forensic excavations of the NWoT-10 test section: a) excavation area, b) looking east, c) rut bowl, d) subgrade rut profile, e) subgrade rut profile and f) subgrade surface.

Appendix D

Displacement and Strain Records for Each Test Section

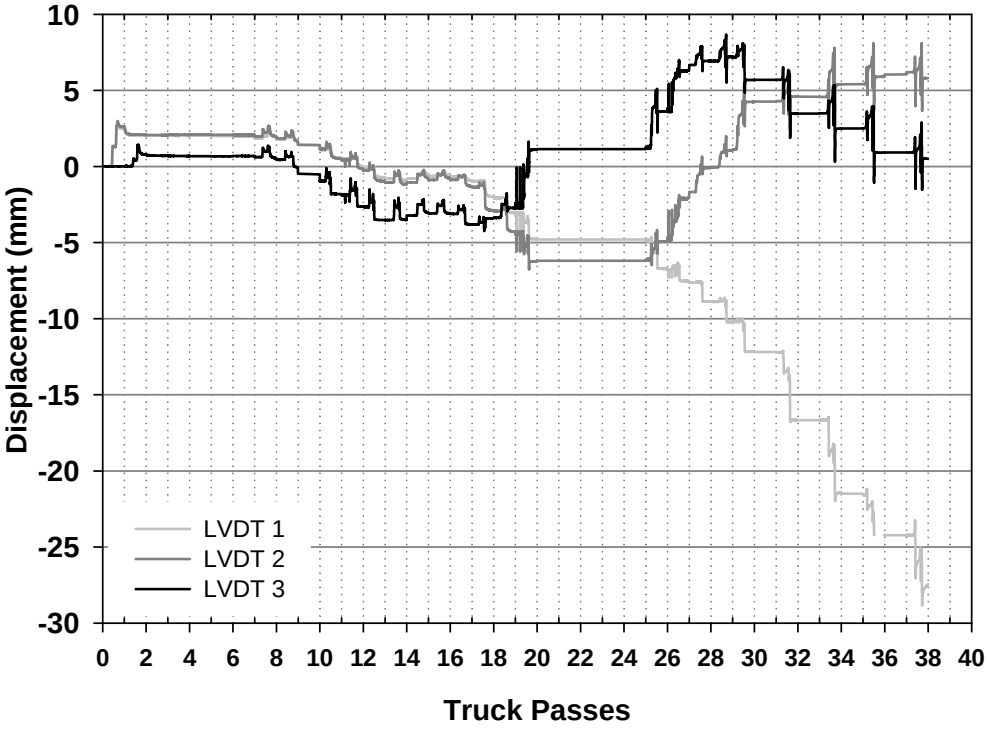

Figure D-1. Displacement profiles of the WeG-1 test section.

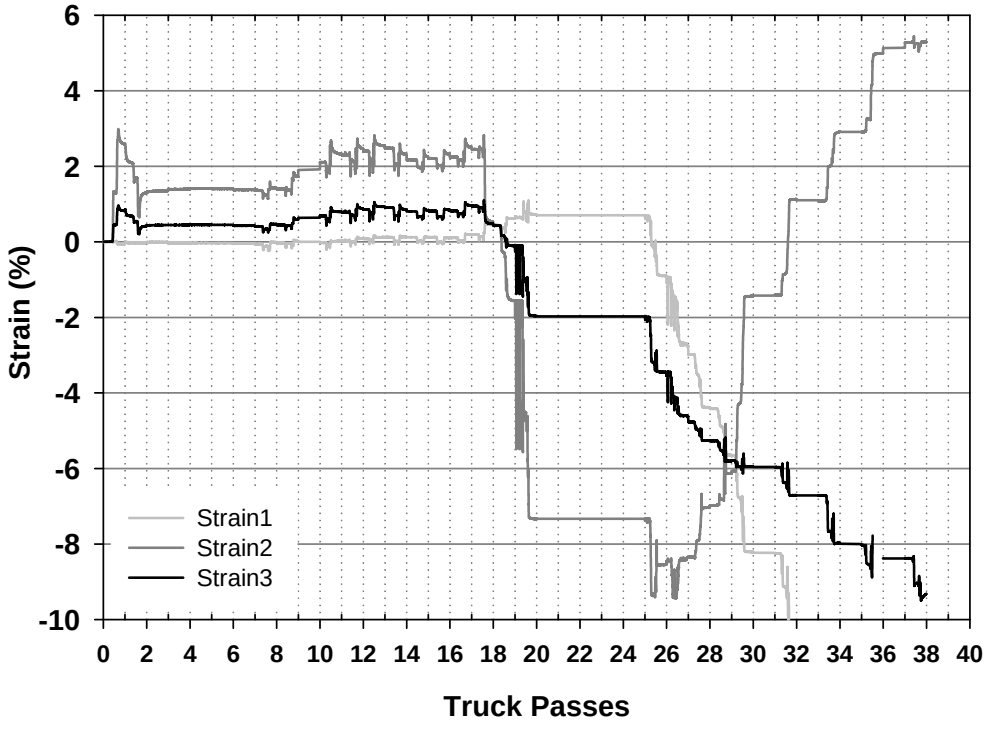

Figure D-2. Strain profiles of the WeG-1 test section.

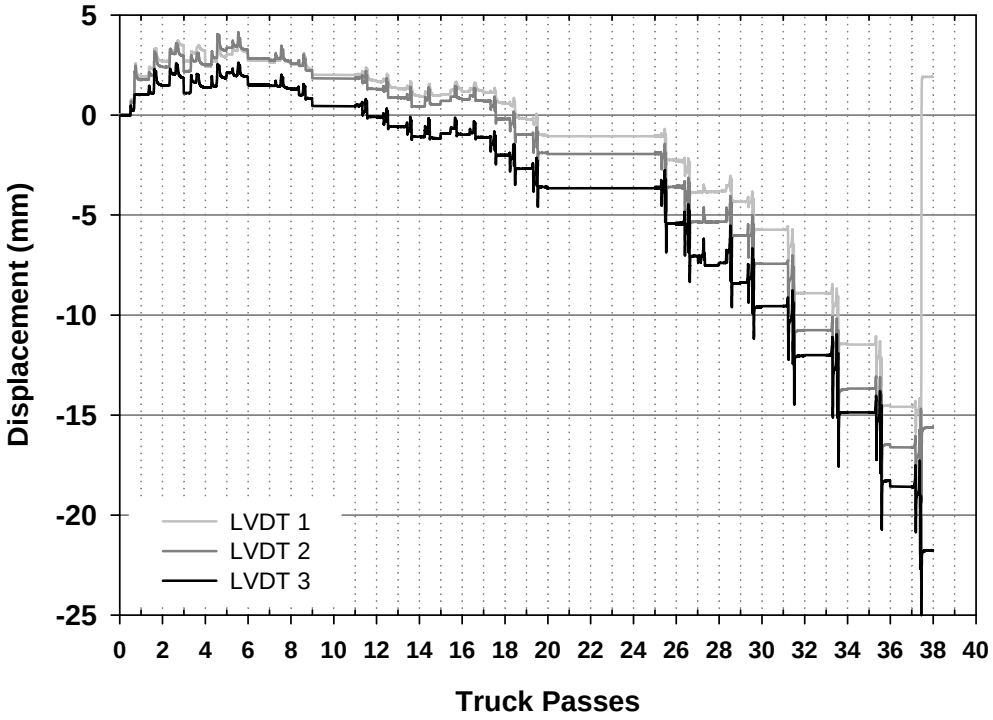

Figure D-3. Displacement profiles of the WeG-2 test section.

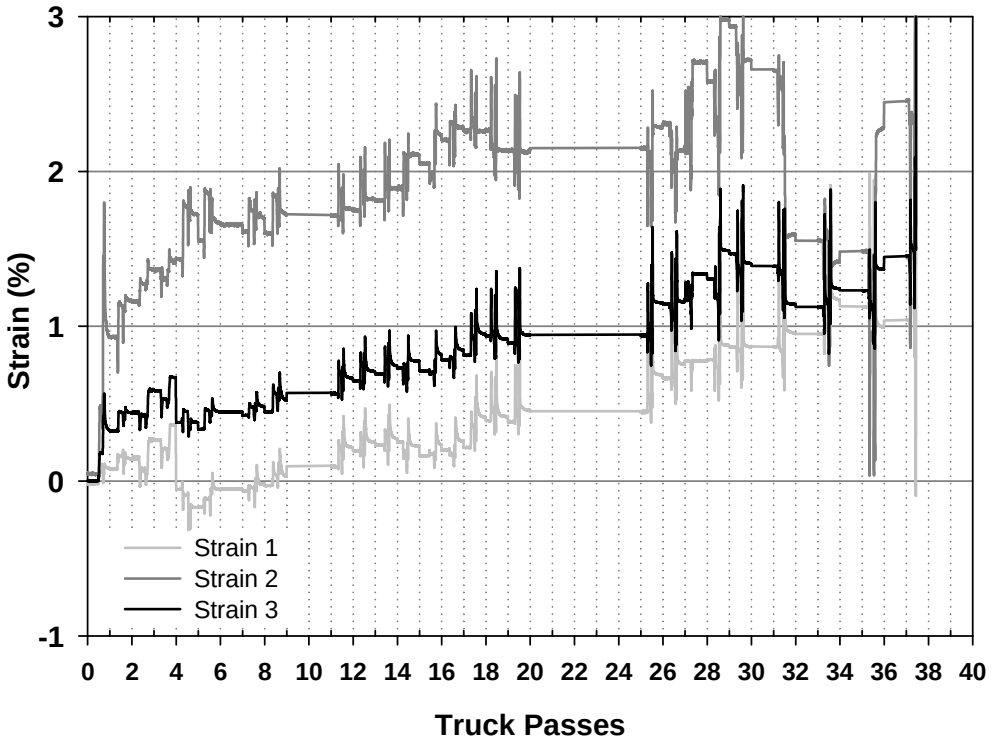

Figure D-4. Strain profiles of the WeG-2 test section.

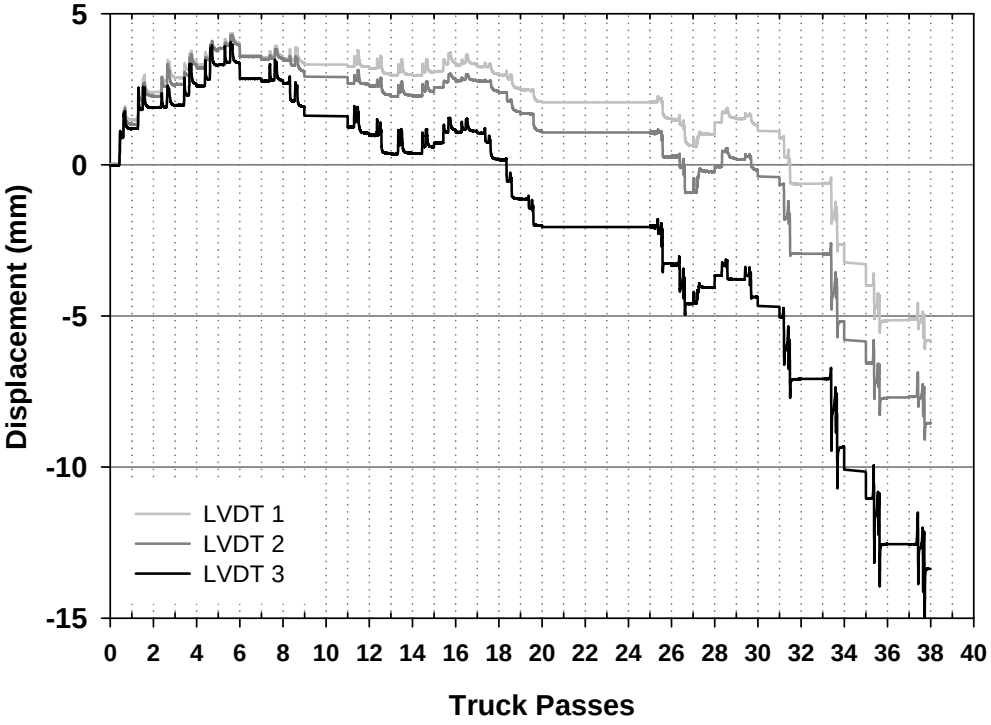

Figure D-5. Displacement profiles of the IFG-3 test section.

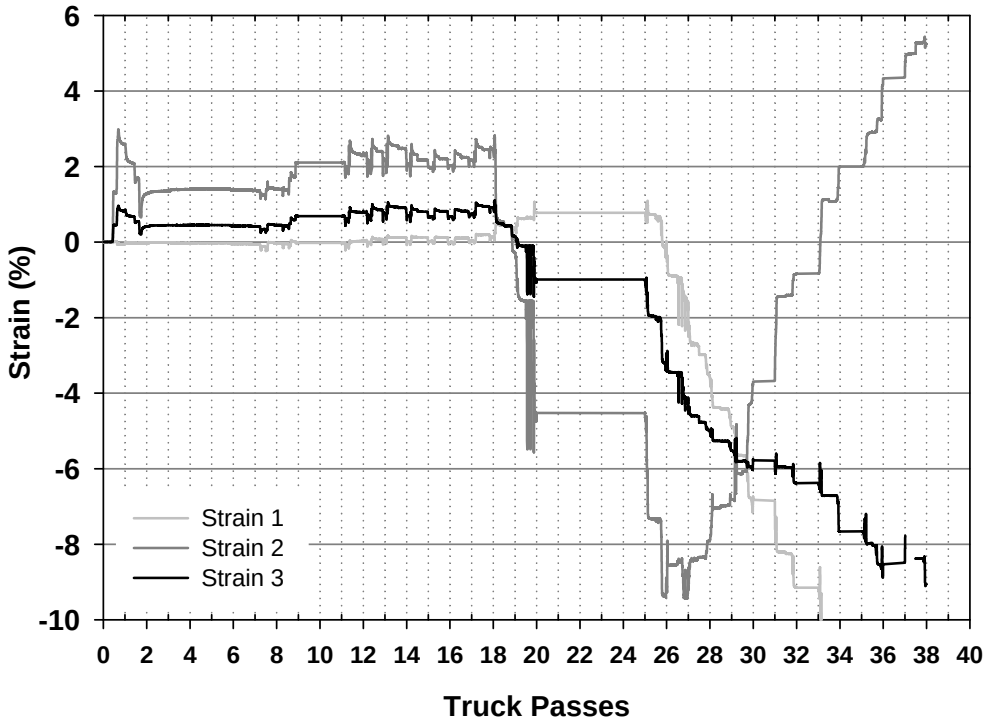

Figure D-6. Strain profiles of the IFG-3 test section.

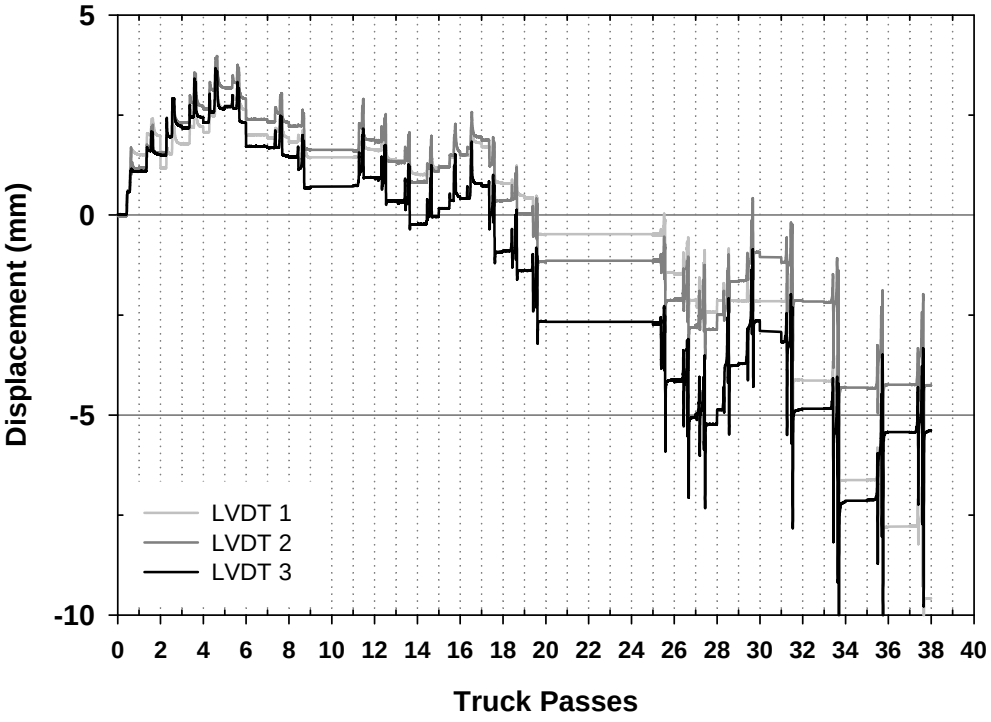

Figure D-7. Displacement profiles of the CoG-4 test section.

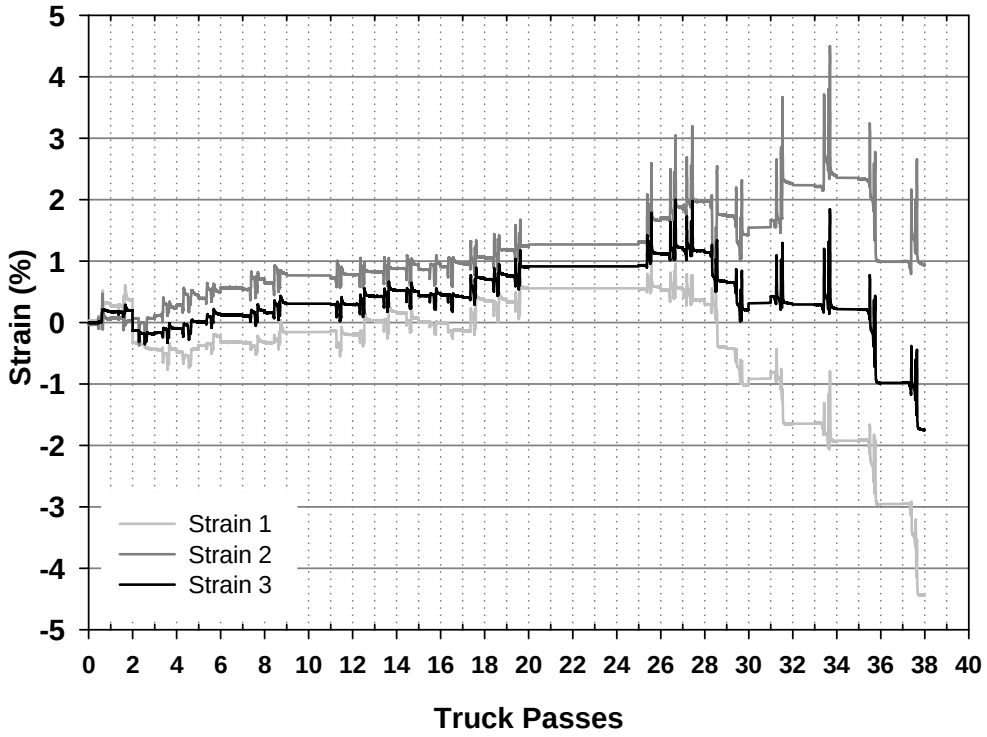

Figure D-8. Strain profiles of the CoG-4 test section.

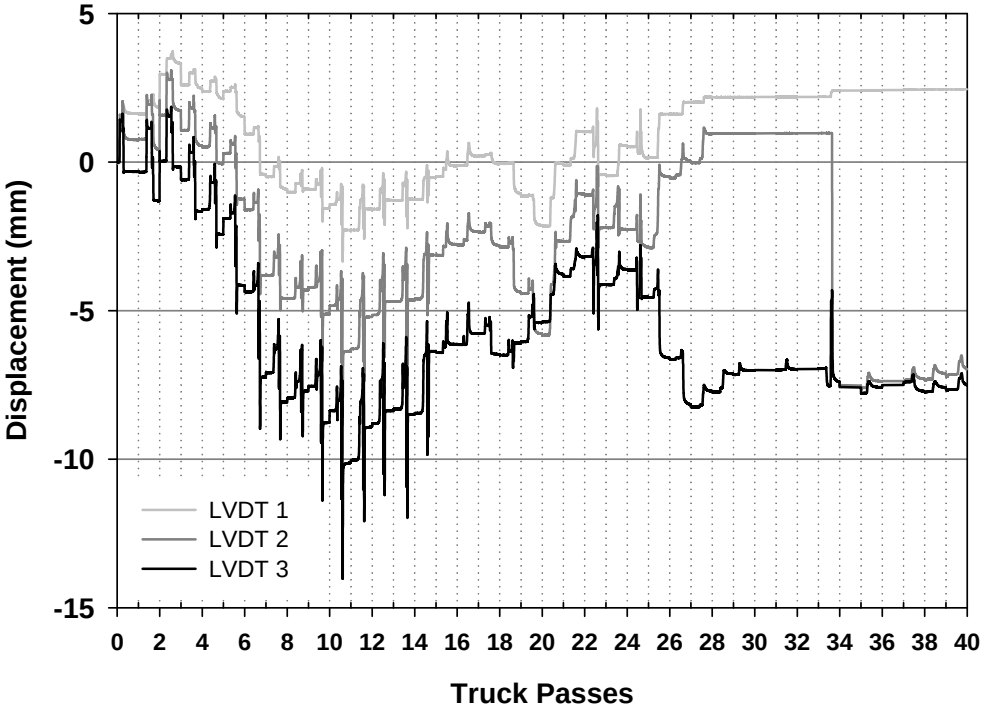

Figure D-9. Displacement profiles of the IFG-5 test section.

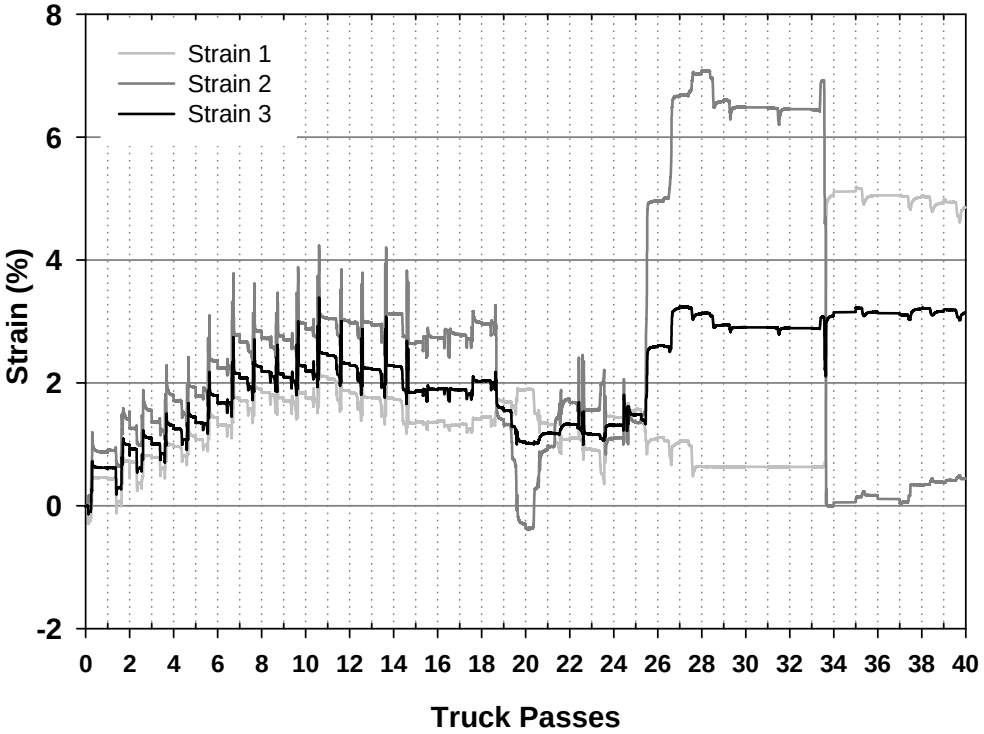

Figure D-10. Strain profiles of the IFG-5 test section.

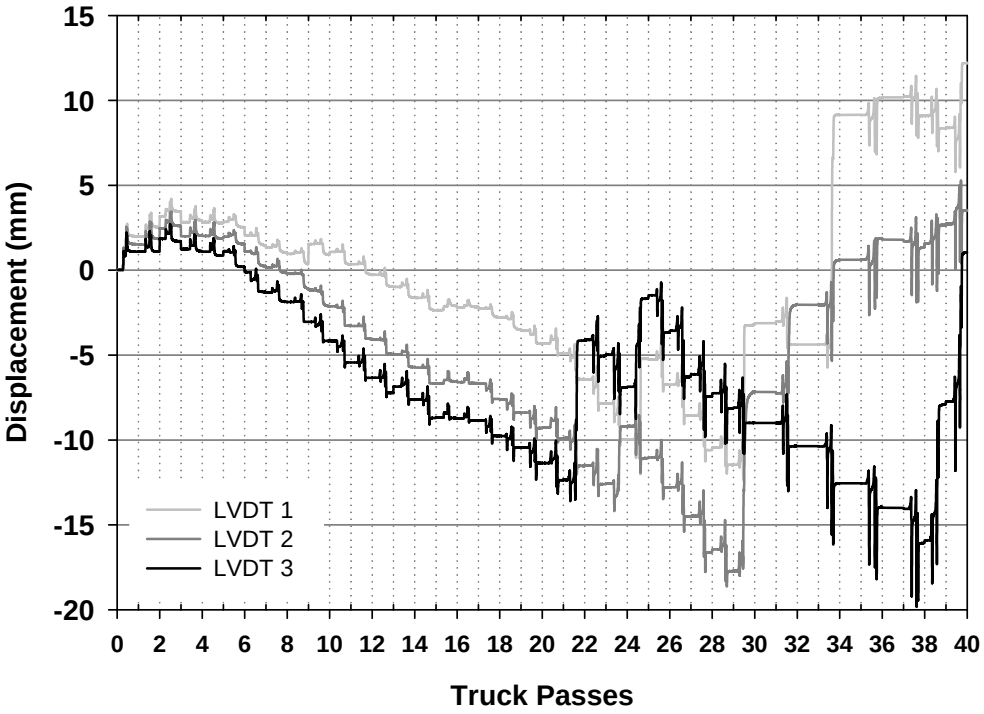

Figure D-11. Displacement profiles of the WeG-6 test section.

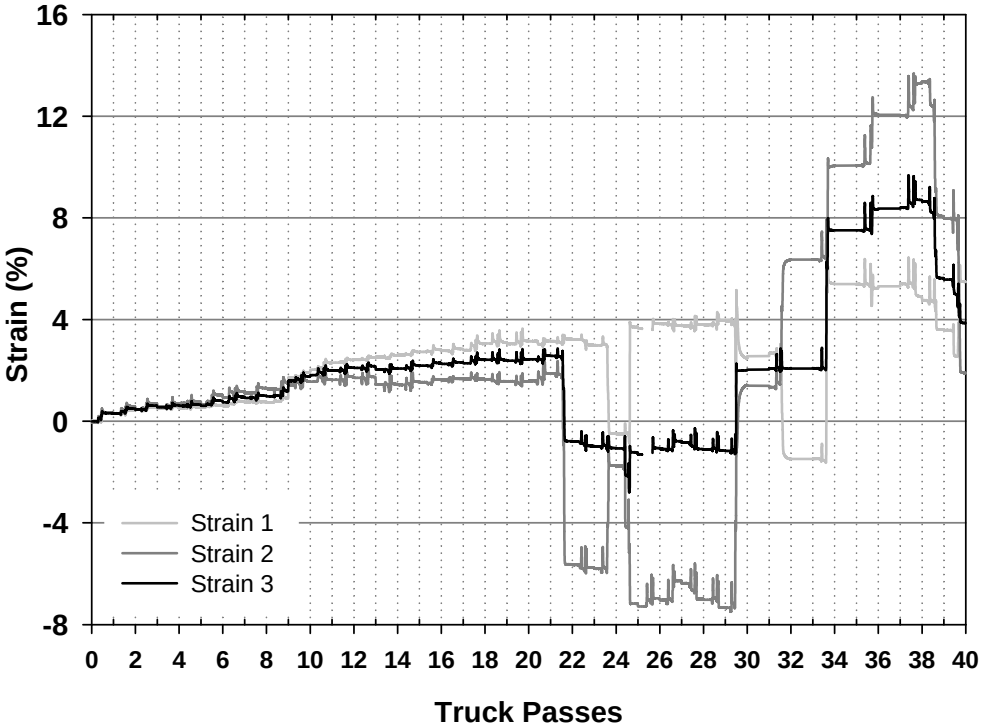

Figure D-12. Strain profiles of the WeG-6 test section.

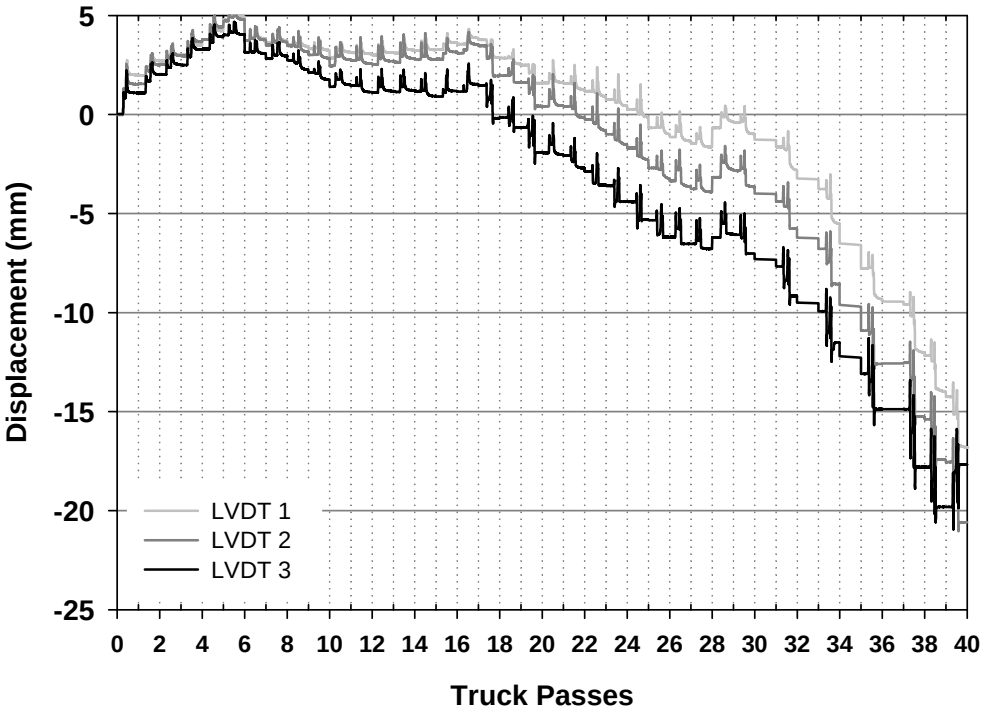

Figure D-13. Displacement profiles of the WoG-7 test section.

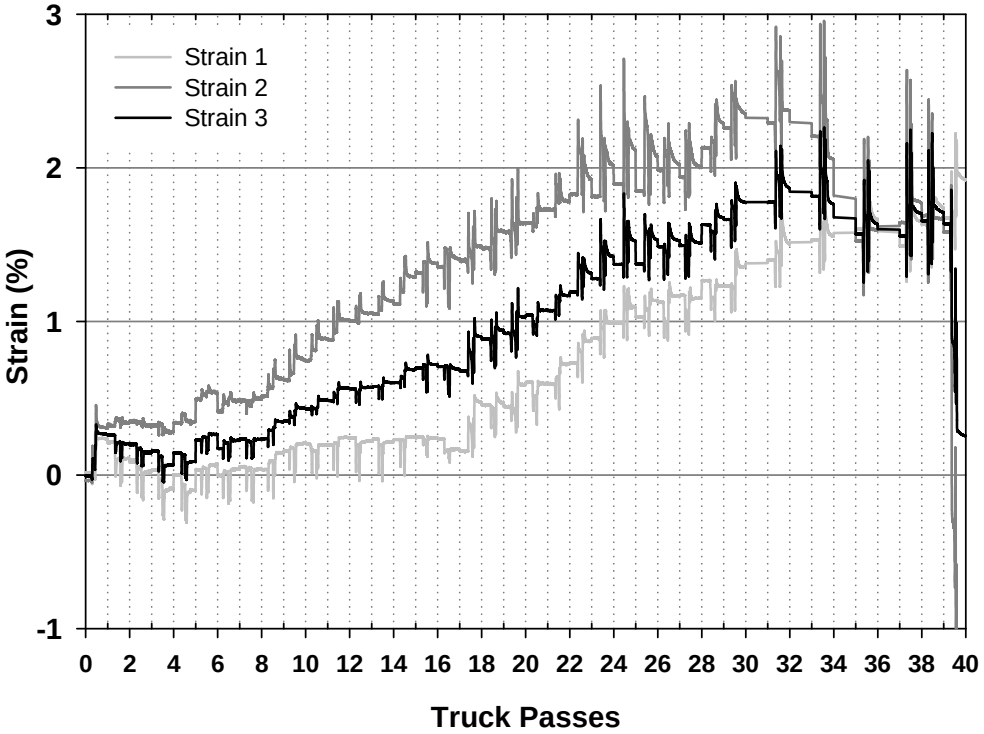

Figure D-14. Strain profiles of the WoG-7 test section.

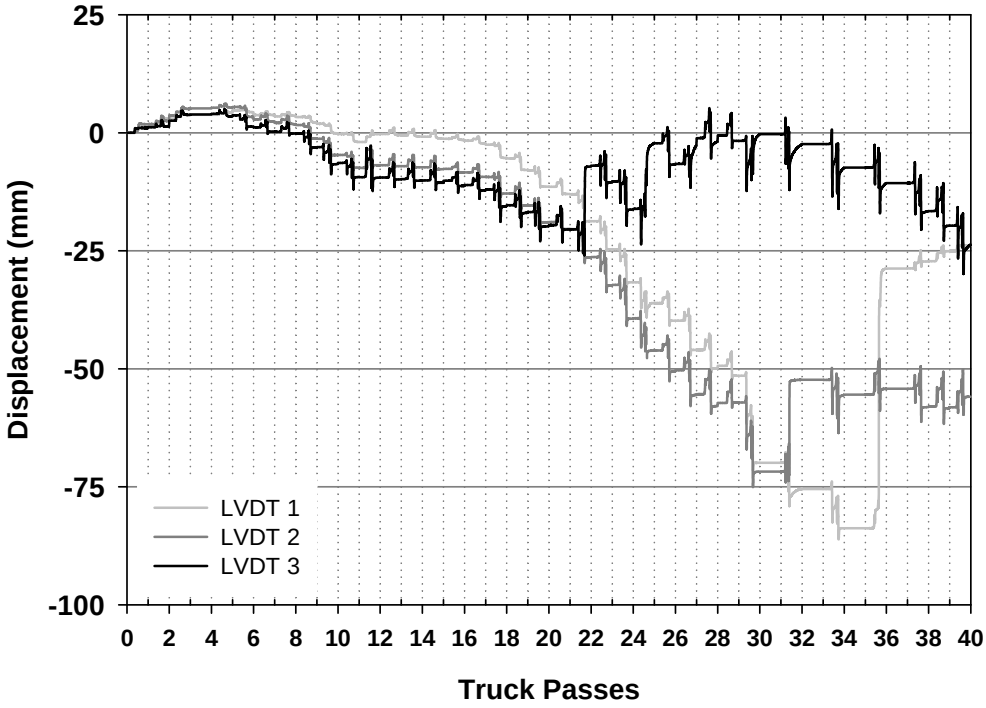

Figure D-15. Displacement profiles of the WoG-8 test section.

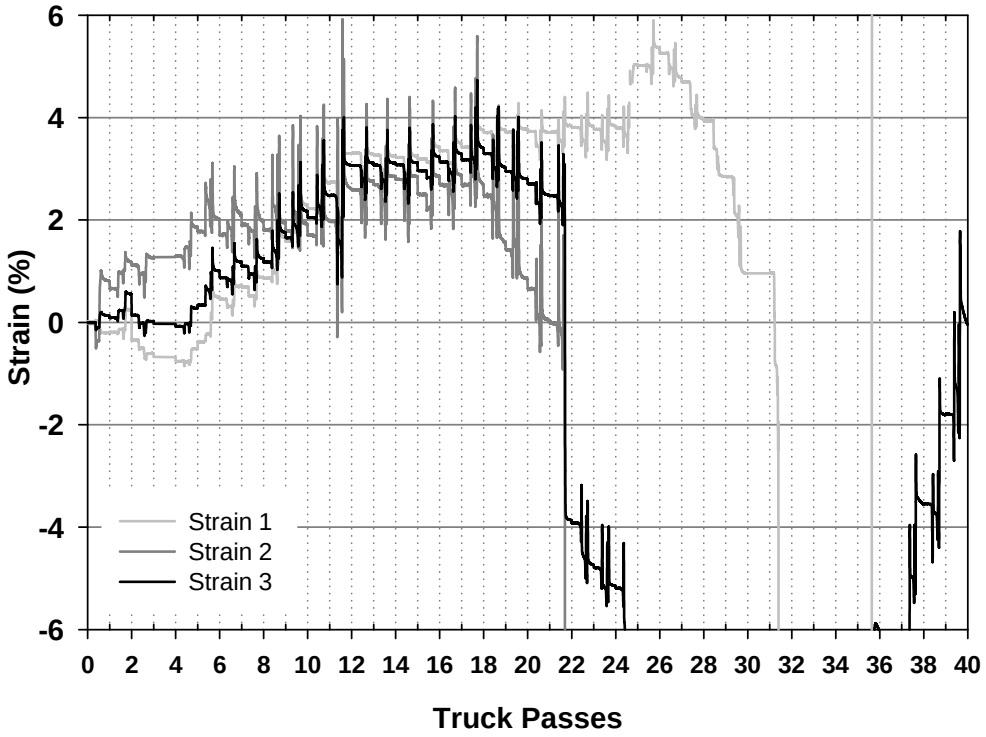

Figure D-16. Strain profiles of the WoG-8 test section.

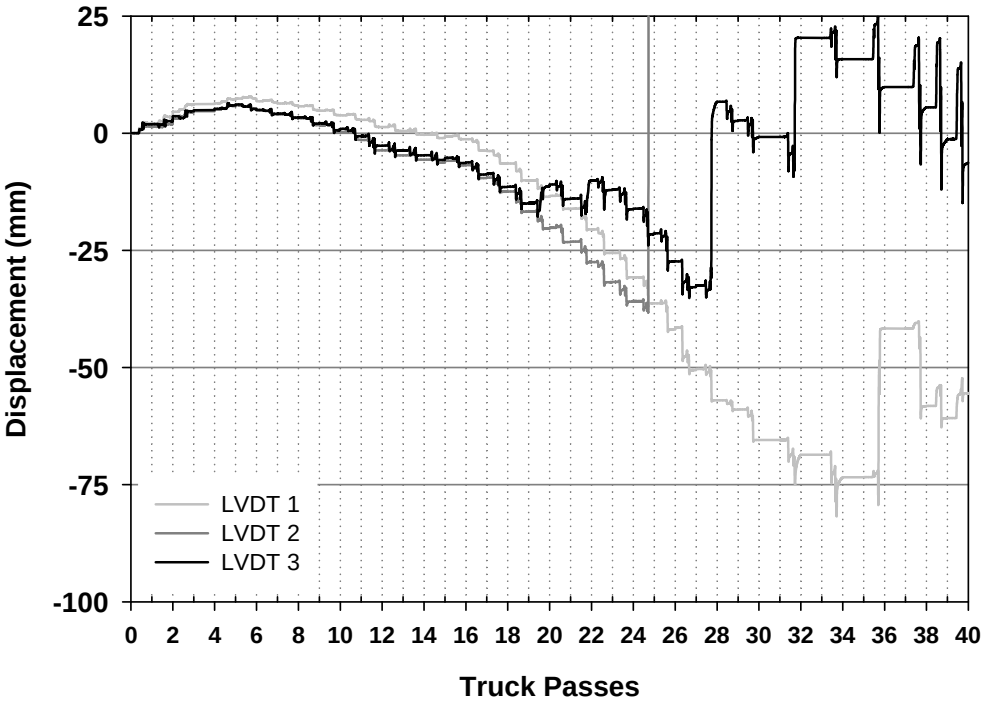

Figure D-17. Displacement profiles of the WoT-9 test section.

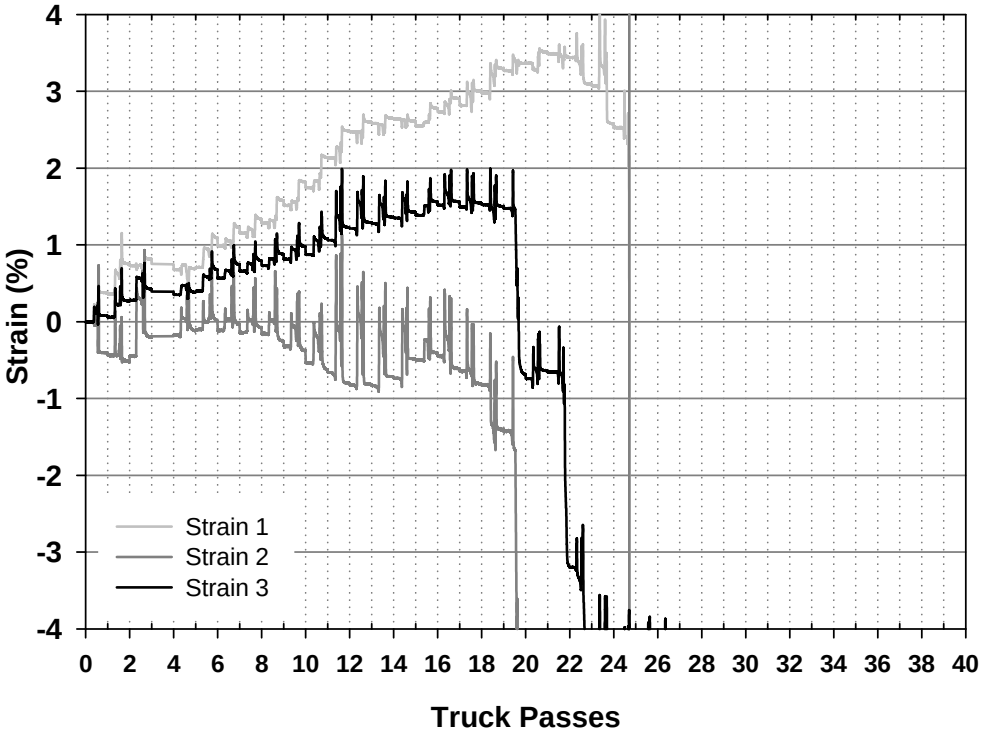

Figure D-18. Strain profiles of the WoT-9 test section.

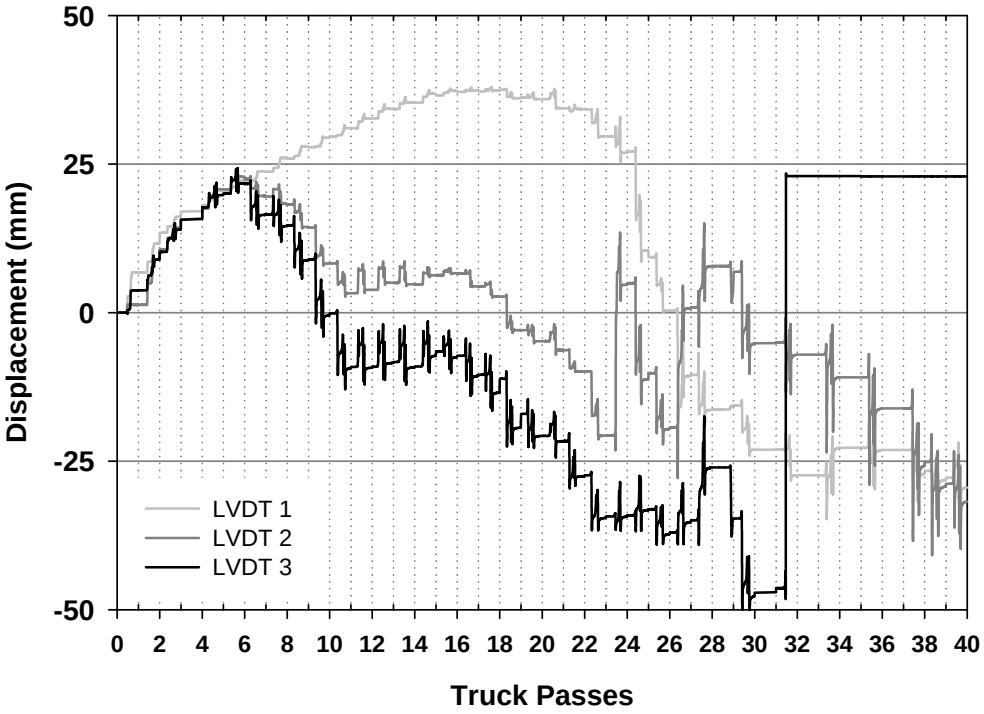

Figure D-19. Displacement profiles of the NWoT-10 test section.

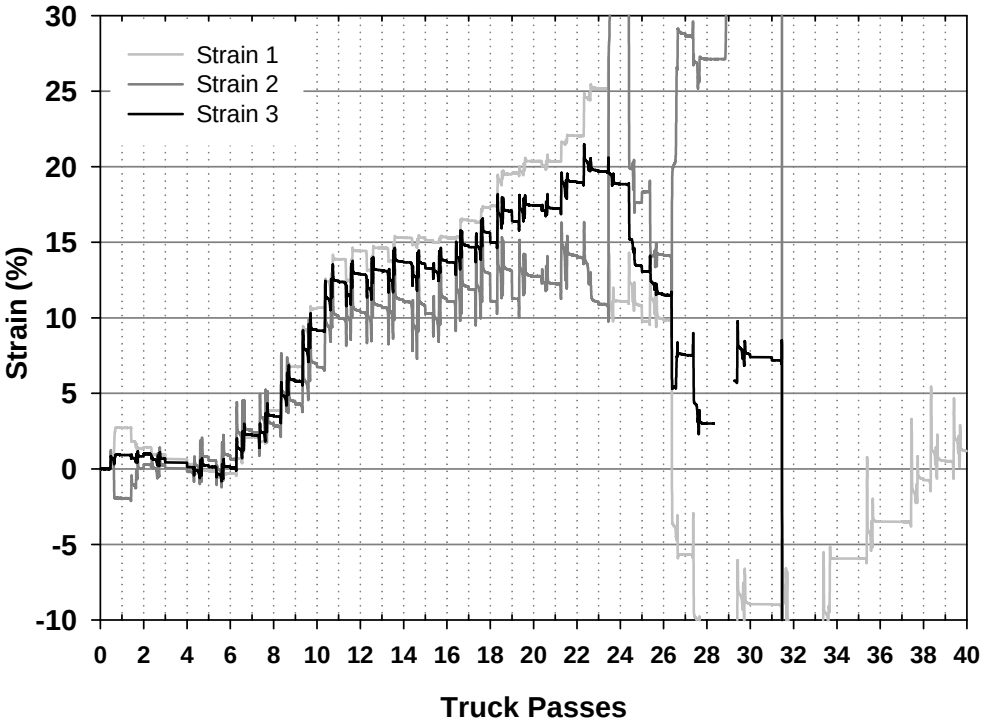

Figure D-20. Strain profiles of the NWoT-10 test section.